THE INFLUENCE OF LANDSCAPE STRUCTURE ON STORAGE AND STREAMFLOW GENERATION IN A PIEDMONT CATCHMENT

by

Shane M. Putnam

A dissertation submitted to Johns Hopkins University in conformity with the
requirements for the degree of Doctor of Philosophy

Baltimore, Maryland

October 2018

©2018 Shane M. Putnam

All Rights Reserved

Abstract

The storage of water and generation of streamflow are fundamental catchment functions. The specific way in which a catchment performs these functions is inextricably tied to the structure of the catchment, including the thickness/texture of soil, depth to impermeable bedrock, and presence of riparian areas with shallow water tables. Accordingly, catchments with different landscape structures will respond differently to hydroclimatic variability. The majority of field investigations into streamflow generation have concentrated on high relief or recently glaciated landscapes where soils are thin and overlie an assumed impermeable bedrock layer. In contrast, relatively little research on streamflow generation has been conducted in deeply weathered regions, such as in the Piedmont Physiographic Province of the eastern United States. Of those studies that have focused on these regions, many have highlighted the potential of deeply weathered landscapes to store large quantities of water, which may be important for maintaining streamflow during droughts.

In the research effort reported here, catchment storage and streamflow generation in a prototypical Piedmont headwater catchment were investigated through field data collection and modeling. The analysis aimed to test hypotheses relating hydrologic function to Piedmont landscape structure. The 37-hectare, forested Pond Branch Catchment of northern Maryland was instrumented to collect data on hillslope spring discharge, hydrometeorological data, riparian well water levels, as well as three years of high frequency precipitation and streamflow stable water isotope data. Additional data were collated from other sources on catchment discharge, soil moisture, and remotely-sensed land surface properties. These data were used in combination with recession analysis, water balance models, and transport modeling using StorAge Selection functions to estimate storage and characterize streamflow generation.

The storage within the hillslope and underlying weathered bedrock was found to be the main driver of the slowly changing baseflow component of streamflow, which made up 85% of total discharge. In addition, the rapidly responding quickflow component of streamflow was proven to be composed of a combination of direct precipitation and return flow from the toe of the hillslope, which was generated as saturation excess overland flow at the riparian-hillslope boundary. The importance of the storage structure in controlling the emergent catchment response to precipitation variability was revealed when a relatively small reduction in rainfall during early spring (when the deep flow system is typically recharged) of water year 2016 produced what may be a decadal drought in the groundwater level, resulting in persistently low baseflow discharge for at least two years after. The role of the deeply weathered landscape structure of Pond Branch in controlling storage and streamflow generation highlights the importance of studying diverse landscapes with different landscape structures in order to gain understanding into catchment functions.

Dissertation Readers (listed alphabetically):

Dr. William P. Ball, Johns Hopkins University

Dr. Grace Brush, Johns Hopkins University

Dr. Ciaran J. Harman, Johns Hopkins University (adviser)

Dr. Harihar Rajaram, Johns Hopkins University

Acknowledgements

I am grateful for everyone who supported me throughout my Ph.D. and helped make this dissertation a reality. First and foremost, I thank my adviser Ciaran Harman. Ciaran taught me to be a true research scientist, always pushing me to explain my question or hypothesis and show how I might go about finding an answer. Ciaran would pull me out of the weeds when I had lost the big picture and was focused on a small detail in the data. Ciaran encouraged me to broaden my skills, sent me to workshops/classes, introduced me to a large network of researchers, and always seemed to have confidence in me even when I had lost it myself. I am indebted for the countless hours that Ciaran spent mentoring me over the last six years and I wish him all the success that he has worked so hard to achieve.

I would like to thank the members of my examination committees as well as numerous other faculty, staff, and students who helped me along the way. Grace Brush taught me to think about the history of the landscape and the relationships between the geology, soil, and vegetation. I will miss spending Saturdays walking around with Grace and her class, identifying trees, discussing the landscape history, and adsorbing as much knowledge as possible. Early in my Ph.D., Naomi Levin and Ben Passey taught me the fundamentals of isotope geochemistry and provided technical support when I was struggling to get the laboratory up and running. Peter Wilcock introduced me to Ciaran, taught me fluid mechanics, and helped foster my academic curiosity while sipping on sherry. William Ball, Harihar Rajaram, Daniel Viete, Darryn Waugh, and Benjamin Zaitchik helped to identify weaknesses in my foundational knowledge, pushed me to think critically about my dissertation questions, and challenged me to identify the broader impacts of my research. Joel Moore at Towson University was eager to discuss my research progress, analyzed hundreds of samples for me, and provided encouragement whenever we ran into each other. Jessica Elroy was always a friend, advocate, and guru of everything relating to academic policies and procedures. When I was stressing over a form or just needed to talk, Jessica was always there. Michael Lester, Huan Luong, Denise Nowlin, Keith Ritchie, and Adena Rojas kept the department running and would always take time out of their day to answer my seemingly incessant questions. Dozens of undergraduate students helped collect and process the samples and data underlying this dissertation. I would especially like to thank Emily Stoll who somehow always made time to filter samples in the lab even though she was working multiple jobs, as well as Eric Morgan who was eager to help me in the field even if I did on occasion have to bribe him with food.

I would like to thank the staff at Oregon Ridge Park as well as all of the homeowners who provided access to the park over the years. Brien Haigley kindly allowed me to park at his house every week so that I could collect weekly water samples. Jerald and Joan Magness allowed me to collect weekly samples and construct a stream gage behind their house as a part of my research in a suburban catchment. Furthermore, Jerald and Joan were always kind and caring, warning me if they saw a snake or offering to give me food if I was working late.

I would like to thank my colleagues and friends who provided feedback on my research as well as the emotional support and necessary distractions which kept me going. My peers, Cassie Cosans, Minseok Kim, Tianqi Liu, Dano Wilusz, and Adam Wlostowski, provided lively discussions during our weekly meetings, feedback on presentations, and were always willing to help in the field, even when it meant carrying car batteries up and down hills. I thank my friends, including Tim Barrick, Ali Barton, Justin Beauchamp, Chris Brueck, Steven Chow, Cassie Cosans, Phillip Flanders, Margaret Flemming, Hanna Gray, Collyn Heier, Robin Hytowitz, Gaige Kerr, Kristin Lang, Sophie Lehmann, Kitty Meader, Mark Natale, Michael Rose, Kristopher Thornsbury, and Dano Wilusz, for supporting me when I most needed it, for joining me in my hobbies, and for all of the fun we have had. I thank Roberto Millar for encouraging me to keep writing over these last few months, for keeping me grounded even when I would wake up in the night panicking, and for all the experiences we have shared together, especially our Jeopardy marathons.

Finally, I would like to thank my family for their lifetime of support as I have pursued my education. I thank Richard V. Putnam, for everything that he has done for me throughout my life, I would not be where I am today without his love and support. I thank Twyla E. Putnam, for believing in my determination and for the sacrifices she made for me. Both Richard and Twyla taught me to work hard, be practical, and to keep on trying even if I wanted to give up. I thank Mary Putnam for always thinking of me whenever I was stressed and for inviting me to the lake, which always provided a much-needed break from my laptop. I thank my siblings, Heather Herd, Richard (Skipper) C. Putnam, and Stephanie Putnam, for being positive role models, for helping me when I needed it, and for encouraging me to achieve my goals.

Contents

Abstract ii

Acknowledgements v

List of Figures xii

List of Tables xxiv

List of Abbreviations and Symbols xxvi

1 Introduction 1

1.1 Motivation 1

1.1.1 Runoff Generation Mechanisms 1

1.1.2 Piedmont Physiographic Province 3

1.1.3 A Prototypical Piedmont Catchment 4

1.2 Dissertation Outline 5

2 The Structure of Storage within a Deeply Weathered Piedmont Catchment 7

2.1 Introduction 7

2.2 Study Site 12
2.3 Methods 16
  2.3.1 Instrumentation & Data Collection 16
  2.3.2 Catchment Storage 20
  2.3.3 Riparian Storage 24
  2.3.4 Soil Storage 24
  2.3.5 Hydraulic and Indirect Storage 25
2.4 Results 31
  2.4.1 Water Balance and Catchment Storage 31
  2.4.2 Riparian Storage 37
  2.4.3 Soil Storage 38
  2.4.4 Hydraulic and Indirect Storage 39
2.5 Discussion 43
  2.5.1 “Hidden” Storage in the Piedmont Saprolite 43
  2.5.2 Challenges in Identifying Hydraulic Storage 47
  2.5.3 Groundwater Drought in the Deeply Weathered Piedmont . . . 49
  2.5.4 Drought Propagation through Structured Storage 50
2.6 Conclusions 52

3 Streamflow Generation in a Forested Piedmont Catchment 54
3.1 Introduction 54
3.2 Methods 60
  3.2.1 Instrumentation & Data Collection 60
  3.2.2 Baseflow Separation 63

3.2.3 Stream Stage Estimation 64

3.3 Results 65

3.4 Inferences about Process 69

3.4.1 Baseflow as Hillslope Storage Release at the Valley Margin . . 69

3.4.2 Quickflow as Riparian Runoff 73

3.4.3 Water Table Response to Storm Events 76

3.4.4 Hillslope Response to Storm Events 82

3.5 Discussion 85

3.6 Conclusions 90

4 Transport Modeling to Elucidate Runoff Generation Mechanisms in a Forested Piedmont Catchment 92

4.1 Introduction 92

4.2 Hypothesis Testing Using rSAS 95

4.3 Methods 99

4.3.1 Instrumentation & Data Collection 99

4.3.2 rSAS Modeling of Saturation Excess Overland Flow 103

4.3.2.1 Direct Precipitation 104

4.3.2.2 Return Flow and Direct Precipitation 107

4.4 Results 108

4.4.1 Direct Precipitation 111

4.4.2 Return Flow and Direct Precipitation 114

4.5 Discussion 116

4.5.1 Stable Water Isotope Data 116

4.5.2 Return Flow 118

4.6 Conclusions 120

5 Conclusion 122

5.1 Summary 122

5.1.1 Key Findings 123

5.1.2 Limitations 125

5.1.3 Broader Impacts 126

5.2 Future Research 129

Bibliography 130

Vita 142

List of Figures

2.1 Observed monthly precipitation (P) and specific discharge (q) for the Pond Branch Catchment compared to the averages for each month over the 2000 to 2017 Water Years. The gray indicates months when precipitation or specific discharge is less than average, while the lighter green or lighter blue indicates months when precipitation or discharge, respectively, is greater than average. From August 2016 through February 2017, the monthly precipitation is less than the monthly average, while specific discharge is below average for the entire 2017 Water Year. Specific discharge remains lower than average in the summer of 2017 despite the higher than average precipitation in the spring and summer of 2017. 11

2.2 (a) Location of the study site (39º 29’ 03” N, 76º 41’ 17” W) in the eastern United States, with the Piedmont Physiographic Province shaded in orange. (b) Overview map of the study site showing the Pond Branch and Baisman Run Catchment boundaries relative to the locations of two USGS Stream Gages and the JHU01 Weather Station. The orthoimage illustrates the dominance of forest cover in the Pond Branch Catchment as well as the presence of suburban areas to the in southwest. (c) Map of the Pond Branch Catchment with instrumentation including the USGS Stream Gage at the outlet, riparian wells, and plots containing volumetric water content (VWC) probes. The numbers “1,” “2,” and “3” correspond to the riparian well numbers referenced in Section 2.3.1. The plots containing VWC probes are labeled according to their relative cardinal direction within the catchment, i.e. “Northern” and “Southern.” The outline of the riparian and swale landscape units are shown, with the remainder of the catchment area defined as the hillslope landscape unit. 13

2.3 (a) Image from the Pond Branch Catchment with annotations showing the divisions between the riparian and hillslope landscape units. Two branches of the stream channel can also be seen in this image, with the main stem on the right. (b) Image of a soil pit dug within the hillslope landscape unit which shows a portion of the subsurface structure including the soil, soil-saprolite boundary, and top section of the saprolite. 15

2.4 Daily forcing data for estimating potential evapotranspiration using the Penman-Monteith Equation, including maximum and minimum temperature (T) and relative humidity (% RH), local atmospheric pressure (atm P), wind speed (V), shortwave radiation (SW), long wave radiation (LW), and leaf area index (LAI). 23

2.5 Summary of the daily data used in combination with the methods described in the previous section to estimate storage for the catchment as whole, hydraulically coupled and uncoupled portions of the landscape, and individual landscape units. Precipitation (P) and specific discharge (q) are in units of millimeters per day; the logarithmic of the specific discharge (log q) has units of logarithmic millimeters per day; the water level (WL) measured in each riparian well is in meters below the land surface; and the volumetric water content (VWC) is in units of cubic meters per cubic meter and therefore dimensionless. The black points in the second pane are days in which the recession rate from the previous day is estimated. The numbers in the fourth pane correspond to the riparian wells labeled in Figure 2.2, and the labels in the last pane correspond to the relative cardinal direction of the two plots containing volumetric water content probes as shown in Figure 2.2. 32

2.6 Daily actual evapotranspiration (ET) for the Pond Branch Catchment. Actual evapotranspiration was calculated as described in Section 2.3.2 by scaling the potential evapotranspiration estimated from the Penman-Monteith Equation. . 34

2.7 Summary of the daily storage time series estimated during this analysis. The α-values in the last two panes correspond to the ratio of the hydraulic area to the total catchment area that is used to estimate the corresponding storage following the method presented in Section 2.3.5. 36

2.8 (a) Individual recession rates (-dq/dt) from Figure 2.5 (gray points), binned average recession rates (black points), standard error for the binned averages (black bars), and the line of best fit, i.e. the catchment sensitivity function, (black line) versus the specific discharge (q) for each of the three α-values used to scale the recession rates. The coefficient of determination (R^2) for each line of best fit is shown in the upper left-hand corner. (b) Binned average recession rates (black points) and the line of best fit (black line) versus the specific discharge for each α-value on a logarithmic-logarithmic plot. (c) Residuals between the line of best fit and the binned average recession rates versus the specific discharge for each α-value on a logarithmic-logarithmic plot. 41

2.9 Hydraulic storage (ΔS_H) versus specific discharge for Pond Branch (q) for each α-value and corresponding catchment sensitivity function. Discharge is plotted on a linear-axis on the left and on a logarithmic-axis on the right. The dashed lines on the left plot map the relationships between hydraulic storage and 1 mm/day of discharge for each α-value. 42

2.10 Dynamic catchment storage (ΔS) versus the two-week average of baseflow calculated from the Pond Branch specific discharge (q). The color map corresponds to the date of the plotted points which range from October 1, 2014 (black) to September 30, 2017 (light gray). Hysteresis indicates that there are multiple catchment stores, some of which are not hydraulically connected to baseflow at all times. 44

2.11 The top pane compares the monthly relative water level observed in a USGS well located approximately 10 kilometers from the research site to the calculated daily dynamic catchment storage (ΔS) over the 2015 to 2017 water years. The water level is plotted on the left y-axis and storage on the right y-axis. The bottom pane shows the complete monthly water level record for the

USGS well, which extends back 62 years to 1955. The dashed lines are the range in the water level observed over the three years in which storage was calculated. 50

3.1 Diagram summarizing dominant runoff generation processes as a function of soils, topography, climate, vegetation, and land use from Dunne (1983) and reproduced by Wagener et al. (2007). 56

3.2 (a) A map of the eastern United States with the Piedmont Physiographic Province shaded in orange and the location of the study site (39º 29’ 03” N, 76º 41’ 17” W) denoted by a red star. (b) Orthoimage of the study site with the location of the Pond Branch Catchment boundary, USGS Stream Gage, and JHU01 Weather Station. This image also shows the dominance of forest cover in the Pond Branch Catchment. (c) Detailed map of the Pond Branch Catchment with instrumentation including the USGS Stream Gage at the outlet, riparian wells, and gaged hillslope springs. The numbers “1,” “2,” and “3” on the map correspond to the riparian well numbers, while the letters “C” and “D” refer to the convergent and divergent hillslope springs, respectively. The outline of the riparian and swale landscape units are shown, with the remainder of the catchment area defined as the hillslope landscape unit. These units are delineated in part based on the contrast in slope between the steep toe of the hillslope and the relatively flat swale and riparian landscape units. In purple is the estimated effective contributing area for each hillslope spring. 59

3.3 (a) Image of the convergent hillslope spring during the construction of its gage. Shown are the plastic barriers used to redirect flow toward the bucket containing a 45º v-notch on the downslope side. (b) Image of the completed convergent hillslope spring gage including the plastic tarp used to prevent direct precipitation on to the saturated area between the gage and the source of the spring. This image was taken at a similar location as the previous one but at a slightly different angle, such that you can see the convergent area upslope of the source of the spring. Note that the instrument in the lower left-hand corner of the image is an autosampler which is used for a different study. 61

3.4 Summary of the 15-minute time series that are used in this analysis to study streamflow generation within the Pond Branch Catchment. Precipitation (P), Pond Branch discharge (q), Pond Branch baseflow (bf), convergent hillslope spring discharge (qC), and divergent hillslope spring discharge (qD) are in units of millimeters per day (mm/d) on the primary y-axis; the logarithmic of Pond Branch discharge (log q) has units of logarithmic mm/d; and the water level (WL) measured in each riparian well and in the Pond Branch channel is in meters above sea level (mASL). Note that all discharge is normalized by the Pond Branch Catchment area but that the discharge for the hillslope springs is included in cubic meters per day on the secondary y-axis for clarity. Pane three shows the results of the baseflow separation of the Pond Branch discharge on a logarithmic scale, with baseflow (bf) in sky blue and quickflow (qf) in cyan. In panes four through six, the largest discharge events are truncated as a result of scaling the y-axis in order to show the variability in the weekly average of the

15-minute time series (solid black line). The numbers in pane seven correspond to the riparian wells labeled in Figure 3.2, while the letter “S” denotes the Pond Branch stage estimate from Section 3.2.3. 68

3.5 Plot of the weekly average discharge (W Avg) for the convergent (qC) and divergent (qD) hillslope spring verses the weekly average baseflow (bf), with linear regression (black line). The slope of each linear regression represents the ratio of the contributing area of the spring to the area contributing to baseflow. See Table 3.1 for the numerical results of the regressions. 73

3.6 Comparison of the cumulative quickflow discharge estimated from baseflow separation and the cumulative runoff which may be generated from direct precipitation on to the riparian area or the riparian plus swale areas. Notice that the quickflow is bounded by the other two cumulative runoff estimates. 76

3.7 Annotated image of a portion of the riparian well transect within the Pond Branch Catchment. The numbers correspond to the well identification numbers. Well #1 is behind the tree in this image, upslope of the break in slope (black dashed line) that divides the hillslope (labeled “Hill”) and the riparian landscape units. Well #2 can be seen in this image and is located within five meters of the right bank of the main channel of Pond Branch (labeled “Channel” and shown as a blue dashed line). Well #3 is out of the frame to the right, approximately 2.5 meters from the left bank of Pond Branch. Between the break in slope and Well #2 is a patch of *Symplocarpus foetidus* (commonly known as Skunk Cabbage), which only grows in soils at or near full saturation. 77

3.8 The topographic profile of the riparian well transect (brown line), with the water table at four time steps over the course of a storm event (before, mid-event, event peak, and post-event). The break in slope denotes the boundary between the hillslope and riparian landscape units with the toe of the hillslope to the left of the break and the riparian unit to the right. The total precipitation amount (P) and maximum precipitation intensity (I_{max}) for each storm is shown in the upper right-hand corner of each plot. (a) The water table response for a storm event on June 27, 2015 with wet antecedent conditions. (b) The water table response for a storm event on November 29, 2016 with dry antecedent conditions. . . . 81

3.9 Analysis of a storm event that occurred on June 23, 2015 to determine if the quantity of hillslope discharge estimated by scaling the spring discharge can account for the quantity of quickflow. Precipitation (P), Pond Branch discharge (Q), convergent spring discharge (QC), and divergent spring discharge (QD) are plotted over a two-day period. Discharge is separated into quickflow (QF) and baseflow (BF) components using baseflow separation as described in Section 3.2.2. The one-hour averages (1 hr Avg) of QC and QD are used to calculate the hillslope discharge (Q_{Hill}) though the unsmoothed data produce similar results. The orange dashed-box shows the interval over which the cumulative sum of P, BF, QF, and Q_{Hill} is calculated with values reported in the upper left-hand corner of each corresponding pane. For this storm, all baseflow can be accounted for by hillslope discharge but only a small proportion of the quickflow can be explained. 84

3.10 Perceptual hydrologic model of the Pond Branch Catchment. The top portion of the figure shows the structure of the landscape including the location of the hillslope and riparian landscape units and its relationship to hydrologic features. The locations of the pictured water tables are approximate but are based on the dynamic range in catchment storage. Note that a vertical exaggeration (VE) of 1.5 is used for this figure. The bottom two boxes show the between event and event response of flow pathways. Between events, hillslope storage sustains baseflow and evapotranspiration (ET) induces diurnal fluctuations in riparian water levels. During precipitation (P) events, water levels at the toe of the hillslope rapidly rise, causing the water table at the hillslope-riparian interface to intersect the surface, creating an area of saturation which generates saturation excess overland flow. This saturation excess overland flow dominates the quickflow component of discharge. 89

4.1 Diagram illustrating the basic concepts of the rank StorAge Selection (rSAS) theoretical framework and the relationship between a rSAS function's probability density function (PDF) and the corresponding time-variable (TV) transit time distribution (TTD). Precipitation (P) enters a control volume (CV) with age zero and then ages as a function of the time (t) elapsed. The water stored in a given CV is ranked by age (shown here conceptually), with the younger water (Δt_5) stacked over the older (Δt_1). Note that Δt_4 is missing from the control volume, indicating that there was no precipitation during that interval. The rSAS function's PDF, here a uniform distribution, specifies the proportion of water of a given age selected from the CV by discharge (q). At each time step, the rSAS PDF determines the TTD, here shown for t_5, where t_5 is the time at the end of Δt_5. 97

4.2 (a) A map of the eastern United States showing the location of the field site (39º 29’ 03” N, 76º 41’ 17” W) relative to state boundaries and the Piedmont Physiographic Province. (b) Detailed map of the field site showing the location of the Pond Branch Catchment boundary, defined landscape units, streams, and all instrumentation used in this chapter. The riparian and swale landscape units are shaded in greenish-blue, with the remainder of the catchment area defined as the hillslope landscape unit. These units are delineated in part based on the contrast in slope between the steep toe of the hillslope and the relatively flat swale and riparian landscape units. A USGS stream gage and an autosampler used to collect 12-hourly water samples are co-located at the catchment outlet, while a precipitation collector used to collect bulk weekly precipitation samples is co-located with the JHU01 weather station. This orthoimage highlights the dominance of forest cover within the Pond Branch catchment. 100

4.3 A figure showing the relationship between the hypothesized quickflow generation mechanism and the choice of the corresponding rank StorAge Selection (rSAS) function for quickflow ($\Omega_{qf}(S_T, t)$). The perceptual model of each runoff generation process is shown on the left and the corresponding $\Omega_{qf}(S_T, t)$, which selects from the age-rank storage column, is shown on the right. P, qf, rf, and WL stand for precipitation, quickflow, return flow, and water level, respectively. A uniform distribution is chosen to represent the selection of water from the age-rank storage column, with different maximum age-rank storage (S_{Tmax}) for each hypothesis. (a) This panel corresponds to the hypothesis that quickflow is generated from saturation excess overland flow, which is produced from direct precipitation. For this hypothesis an S_{Tmax} of 0.245 mm is chosen to represent the selection of the very youngest water within the age-rank storage column. (b) This panel corresponds to the hypothesis that quickflow is generated from saturation excess overland flow, which is composed of both direct precipitation and return flow from the toe of the hillslope. Here the S_{Tmax} parameter of $\Omega_{qf}(S_T, t)$ is optimized in order to represent the selection of water from the tension saturated zone at the toe of the hillslope and from the youngest water in storage. 105

4.4 Summary of all of the time series used in this chapter. Precipitation (P), specific discharge (q), and actual evapotranspiration (ET) are in units of millimeters per six hours (mm/6hrs); the logarithmic of the specific discharge (log q) has units of logarithmic mm/6hrs; and the delta-O-18 ($\delta^{18}O$) of P and q are in unites of per mil (‰) relative to Vienna Standard Mean Ocean Water (VSMOW). In pane three the logarithmic of the specific discharge is separated into its baseflow (bf) and quickflow (qf) components using baseflow separation. The $\delta^{18}O$ of P is determined from bulk weekly samples while the $\delta^{18}O$ of q is from 12-hourly grab samples. Notice that the y-axes for $\delta^{18}O$ of P and q are not the same. 109

4.5 The predicted δ^{18}O of discharge (q) in per mil (‰) for different values of the maximum age-rank storage (S_{Tmax}) for the rank StorAge Selection (rSAS) function for quickflow, along with the observed δ^{18}O of Pond Branch discharge. The first pane, with an S_{Tmax} of 0.254 mm, corresponds to the hypothesis that quickflow is dominated by direct precipitation. The second pane, with an optimized S_{Tmax} of 18.5 mm, corresponds to the hypothesis that quickflow is composed of both direct precipitation and return flow. The last pane shows the results of a sensitivity analysis in which S_{Tmax} is varied between 5.0 mm and 100 mm. 112

4.6 A two-week window of the results presented in Figure 5. The y-axis is rescaled to a narrower range in order to compare the predicted δ^{18}O of discharge (q) in per mil (‰) for different values of the maximum age-rank storage (S_{Tmax}) to the observed δ^{18}O of Pond Branch discharge. The first two panes correspond to separate quickflow generation hypotheses while the last pane shows the results of a sensitivity analysis. 113

List of Tables

2.1 Comparison of the total of the water balance terms for the three years over which daily catchment storage was calculated where P, q, ET, ΔS, and ΔS_{range} stand for the precipitation, specific discharge, actual evapotranspiration, dynamic catchment storage, and range in the dynamic catchment storage, respectively. The last row in the table is the 17-year annual water year average calculated from the same data used to construct Figure 2.1, such that ET, ΔS, and ΔS_{range} were not available (NA). 33

3.1 Summary of the slope (m), coefficient of determination (R^2), and probability value (p-value) for the linear regression shown in Figure 3.5 for each hillslope spring. The slope of the linear regression is multiplied by the area contributing to baseflow, which is assumed to be the hillslope area, to calculate the corresponding contributing area of the spring (A_{spring}). A_{spring} is divided by the hillslope length (L_{hill}) in order to calculate the effective contributing width of the spring (W_{spring}). The 99 % confidence interval is included for both A_{spring}

and W_{spring} as a measure of the bounds within which the observed contributing width must fall within in order to validate. 73

4.1 Summary of the optimized or selected parameters for each hypothesis and corresponding set of rank StorAge Selection (rSAS) functions, as well as the resulting modified Kling-Gupta Efficiency (KGE). The maximum age-rank storage (S_{Tmax}) for quickflow (qf) is chosen *a priori* for the direct precipitation hypothesis and optimized for the hypothesis that quickflow is composed of both return flow and direct precipitation. For baseflow (bf), a gamma distribution is chosen for the rSAS function with shape parameter α_{bf} and scale parameter θ_{bf}. The mean μ_{bf} of the gamma distribution is the product of α_{bf} and θ_{bf}. For evapotranspiration (ET), a uniform distribution is chosen and the S_{Tmax} parameter is optimized. S_{Tmax}, θ_{bf}, and μ_{bf} are in units of millimeters (mm) of storage. 114

List of Abbreviations and Symbols

A	Contributing area or cross-sectional area (context dependent)
Avg	Average
a	Recession constant of the Eckhardt (2015) digital filter
atm P	Atmospheric pressure
BES	Baltimore Ecosystem Study
BF	Baseflow discharge
BFI_{max}	Maximum baseflow index parameter of the Eckhardt (2015) digital filter
BMP	Best management practice
bf	Specific baseflow discharge
C	Convergent hillslope or Celsius (context dependent)
CDF	Cumulative distribution function
CV	Control volume
D	Divergent hillslope
DEM	Digital elevation model
d	Day

dq/dt	Recession rate of specific discharge
Est	Estimated
ET	Actual evapotranspiration
f	Frequency
GNSS	Global Navigation Satellite System
g(q)	Sensitivity function
H	Hydraulic
Hill	Hillslope
hr	Hour
I	Indirect or precipitation intensity (context dependent)
JHU	Johns Hopkins University
JHU01	Johns Hopkins University 01 weather station
KGE	Kling-Gupta Efficiency
Km	Kilometers
k	Scaling factor used to estimate actual evapotranspiration from potential evapotranspiration
kPa	Kilopascal
L	Length
LAI	Leaf area index
LHL	Landscape Hydrology Lab
LTER	Long Term Ecological Research
LW	Longwave radiation
log	Logarithmic

mASL	Meters above sea level
mm	Millimeters
m	Slope or meters (context dependent)
max	Maximum
min	Minimum
NA	Not available
NLDAS	North American Land Data Assimilation System
NOAA NCEI	National Ocean and Atmospheric Administration Nation Centers for Environmental Information
n	Manning’s roughness coefficient
P	Precipitation
$\overleftarrow{P}(T,t)$	Cumulative backward transit time distribution
PDF	Probability density function
PET	Potential evapotranspiration
p	Significance level
Q	Discharge
QF	Quickflow discharge
q	Specific discharge
qf	Quickflow specific discharge
R	Riparian, wetted perimeter, ratio, or recharge to hydraulic storage (context dependent)
R^2	Coefficient of determination
RH	Relative humidity

rf	Return flow
rip	Riparian
rSAS	rank StorAge Selection
S	Soil, stage, or storage (context dependent)
S_f	Friction slope
S_{ref}	Reference storage used to calculate relative catchment storage
S_T	Age-rank storage
S_{Tmax}	Maximum age-rank storage parameter
SW	Shortwave radiation
s	Seconds
T	Age or temperature (context dependent)
TTD	Transit time distribution
TV	Time-variable
t	Time
USGS	United States Geological Survey
V	Wind speed
VSMOW	Vienna standard mean ocean water
VWC	Volumetric water content
W	Contributing width, week, or Watts (context dependent)
WL	Water level
WY	Water year

α	Ratio of the hydraulic area to the total catchment area or shape parameter of the gamma distribution (context dependent)
ΔS	Relative storage
$\delta^{18}O$	Delta-oxygen-18 isotope ratio
θ	Scale parameter of the gamma distribution
μ	Mean of the gamma distribution
τ	Dummy integration variable
$\Omega(S_T, t)$	CDF of the rank StorAge Selection function
‰	Per mil

Chapter 1

Introduction

1.1 Motivation

1.1.1 Runoff Generation Mechanisms

Runoff generation mechanisms describe the processes and flow pathways that produce the increase in stream discharge often observed during and after precipitation events. An understanding of how a catchment responds to precipitation is essential for predicting both the quantity and composition of streamflow and is especially important in catchments where water quality is a primary concern. Since the 1930's, a variety of mechanisms have been proposed that describe runoff generation, including infiltration excess overland flow (Horton, 1933), saturation excess overland flow (Dunne & Black, 1970b, 1970a), subsurface storm flow (Hewlett & Hibbert, 1963; Hursh & Brater, 1941; McDonnell, 1990; Mosley, 1979), and groundwater ridging (Abdul & Gillham, 1984; Ragan, 1968; Sklash & Farvolden, 1979). In recent decades, the study of runoff generation mechanisms has been aided by the use of environmental tracers such as the stable isotopes of oxygen and hydrogen, which provide a way of “fingerprinting” the various sources of water that compose discharge. This has led to the discovery that storm event discharge often contains significant quantities of pre-event water (Pinder & Jones, 1969).

The production of runoff during a storm event is unavoidably linked to the structure of the landscape, with all runoff generation mechanisms relating some property of a landscape to its ability to generate storm flow. For example, in the process of infiltration excess overland flow as described by Horton (1933), runoff is generated when the precipitation intensity exceeds the infiltration rate of the soil. This infiltration rate depends on the soil type, as well as the history of land use. Some studies have highlighted the importance of landscape structure in producing runoff, with the connectivity between hillslopes, riparian areas, and stream channels have been identified as a major control on the storm flow response of discharge (Jencso et al., 2009; Jencso & McGlynn, 2011; McGlynn et al., 2004).

Most of this past work has focused on steep catchments with thin soils overlying impermeable bedrock and narrow valley bottoms with streams tightly coupled to the hillslopes (Jencso et al., 2009) or on recently glaciated catchments with similarly thin soils overlying scoured bedrock (Dunne & Black, 1970a). Whereas, in much of the world, including the Piedmont Province of the eastern United States, the landscape is of low to moderate relief and well-developed soil overlies a thick layer of chemically weathered bedrock known as saprolite.

1.1.2 Piedmont Physiographic Province

The Piedmont Physiographic Province is a geographic area in the eastern United States between the Atlantic Coastal Plain and the Appalachian Mountains, extending from Alabama in the south to New Jersey in the north. This physiographic province is underlain by hard, crystalline, igneous and metamorphic bedrock of the ancient Appalachian Mountain system and is characterized by gently rolling foothills and deeply weathered bedrock (Dowd et al., 1993). In the Piedmont, the soil mantles a highly permeable 10 to 20 meter thick layer of chemically weathered bedrock known as saprolite (Pavich, 1989). This saprolite maintains the large-scale structure and volume of the bedrock but has about one-third of the mass (Pavich, 1989), resulting in a total porosity increase from virtually zero in bedrock to 40 to 50% in saprolite (Dowd et al., 1993). The average relief in the Piedmont is approximately 50 meters (Markewich et al., 1990), with rounded hillslopes giving way to moderately steep side slopes that intersect gently sloping valley bottoms (Richardson, 1980).

Previous research has highlighted the potential of saprolite to store large quantities of water, both within the Piedmont and in other deeply weathered regions. Holbrook et al. (2014) estimated there to be as much as 5 m^3/m^2 of storage at one site in the southern Sierra Mountains of California. Within the Chesapeake Bay Watershed, Bachman et al. (1998) attributed a comparatively high baseflow index observed within Piedmont Catchments to the presence of saprolite. In the Pond Branch Catchment of the Maryland Piedmont, Cleaves et al. (1970) estimated that water stored within the saprolite could sustain baseflow discharge for 25 to 349 days and observed a period of 187 days during which baseflow was maintained in the absence of significant precipitation. Despite the storage potential within saprolite, few if any studies have linked direct observations of discharge to its storage or studied its influence on the emergent catchment scale water balance.

1.1.3 A Prototypical Piedmont Catchment

The Pond Branch Catchment is analyzed in this dissertation to test hypotheses relating Piedmont landscape structure to storage and streamflow. Pond Branch is a 37-hectare, forested, second-order catchment located 12 kilometers north of the northern boundary of Baltimore City, Maryland, within the Piedmont Physiographic Province. This catchment has been studied since the 1960's (e.g. Cleaves et al. (1970)) and has served as the forested "reference" site for the Baltimore Ecosystem Study Long Term Ecological Research Network since 1998 (Groffman et al., 2004). The unglaciated catchment is underlain by medium- to coarse-grained micaceous schist (Otton et al., 1975), which has weathered in place to form up to 25 meters of saprolite (Cleaves et al., 1970). Seismic refraction tomography conducted in the spring of 2014 indicates that the saprolite is thickest under the hillslopes and thins toward the valley margin (St Clair et al., 2015), with bedrock outcropping within the stream channel near the catchment outlet. Soils are generally one to two meters thick and grade from channery loam on the ridges to silt loam in the valley bottom (Cleaves et al., 1970). Moderately steep side slopes converge on the flat valley bottom forming a well-defined riparian area where water tables are generally within a meter of the surface and multiple channels anastomose. Land cover is 97% deciduous forest and 3% herbaceous vegetation (Cleaves et al., 1970).

Given this dominance of forest cover, it was surprising to discover that there are still two distinct time scales of responses in the discharge measured at the catchment outlet, namely a rapidly responding and recessing quickflow component and a slowly changing baseflow component. Numerous studies have documented the ability of forests to attenuate streamflow variability, including Roa-García et al. (2011), who compared the quickflow response of adjacent forest and grassland catchments, finding that forest catchments not only attenuate the quickflow peak but also reduce the overall amount of quickflow. Roa-García et al. (2011) attributed the attenuation of forest catchments, in part, to the higher total porosity of the forest soils. In Pond Branch, the contrast in the temporal frequency of the quickflow and baseflow in a catchment dominated by forest cover and the potential influence of landscape structure on these two components provide further motivation for the hypotheses tested.

1.2 Dissertation Outline

In this work, field data from the Pond Branch Catchment are combined with modeling to test hypotheses relating Piedmont landscape structure to storage and streamflow generation. Data include spring and catchment discharge, hydrometeorological measurements, riparian well water levels, soil moisture, and three years of high frequency precipitation and streamflow stable water isotope data. These data are used along with recession analysis, water balance models, and the StorAge Selection transport modeling framework. In Chapter 2, the influence of Pond Branch Catchment storage structure on the emergent catchment scale storage and discharge is explored by calculating storage for individual landscape units, hydraulically coupled and uncoupled portions of the landscape, and for the catchment as a whole. During the three-year study period, catchment scale storage transitioned from near normal to a decadal drought, providing further insights into the way in which landscape structure, and the resulting structure of storage, dampens hydroclimatic variability. In Chapter 3, Pond Branch streamflow is decomposed into baseflow and quickflow components, and the generation of each component is explored using discharge and water level measurements. Specifically, the hypotheses that (1) the quantity of baseflow can be accounted for by water released from hillslope storage and (2) the quantity of quickflow can be accounted for by runoff generated from direct precipitation on to the riparian area are tested. In Chapter 4, stable water isotope data are used to provide information on the composition of quickflow, which is then employed along with transport modeling to further explore the quickflow generation mechanism or mechanisms identified in Chapter 3. Finally, in Chapter 5, the results of each of the previous chapters are summarized before discussing the limitations and broader impacts of this dissertation as well as potential future research.

Chapter 2

The Structure of Storage within a Deeply Weathered Piedmont Catchment

2.1 Introduction

The structure of a landscape, i.e. the topography, depth/type of soil, the presence of shallow bedrock or a thick layer of saprolite, and the ability of different parts of the landscape to store and release water at different time scales controls the partitioning of precipitation between different terms of a catchment's water balance and its emergent response to hydroclimatic forcing. For example, within the Chesapeake Bay Watershed, Bachman et al., (1998) compared streamflow and water quality data for watersheds across physiographic provinces and lithologies, each with their own landscape structure, and found that compared to the physiographic provinces underlain by siliciclastic rocks, the crystalline Piedmont had a higher proportion of its total discharge as baseflow.

The Piedmont is a physiographic province extending from just north of New York City southward along the eastern United States into Alabama and is bounded by the Atlantic Coastal Plain to the east and the Blue Ridge and Appalachian Mountains to the west. This geographic area is underlain by hard, crystalline, igneous and metamorphic rocks of the ancient Appalachian Mountain system (Dowd et al., 1993), which have been sheared, fractured, and folded (Trapp Jr. & Horn, 1997). From Maryland to Alabama, the metamorphic rocks of the Piedmont have weathered in place to form a 0.5 – 2.0 meter (m) thick clay-rich soil overlying 10 - 20 m of saprolite (Markewich et al., 1990; Pavich, 1989). This saprolite maintains the large-scale structure and volume of its parent rock but has about one-third of the mass (Pavich, 1989), resulting in a total porosity increase from virtually zero in bedrock to 40 to 50% in saprolite (Dowd et al., 1993). Saprolite is generally thickest under the convex uplands of the Piedmont and thins towards the valley bottom where bedrock may outcrop (Pavich, 1989; Richardson, 1980). The rounded uplands give way to steep valley side slopes, forming v-shaped stream valleys with narrow (Pavich, 1989), but sometimes quite level valley floors (Richardson, 1980). In Maryland, the Piedmont encompasses 25% of the land surface area and contains 4.6% of the state's wetlands, of which non-tidal wetlands in deciduous forests dominate (Tiner & Burke, 1995).

Bachman et al. (1998) attributed the higher proportion of baseflow in the Piedmont to its thick layer of saprolite, which they suggested may act as an unconsolidated-rock aquifer. Similarly, Cleaves et al. (1970) estimated that water stored within the saprolite of a headwater Piedmont catchment, Pond Branch, could sustain baseflow discharge for 25 to 349 days and observed a period of 187 days during which baseflow was maintained in the absence of significant precipitation. However, a thick saprolite layer is not unique to the Piedmont and is common both within the continental United States and in tropical to subtropical latitudes around the world (Salama et al., 2017; Wald et al., 2012). In fact, saprolite has been identified as a vital reservoir of water during the dry season in arid and semi-arid mountainous terrain (Riebe et al., 2016), including in the southern Sierra Mountains of California where the storage capacity was estimated to be as much as 5 m^3/m^2 at one site (Holbrook et al., 2014).

Additional landscape units such as the soil, unsaturated zone, or wetlands may also impart their own influence on the emergent storage and discharge of a catchment. In their analysis of the Pond Branch Catchment, Duncan et al. (2015) suggested that the wetlands found in the riparian area of the valley bottom likely serve as a large storage reservoir of water under baseflow conditions. At the Maimai research catchments in New Zealand, McGlynn & McDonnell (2003) found that baseflow discharge was in fact dominated by runoff from the riparian area. In contrast, in the Susannah Brook Catchment of Western Australia, Ocampo et al. (2006) found that the riparian zone did not store significant quantities of water but was instead important for controlling the storm response. The effect of the riparian area, as well as other landscape units, i.e. the saprolite and soil, on controlling the emergent storage and discharge at the catchment scale varies between studies as a result of the structure of the units themselves as well as the connectivity between the units.

McGlynn & McDonnell (2003) advocated for breaking apart a catchment into individual landscape units in order to understand which parts of the landscape contribute to different parts of the catchment hydrograph. They applied this approach at Maimai where soils are shallow and overlie an assumed impermeable bedrock layer. In fact, most catchment scale studies relating landscape structure to hydrologic response have focused on steep watersheds with thin soils overlying impermeable bedrock (Anderson & Burt, 1978; Dunne & Black, 1970b; McGlynn & McDonnell, 2003; Sidle et al., 2000). In contrast, little attention has been paid in complicated hydrologic settings such as the Piedmont where the deeply weathered zone below the first 1-2 meters of the Earth's surface contains flowpaths and void space for water storage (Dowd et al., 1993; Riebe et al., 2016). In the southern Piedmont at the Panola Mountain Research Watershed, Peters & Aulenbach (2011) estimated both soil and catchment scale storage; however, the geology at Panola is not representative of the rest of the Piedmont, with most of the catchment underlain by less than one meter of saprolite. In other Piedmont studies, deep groundwater storage has been estimated (LeGrand, 1967; Richardson, 1980) or the potential for large quantities of stored water within catchments has been implied from estimates of baseflow or groundwater age (Bachman et al., 1998; Lindsey et al., 2003). However, storage within the saprolite or riparian area were not quantified in those studies. In addition, the role of these individual landscape units within deeply weathered landscapes such as the Piedmont in controlling the emergent storage and discharge behavior at the catchment scale has not been explored.

In this study, we use data from the Pond Branch Catchment to calculate storage for individual landscape units, for hydraulically coupled and uncoupled portions of the landscape (Riegger & Tourian, 2014), and for the catchment as a whole over a three-year period. The catchment water balance is used to estimate catchment scale storage; riparian wells and soil moisture data are used to estimate storage for riparian and soil landscape units, respectively; and recession analysis is used to estimate the hydraulically coupled and uncoupled portions of the catchment scale storage, referred to as the hydraulic and indirect storage, respectively.

During the three-year study period, catchment scale storage and baseflow discharge transitioned from near normal to a decadal drought, with below average discharge at the outlet of Pond Branch for the last 13-months of the study period (bottom pane of Figure 2.1). The onset of the below average discharge came a month after the beginning of a seven-month period in which there was below average precipitation (top pane of Figure 2.1). The propagation of this drought through the individually calculated catchment stores was studied in order to gain insights into the role of landscape structure in controlling the storage and release of water, as well as its influence in dampening or magnifying hydroclimatic variability in deeply weathered landscapes.

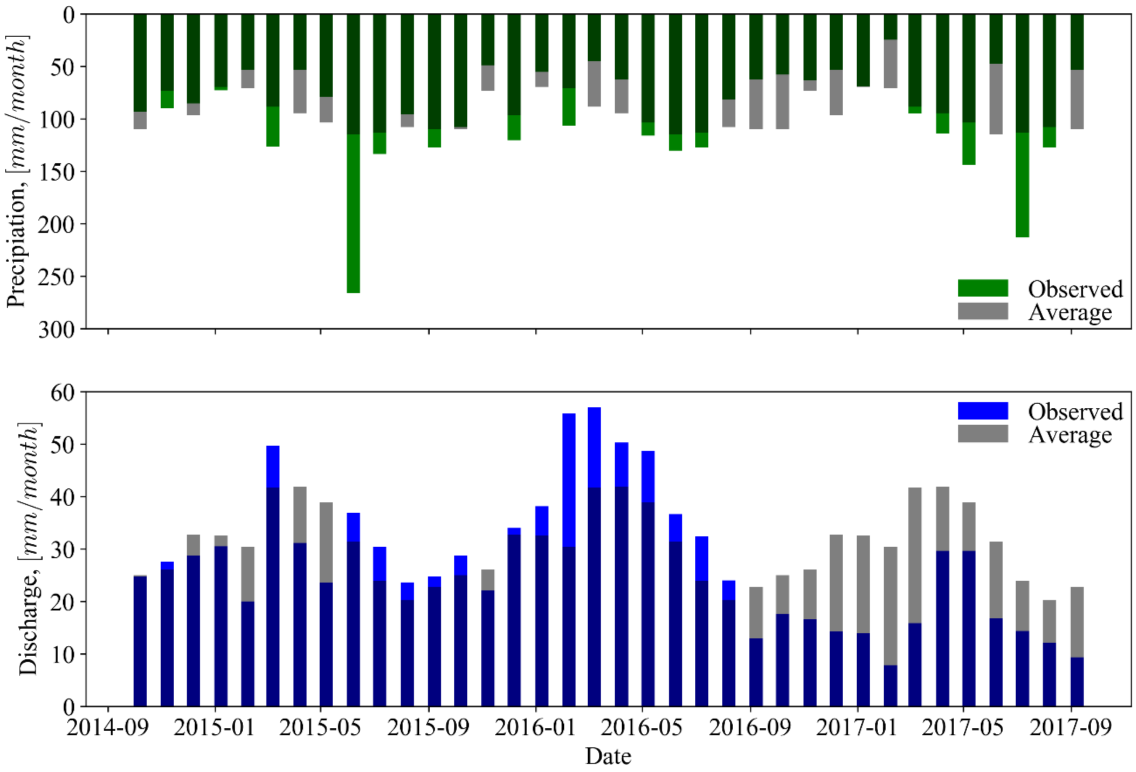

Figure 2.1: Observed monthly precipitation (P) and specific discharge (q) for the Pond Branch Catchment compared to the averages for each month over the 2000 to 2017 water years. The gray indicates months when

precipitation or specific discharge is less than average, while the lighter green or lighter blue indicates months when precipitation or discharge, respectively, is greater than average. From August 2016 through February 2017, the monthly precipitation is less than the monthly average, while specific discharge is below average for the entire 2017 water year. Specific discharge remains lower than average in the summer of 2017 despite the higher than average precipitation in the spring and summer of 2017.

2.2 Study Site

Pond Branch is a 37-hectare catchment located 12 kilometers (km) north of the northern boundary of Baltimore City, Maryland, within the Piedmont Physiographic Province of the eastern United States (Figure 2.2). The second-order catchment is located entirely within a county park and is a subcatchment of the 379 ha, fourth-order Baisman Run Catchment (Duncan et al., 2015; Wolman, 1987). Baisman Run drains to the east via Beaverdam Run into Loch Raven Reservoir, one of Baltimore City's three drinking water reservoirs, before entering the Gunpowder Falls which flows directly into the Chesapeake Bay, the largest estuary in the United States (Bachman et al., 1998). Pond Branch is almost entirely forested with only 3% classified as other cover (herbaceous vegetation) by Cleaves et al. (1970). A buried gas pipeline bisects the midsection of the catchment nearly orthogonal to the mainstem of the stream channel. The upper third (34%) of the Baisman Run Catchment is low-density residential while the other 66% is dominated by second growth, deciduous forest (Groffman et al., 2004). Both Baisman Run and Pond Branch have been the focus of numerous studies since the 1960's (e.g., (Cleaves et al., 1970; Wolman, 1987)), with Pond Branch serving as a forested "reference" site for the Baltimore Ecosystem Study (BES) Long Term Ecological Research Network (LTER) since 1998 (Groffman et al., 2004).

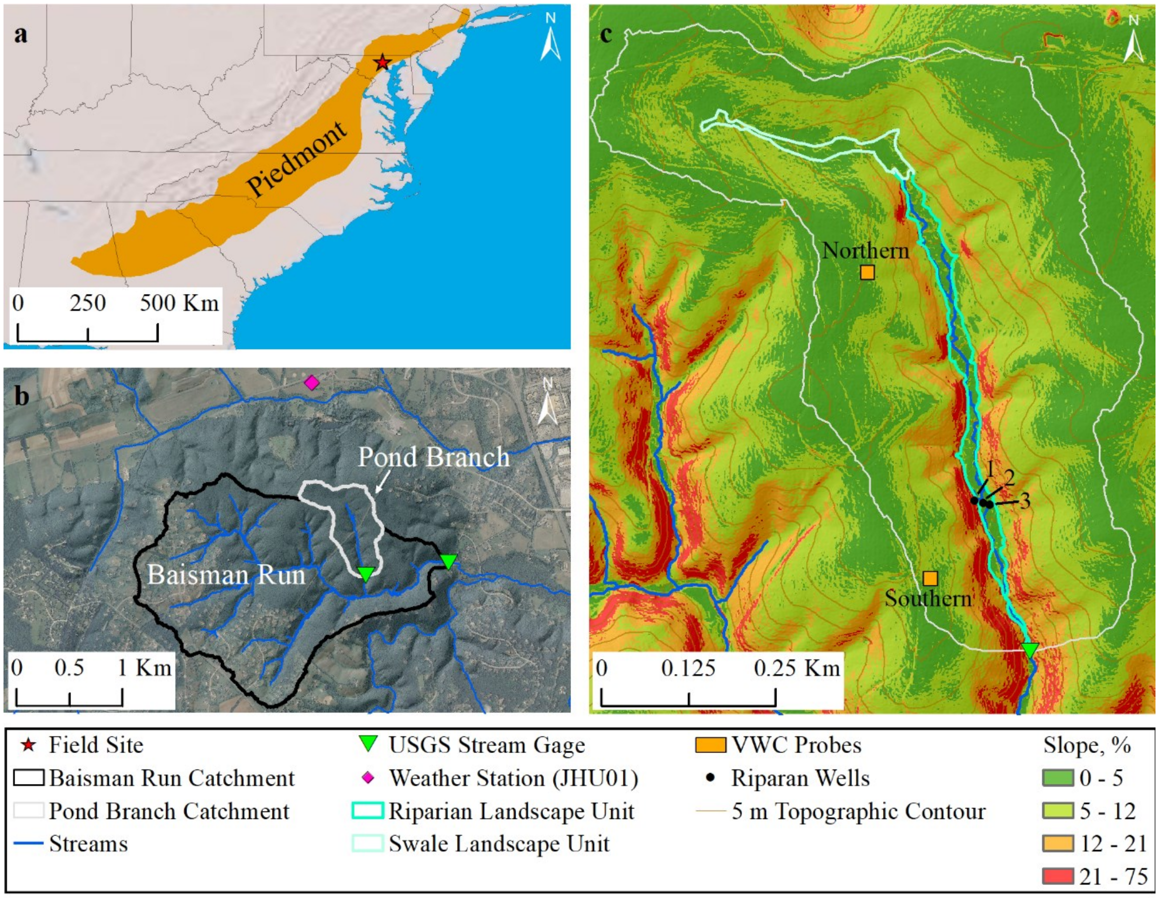
a
Piedmont
0 250 500 Km
b
Pond Branch
Baisman Run
0 0.5 1 Km
c
Northern
Southern
1
2
3
0 0.125 0.25 Km
N
Field Site
Baisman Run Catchment
Pond Branch Catchment
Streams
USGS Stream Gage
Weather Station (JHU01)
Riparian Landscape Unit
Swale Landscape Unit
VWC Probes
Riparan Wells
5 m Topographic Contour
Slope, %
0 - 5
5 - 12
12 - 21
21 - 75

Figure 2.2: (a) Location of the study site (39º 29' 03" N, 76º 41' 17" W) in the eastern United States, with the Piedmont Physiographic Province shaded in orange. (b) Overview map of the study site showing the Pond Branch and Baisman Run Catchment boundaries relative to the locations of two USGS Stream Gages and the JHU01 Weather Station. The orthoimage illustrates the dominance of forest cover in the Pond Branch Catchment as well as the presence of suburban areas to the in southwest. (c) Map of the Pond Branch Catchment with instrumentation including the USGS Stream Gage at the outlet, riparian wells, and plots containing volumetric water content (VWC) probes. The numbers "1," "2," and "3" correspond to the riparian well numbers referenced in Section 2.3.1. The plots containing VWC probes are labeled according to their relative cardinal direction within the catchment, i.e. "Northern" and "Southern." The outline of the riparian and swale landscape units are shown, with the remainder of the catchment area defined as the hillslope landscape unit.

As is common throughout the Piedmont, Baisman Run and Pond Branch are underlain by crystalline bedrock. This bedrock is composed of uniform, medium- to coarse-grained biotite-plagioclase-muscovite-quartz schist with lesser amounts of fine- to medium-grained, slabby weathering schist near the Baisman Run outlet (Otton et al., 1975). Within these unglaciated catchments, this schist has weathered in place to form up to ~ 25 meters (m) of saprolite (Cleaves et al., 1970). Seismic refraction surveys conducted in the Spring of 2014 within Pond Branch indicate that the saprolite is thickest under the uplands and thins toward the valley bottom (St Clair et al., 2015), with bedrock outcropping in the valley bottom near the catchment outlet. This saprolite profile has been documented elsewhere within deeply weathered landscapes, including at the Calhoun Critical Zone Observatory in South Carolina (St Clair et al., 2015) and by Pavich (1989) in describing weathering across the Piedmont. Overlying the saprolite is 1 to 2 m of soil which grades from channery loam on the ridgetops, to loam on the hillsides, and to silt clay loam and silt loam in the valley bottom (Duncan et al., 2015; NRCS Soil Survey).

Elevations range from 132 to 194 m above sea level within the Pond Branch Catchment, with approximately 20 to 25 m of local relief from valley bottom to watershed divide along a transect perpendicular to the main stream channel. The 62 meters of relief found in Pond Branch is similar to the mean of 50 m for the Piedmont reported in Markewich et al. (1990). Slopes range from 0 to 45 degrees, have a mean of 7 degrees, are steepest at the toe of the hillsides, and are near zero both on the ridgetops and in the valley bottom. The distinct break in slope between the hillside and the valley bottom is partially used to demarcate two landscape units discussed within this analysis. Here we define the riparian landscape unit as the flat valley bottom area between the break-in-slope of the surrounding hillsides and down-valley of a 1 to 2-meter-deep head cut where channel initiation occurs at the upper end of the catchment (Figure 2.3a). Within the riparian landscape unit is the Pond Branch stream channel, which is fed by multiple side channels that drain numerous seeps and springs located at the toe of the hillside. As is common in the Piedmont, wetlands can be found throughout this riparian unit where water tables are generally within a meter of the land surface. Up-valley of the aforementioned head cut is a broad, flat, zero-order valley or swale which is distinguished from the surrounding hillside by its low slope and high upslope contributing area. The remainder of the catchment area is defined as the hillslope landscape unit which is underlain by a thick layer of saprolite (Figure 2.3b). The riparian, swale, and hillslopes units make up 3.7%, 1.5%, and 94.8% of the catchment area, respectively.

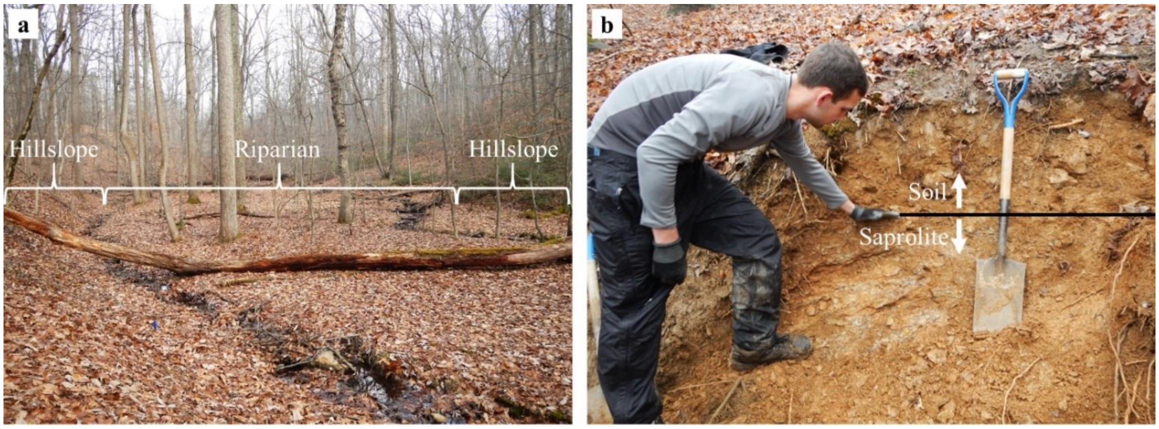

Figure 2.3: (a) Image from the Pond Branch Catchment with annotations showing the divisions between the riparian and hillslope landscape units. Two branches of the stream channel can also be seen in this image, with the main stem on the right. (b) Image of a soil pit dug within the hillslope landscape unit which shows a portion of the subsurface structure including the soil, soil-saprolite boundary, and top section of the saprolite.

Pond Branch is at the northern limit of the humid subtropical climate zone which extends southward encompassing all of the Piedmont into Alabama. The mean annual temperature is 13 ºC and temperatures vary greatly between seasons, with hot humid summers when maximum daily temperatures exceed 30 ºC and cold winters with minimum daily temperatures below – 4 ºC (1981-2010 climate normals at Baltimore Washington International Airport) (NOAA NCEI). Precipitation is distributed relatively uniformly throughout the year, varying between a minimum of 74 millimeters (mm) in February to a maximum of 103 mm in July, resulting in a mean annual precipitation of 1064 mm (NOAA NCEI). Storms in late fall, winter, and early spring are typically long duration, low intensity events often associated with large low-pressure systems, while storms in late spring, summer, and early fall are short duration, high intensity events often associated with afternoon thunderstorms. Snowfall can occur several times per year between November and March but significant snow packs are rare and most snow melts within a few days of falling. Average streamflow is generally highest in late winter and early spring before it begins to decline at the onset of the growing season, reaching a minimum in summer or early fall. Much of the Pond Branch stream network is perennial except during extreme droughts, such as occurred in 2002 when surface flows ceased entirely for a period of a few months.

2.3 Methods

2.3.1 Instrumentation & Data Collection

In 1998, the BES LTER began reactivating and installing instrumentation within the Pond Branch and Baisman Run Catchments. That infrastructure and corresponding datasets served as a foundation for the instrumentation plan that was designed and executed as a part of this study. See Figure 2.2 for the location of all instrumentation described below.

Records of 15-minute stream stage and discharge were obtained from United States Geological Survey (USGS) Stream Gages at the outlets of Pond Branch and Baisman Run. Discharge at the outlet of Pond Branch was measured using a triple v-notch weir and float device beginning in April 1998 (USGS Site Number 01583570). In August 2013, the USGS replaced the float with an acoustic sensor mounted above the weir pool in order to increase the resolution of the stage and potentially observe suspected diurnal variations in water level. Discharge at the outlet of Baisman Run was measured using a compound weir and bubbler system beginning in November 1999 (USGS Site Number 01583580). The weir at Pond Branch was frequently affected by leaf build up in the fall and freezing in the winter which caused a backwater effect that resulted in unreliable discharge estimates. As a result, discharge data for Pond Branch were unavailable for approximately 8% of the time-series between October 1, 2000 and September 30, 2017. In contrast, the discharge time-series for Baisman Run was less affected by leaves and ice and so was used to fill in the gaps in the Pond Branch record. A quadratic function was fit to the relationship between Pond Branch and Baisman Run discharge (Nash-Sutcliffe Efficiency=0.73) and used to estimate missing observations of Pond Branch discharge. Remaining gaps in the Pond Branch record (3.3% of the total record) were filled by linear interpolation.

Riparian water levels were observed every 15-minutes between September 2014 and June 2017 in three wells located along a transect bisecting the main channel of Pond Branch. The wells are aligned approximately west to east, one-third of the way up the channel from the outlet, with the western most well (Well #1) at the toe of the hillslope, the middle well (Well #2) located just west of the channel, and the eastern most well (Well #3) located on the east side of the channel (Figure 2.2c). The wells were installed by the BES to a depth of 1 to 2 meters within the riparian area between 2001 and 2009 (Duncan et al., 2013) and were outfitted for this study with non-vented pressure transducers (Solinst Levelogger) in September 2014. In one of the wells, another pressure transducer (Solinst

Barologger) was suspended within the air column to measure atmospheric pressure changes. Manual water level measurements were made with a water level meter (Heron dipper-T) before and after offloading the pressure transducers. The 15-minute time series of water levels for each well was calculated by first taking the rolling one-hour average of the pressure transducer data to remove noise and then subtracting the atmospheric pressure from the submerged pressure transducer data to get the depth of the water above the submerged pressure transducer. These depths were then converted into the depth of water below the land surface and subtracted from the manual water level measurements to calculate offsets for before and after the pressure transducers were offloaded. A time series of offsets was then constructed and used to bring the water levels calculated from the pressure transducer into agreement with the manual observations.

Soil moisture in two hillslope plots was logged hourly beginning in the summer of 2011 by the BES. The two plots were located within the Pond Branch Catchment approximately 450 m apart directly north-south on the western ridgetop where slopes are less than 10%. Each plot contained five Decagon 5TM probes buried horizontally at 10 cm and arranged with a single probe in the center and the remaining four probes 5 m away from the center in the four cardinal directions (Groffman and Dillon, 2010). The volumetric water content measured by each Decagon 5TM probe was stored on a central datalogger (Decagon Em50). The average hourly soil moisture for the hillslope was calculated by first taking the average of the volumetric water content measured by the five probes in each plot and then taking the average of the two plots. The average soil moisture for the hillslope could have also been calculated by taking the average of all ten probes, however, by taking the average of the five probes first, the variability in soil moisture between plots could be compared. Soil moisture data were available 97.2% of the time between October 1, 2014 and September 30, 2017 with any remaining gaps in the hillslope average filled by taking a linear interpolation.

Meteorological measurements were made every 5 minutes beginning in June 2014 by a weather station (JHU01) located approximately 1-kilometer (km) north of the Pond Branch Catchment at an elevation of 114 m above sea level. JHU01 was installed far away from any tall objects within a field where the grass was maintained at a consistent height. The station was custom built using components from Campbell Scientific and was designed to measure atmospheric pressure, temperature, humidity, incoming shortwave radiation, wind speed and direction, and precipitation amount. A tipping bucket rain gage (Texas Electronics TR-525USW) was installed with an alter-type wind screen (Novalynx 260-953) to improve the catch and each winter a snowfall adapter (Campbell Scientific CS705) with an antifreeze reservoir was secured to the gage in order to quantify the liquid water equivalent of frozen precipitation. Wind speed and direction were measured with an anemometer (R.M. Young 05103) mounted 2 m above the grass surface, and incoming shortwave radiation and barometric pressure were measured with a pyranometer (Hukseflux LP02) and a barometer (Setra 278), respectively. The temperature and relative humidity were determined using a single sensor (Rotronic HC2-S3) which began malfunctioning in November 2015 and continued to do so until January 2017 when it was replaced. As a result, the relative humidity and temperature recorded by a second weather station (CW1032) was used in the analyses that follow. CW1032 is a Davis Vantage Pro Weather Station located approximately 7 km southeast of the Pond Branch outlet in a residential area and is operated by a homeowner within the Citizen Weather Observer

Program (CWOP). Data from JHU01 were stored on a datalogger (Campbell Scientific CR1000) and downloaded via a cellular gateway (AirLink Raven XT) every hour, while data from CW1032 were publicly available for download from a CWOP affiliated website.

2.3.2 Catchment Storage

Storage for the Pond Branch Catchment was calculated over a three-year period using the following mass balance equation:

$$\Delta S(t) = S(t) - S(0) - S_{ref} = \int_0^t (P(t) - q(t) - ET(t))\ d\tau - S_{ref} \tag{2.1}$$

where $S(t)$ [L] is the total catchment storage at time t [T], $\Delta S(t)$ is storage relative to a reference state S_{ref}, $P(t)$ [L/T] is the total precipitation, $q(t)$ [L/T] is the specific discharge, $ET(t)$ [L/T] is the actual evapotranspiration (including evaporated interception water), and τ is a dummy integration variable. Equation 2.1 assumes that the transfer of water into or out of the catchment by other pathways is negligible. Markewich (1990) suggested that groundwater in the Piedmont moves along joints, foliation, bedding planes, and faults, in which case inter-basin flow would likely be significant. However, more recently, Vepraskas (2005) showed that there was virtually no preferential flow along veins and fractures within mica-schist saprolite, providing some support for the assumption that inter-basin transfer within the mica-schist saprolite of the Pond Branch Catchment may be negligible. $\Delta S(t)$ represents the dynamic component of the total catchment storage, which can be defined as the change in storage over a given period of time relative to a reference state S_{ref}, whereas the total catchment storage is difficult to quantify given ill-defined boundary conditions that define the extent of the storage volume, or initial conditions representing the volume at time $t = 0$ (Sayama et al., 2011).

In order to solve Equation 2.1 and estimate daily catchment scale dynamic storage from October 1, 2014 to September 30, 2017, time-series of $P(t)$, $q(t)$, and $ET(t)$ were needed. The total precipitation for each day, $P(t)$, was calculated by taking the sum of the 5-minute precipitation data from the JHU01 weather station. It was assumed that these data represented the spatial average of precipitation over the catchment which at no point is more than 2 km's from the rain gage, even though for some storms, especially thunderstorms, precipitation amounts may have varied across the catchment. In addition, the use of the snowfall adapter meant that snow was converted to its liquid water equivalent at the time it fell. This snow is typically stored as snowpack on the land surface for only a week or two, during which time it contributes to the catchment storage calculated here. The specific discharge for each day, $q(t)$, was calculated by taking the sum of the gap-filled 15-minute time-series of discharge for Pond Branch and then dividing by the catchment area.

The actual evapotranspiration for each day, $ET(t)$, was calculated by multiplying the potential evapotranspiration ($PET(t)$) estimated using the Penman-Monteith Equation by a scaling factor, so $ET(t) = k\ PET(t)$ (Monteith, 1965). The Penman-Monteith Equation was solved at a daily time-step using time-series of forcing data and a set of assumed constants. The forcing data included temperature and relative humidity from the CW1032 weather station; incoming shortwave radiation, wind speed, and local atmospheric pressure from the JHU01 station; area-averaged hourly incoming longwave radiation from the North American Land Data Assimilation System (NLDAS) primary forcing data set (NLDAS_FORA0125_H); and hourly leaf area index from the Noah land-surface model for NLDAS ((NLDAS_NOAH0125_H) (Figure 2.4). Constants for a broadleaf forest including maximum leaf conductance, height of the principal land-cover, and shelter factor were selected from Dingman (2008), while average values of the albedo and emissivity for a deciduous forest were used from Brutsaert (2005).

In order to close the water balance and estimate the appropriate scaling factor for $ET(t)$, it is common to assume that the change in catchment scale dynamic storage, $\Delta S(t)$, is equal to zero given a sufficiently long water balance (Dingman, 2008). However, in a catchment experiencing a drought or with considerable year-to-year storage variability this assumption may not hold. In order to test whether storage was similar at the beginning and end of the 2015 to 2017 water-year the baseflow was compared, under the assumption that baseflow may be a proxy for catchment storage. Baseflow at the beginning of October 2014 was approximately four times higher than at the end of September 2017, suggesting that the assumption that the change in storage was zero over the three-year water balance was not valid. In contrast, baseflow was nearly identical at the beginning and the end of the 2015 water-year's water balance. Thus, it was assumed that $\Delta S(t)$ was equal to zero at the start and end of this first year of the three-year water balance. Total ET over 2015 was calculated by solving Equation 2.1 with $\Delta S(t) = 0$, and then a scale factor k for the $PET(t)$ was determined by taking the ratio of this total to the sum of the $PET(t)$ from the Penman-Monteith Equation for the 2015 water-year. The $ET(t)$ was then calculated at the daily time-step for the three-year water balance by multiplying the daily $PET(t)$ by this scale factor. Finally, the time series of $ET(t)$, $P(t)$, and $q(t)$ were used to solve Equation 2.1 and calculate the daily catchment scale dynamic storage from October 1, 2014 to September 30, 2017.

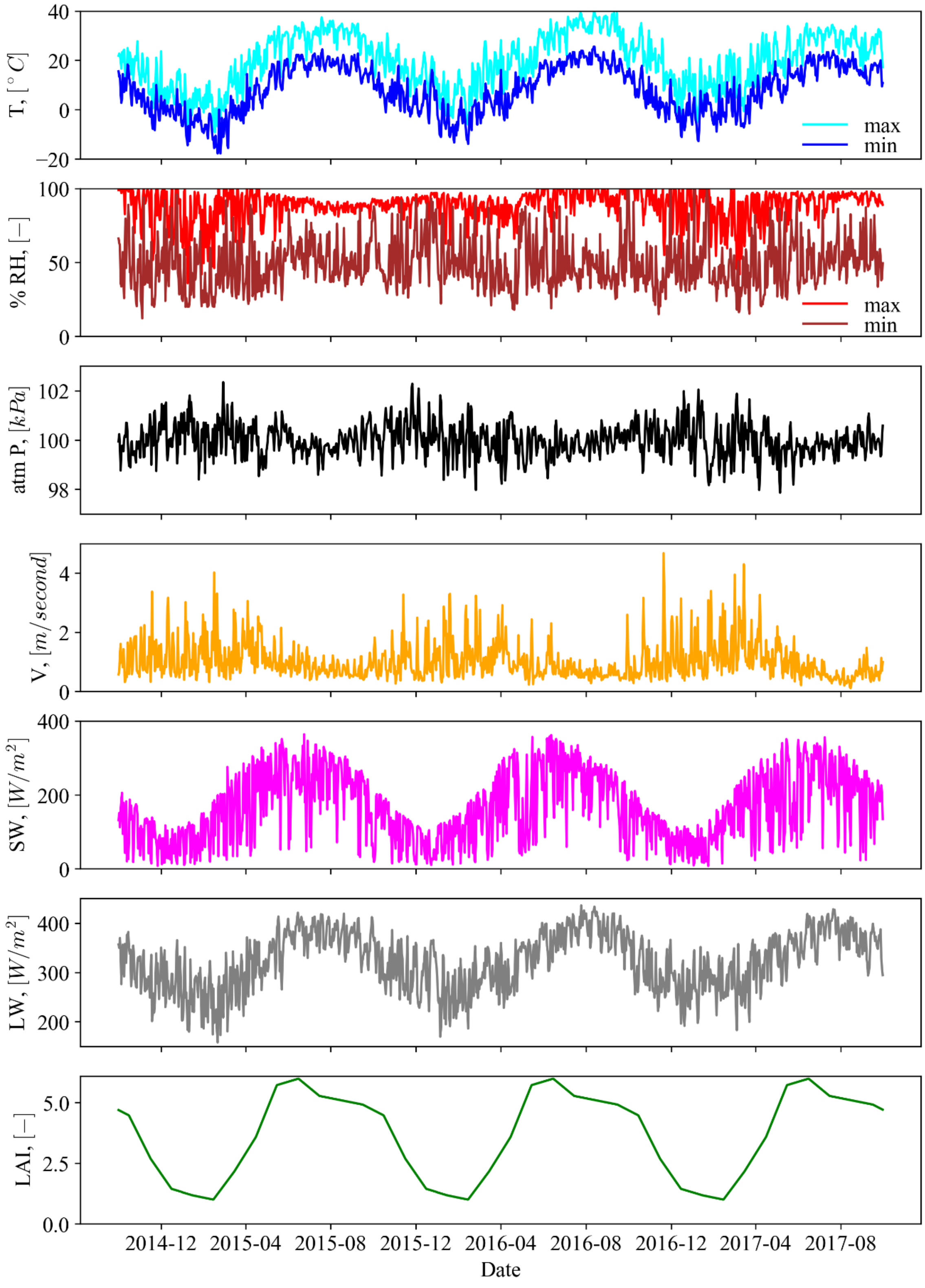

Figure 2.4: Daily forcing data for estimating potential evapotranspiration using the Penman-Monteith Equation, including maximum and minimum temperature (T) and relative humidity (% RH), local

atmospheric pressure (atm P), wind speed (V), shortwave radiation (SW), long wave radiation (LW), and leaf area index (LAI).

2.3.3 Riparian Storage

Storage within the riparian landscape unit was calculated between October 2014 and June 2017 by assuming that the riparian well data were representative of the water table in the entire catchment's riparian zone. The daily average of the corrected 15-minute time series of water level for each of the three riparian wells described in Section 2.3.1 was multiplied by the specific yield for a silt loam soil in order to calculate storage depth within the riparian aquifer. Riparian storage depth was scaled by the ratio of the riparian area to the Pond Branch Catchment area to convert the storage to a per unit catchment area quantity, making it directly comparable to the catchment storage estimated in the previous section. The riparian area was calculated using ArcGIS and a 1-m resolution digital elevation model (DEM) to manually define the boundary between the hillslope and riparian landscape units based on the contrast in the calculated slope between the two units and firsthand field observations. Finally, the scaled riparian storage was adjusted so that the minimum observed value for each well, i.e. the maximum observed depth below the surface, was set to zero. This estimated riparian storage once again represents the dynamic component of the total storage since it is based on relative changes in water level and not on the absolute volume of water within the riparian landscape unit.

2.3.4 Soil Storage

Soil storage in the top 20 cm was calculated between October 1, 2014 and September 30, 2017. Storage was only calculated for the upper 20 cm of soil given the placement of the volumetric water content probes at 10 cm depth. The total soil storage is likely to be much larger, given a soil profile that is approximately 150 cm, but less variable than the storage near the surface. The upper 20 cm of soil storage was estimated by first taking the daily average of the hourly hillslope soil moisture, which was calculated, as described in Section 2.3.1, by taking the average of the hourly volumetric water content measured within two hillslope plots. It was assumed that the daily average soil moisture represented an average of the upper 20 cm of soil over the entire hillslope, such that the hillslope soil storage depth was calculated by multiplying the daily average hillslope soil moisture by 20 cm. This hillslope soil storage depth was then scaled by the ratio of the hillslope area to the Pond Branch Catchment area to convert storage to a per unit catchment area quantity, which could then be directly compared to the catchment and riparian storage estimates. The hillslope area was determined in the previous section by subtracting the areas of the riparian and swale landscape units calculated in ArcGIS from the total catchment area. In contrast to the riparian and catchment storage, the estimated soil storage is not the dynamic component of the absolute storage but is instead the absolute soil storage since it was calculated using the volumetric water content.

2.3.5 Hydraulic and Indirect Storage

The catchment-scale dynamic storage calculated in Section 2.3.2 is assumed to be composed of two stores, one that is hydraulically coupled to discharge and one that is hydraulically uncoupled (Riegger & Tourian, 2014), referred to as hydraulic and indirect storage, respectively (Dralle et al., 2018). Here, hydraulically coupled means that the potential energy of a store directly influences discharge, while hydraulically uncoupled means that the potential energy of a store does not directly influence discharge. Therefore, by definition, the catchment scale dynamic storage, $\Delta S(t)$ [L], from Equation 2.1 is equivalent to the sum of the hydraulic, $\Delta S_H(t)$ [L], and indirect storage, $\Delta S_I(t)$ [L]:

$$\Delta S(t) = \Delta S_I(t) + \Delta S_H(t) \tag{2.2}$$

The indirect storage can be thought of as any storage which is hydraulically disconnected from discharge at the catchment outlet. Examples of indirect storage include snow/ice and perched surface water ponds (Riegger & Tourian, 2014), as well as unsaturated and tension-saturated zone storage in the soil, saprolite, and riparian area. Hydraulic storage is the component of the catchment storage whose hydraulic gradients drive discharge and includes saturated storage in the soil, saprolite, and riparian area which drains freely to surface discharge. When estimating hydraulic storage, some have assumed that it is equivalent to catchment scale dynamic storage, however, the presence of hysteresis loops in storage-discharge relationships often reveal the non-monotonic relationship between catchment scale dynamic storage and discharge created by indirect storage. Here hydraulic storage is calculated using a modified version of the recession analysis described by Kirchner (2009), and then indirect storage is calculated using this hydraulic storage along with Equation 2.2 and the catchment scale dynamic storage.

In order to estimate the hydraulic storage, $\Delta S_H(t)$, a water balance is first written for this component of the catchment storage:

$$\frac{dS_H}{dt} = R(t) - \alpha ET(t) - q(t) \tag{2.3}$$

where $R(t)$ [L/T] is the recharge to the hydraulic storage from precipitation, infiltration, and redistribution from indirect storage, $ET(t)$ [L/T] is the total actual evapotranspiration, α [-] is the ratio of the hydraulic area to the total catchment area, and $q(t)$ [L/T] is the specific discharge at the catchment outlet. The hydraulic area is defined as the area of the catchment from which evapotranspiration directly removes water from hydraulic storage. Assuming that stream discharge, $q(t)$, is solely a function of the hydraulic storage, $\Delta S_H(t)$, the chain rule allows us to assume that the rate of change of discharge with respect to time, dq/dt, is equal to the product of the derivative of discharge with respect to hydraulic storage, dq/dS_H, and the rate of change of hydraulic storage dS_H/dt. Substitution into Equation 2.3 allows us to equate the rate of change of discharge through time to the water balance of hydraulic storage as:

$$\frac{dq}{dt} = \frac{dq}{dS_H}\frac{dS_H}{dt} = \frac{dq}{dS_H}(R(t) - \alpha ET(t) - q(t)) \tag{2.4}$$

Making the additional assumption that the storage-discharge relationship is a strictly increasing function and thus invertible, Kirchner (2009) defines a function relating dq/dS_H and q:

$$g(q) = \frac{dq}{dS_H} \tag{2.5}$$

which is termed the "sensitivity function" and modified here to be explicit that hydraulic storage (and not dynamic catchment storage ΔS) is represented by this relationship. In Kirchner (2009), the storage term in Equation 2.5 is defined as the dynamic storage and is recognized to be less than the total catchment storage, however, as described above, the catchment scale dynamic storage includes both hydraulic and indirect storage components, making it necessary to distinguish between the total dynamic storage and the hydraulic storage, which can be estimated using this approach. Equation 2.5 can then be substituted into Equation 2.4 to yield:

$$\frac{dq}{dt} = g(q)(R(t) - \alpha ET(t) - q(t)) \tag{2.6}$$

If we restrict ourselves to considering times when the recharge term $R(t)$ is negligible, this can be further simplified and rearranged to produce:

$$g(q) = -\left.\frac{{}^{dq}\!/_{dt}}{q(t)+\alpha ET(t)}\right|_{R=0} \tag{2.7}$$

The recharge term $R(t)$ might be assumed to be negligible when there is no precipitation, and indeed precipitation last occurred sufficiently long ago that redistribution from indirect storage has completed. This equation is equivalent to Equation 7 of Kirchner (2009) given an α of zero; however, by varying α between zero and one, the assumption that the evapotranspiration flux is small compared to discharge can be relaxed, and the flux of evapotranspiration can be scaled by the fraction of the catchment area from which evapotranspiration removes water directly from hydraulic storage. Given Equation 2.7 and time-series of dq/dt, $ET(t)$, and $q(t)$ as well as values of α, the sensitivity function, $g(q)$, can be determined. Finally, the hydraulic storage, $S_H(t)$, can be calculated by inverting Equation 2.5 and integrating:

$$\Delta S_H(t) = S_H(t) - S_{H,min} = \int_{q_{min}}^{q(t)} \frac{dq}{g(q)} \tag{2.8}$$

where q_{min} is the minimum observed discharge and $q(t)$ is the discharge at time, t.

Hydraulic storage for the Pond Branch Catchment is estimated using Equations 2.7 and 2.8 in combination with the data described in Section 2.3.1. First, the daily average specific discharge is calculated from the gap-filled 15-minute Pond Branch discharge data in order to smooth over small fluctuations in discharge that are not a part of the long-term recession of the catchment hydrograph, including diel cycles induced by evapotranspiration. The recession rate, $-dq/dt$, is calculated at a daily timestep for pairs of consecutive days in which there is no measurable precipitation on either day as well as no precipitation in the 12 hours before the first day or one hour after the second day. These conditions are made in order to satisfy the assumptions made by Equation 2.7, including no precipitation on either day as well as no redistribution, i.e. that redistribution happens within the 12 hours after a precipitation event. Field notes and observations are used to manually remove recession rates affected by melting snow or by errors in the discharge measurement created by ice or leaves at the gage. The average discharge, $q(t)$, is calculated for each corresponding recession rate along with the average evapotranspiration, $ET(t)$, using the daily actual evapotranspiration from Section 2.3.2. Three values of α are selected: 0.0, corresponding to the assumption that the evapotranspiration flux is small compared to discharge; 0.051, corresponding to the fraction of the catchment area represented by the swale and riparian landscape units, which may be assumed to represent the surface expression of the hydraulic storage area; and 1.0, corresponding to the entire catchment area, suggesting that evapotranspiration can affect hydraulic storage deep within the hillslope landscape unit. Recession plots are constructed for each α value by plotting $q(t)$ verses the right-hand side of Equation 2.7 multiplied by $q(t)$. The data are binned following the method outlined in Kirchner (2009) in order to estimate an average recession rate at each discharge value while removing scatter in $-dq/dt$ when $q(t)$ is small (Kirchner, 2009). Each bin spans at least 1% of the logarithmic-range of $q(t)$ and includes enough points such that the standard error of $-dq/dt$ is less than or equal to half of its mean (Kirchner, 2009). A quadratic function is fit to the logarithmic of the binned $-dq/dt$ and $q(t)$ data for each α value using polynomial least squares regression with inverse variance weighting. Inverse weighting is used to prevent the recession from being skewed by highly uncertain points (Kirchner, 2009). Each quadratic function represents the logarithmic of the sensitivity function, $g(q)$, for its respective α value. Given each $g(q)$, the hydraulic storage, $\Delta S_H(t)$, is calculated using Equation 2.8 by integrating between the minimum observed discharge, q_{min}, and the discharge at time, $q(t)$. $\Delta S_H(t)$ is determined only on days in which there is no precipitation, resulting in hydraulic storage estimates for 40.1% of the days between October 1, 2014 and September 30, 2017. A linear interpolation is used to estimate storage on days in which there is precipitation, and then the hydraulic storage is adjusted so that the minimum observed values is set equal to the minimum riparian storage from Section 2.3.3 since riparian storage can be assumed to be a component of the total hydraulic storage.

Indirect storage, $\Delta S_I(t)$, is calculated over a three-year period using daily time-series of the catchment scale dynamic storage, $\Delta S(t)$, and hydraulic storage, $\Delta S_H(t)$, to solve Equation 2.2. As described above, $\Delta S_H(t)$ is estimated using three different ratios of the hydraulic area to the total catchment area, α, however, only one of the three $\Delta S_H(t)$ estimates is used to calculate $\Delta S_I(t)$. Specifically, $\Delta S_H(t)$ with the corresponding highest coefficient of determination, R^2, for the regression used to estimate the sensitivity function, $g(q)$, is selected to calculate $\Delta S_I(t)$. The $\Delta S(t)$ estimated in Section 2.3.2. is then scaled by the sum of $\Delta S_H(t)$ and the soil storage from Section 2.3.5 since $S(t)$ must always be greater than the sum of these two individual stores. Finally, $\Delta S_I(t)$ is calculated at a daily timestep by subtracting the selected $\Delta S_H(t)$ from the scaled $\Delta S(t)$. The indirect and hydraulic storage estimated in this section represent the dynamic components of the total indirect and hydraulic storage, respectively, since neither method used to calculate either store is able to determine the absolute storage volumes.

2.4 Results

2.4.1 Water Balance and Catchment Storage

The catchment scale water balance was calculated at a daily time step from October 1, 2014 until September 30, 2017. The water balance was estimated only for complete water years and the JHU01 weather station was not installed until June 2014 such that only the 2015, 2016, and 2017 water years could be estimated for this analysis. Data from other precipitation gages or weather stations could be used to extend the duration of the water balance estimate; however, additional corrections/assumptions would have to be made in order to account for instrument bias, making inter-year comparisons of storage more uncertain.

The daily time-series of precipitation ($P(t)$) is shown in Figure 2.5 and the total for each water year is shown in Table 2.1, with the annual water year average of 1152 mm from 2000 to 2017 shown in the last row (NOAA NCEI). $P(t)$ was approximately 100 mm above average for the first water year and approximately 100 mm below average for the final two water years. In addition, the monthly $P(t)$ was consistently less than average for a seven-month period beginning in August 2016 and ending in February 2017 (Figure 2.1).

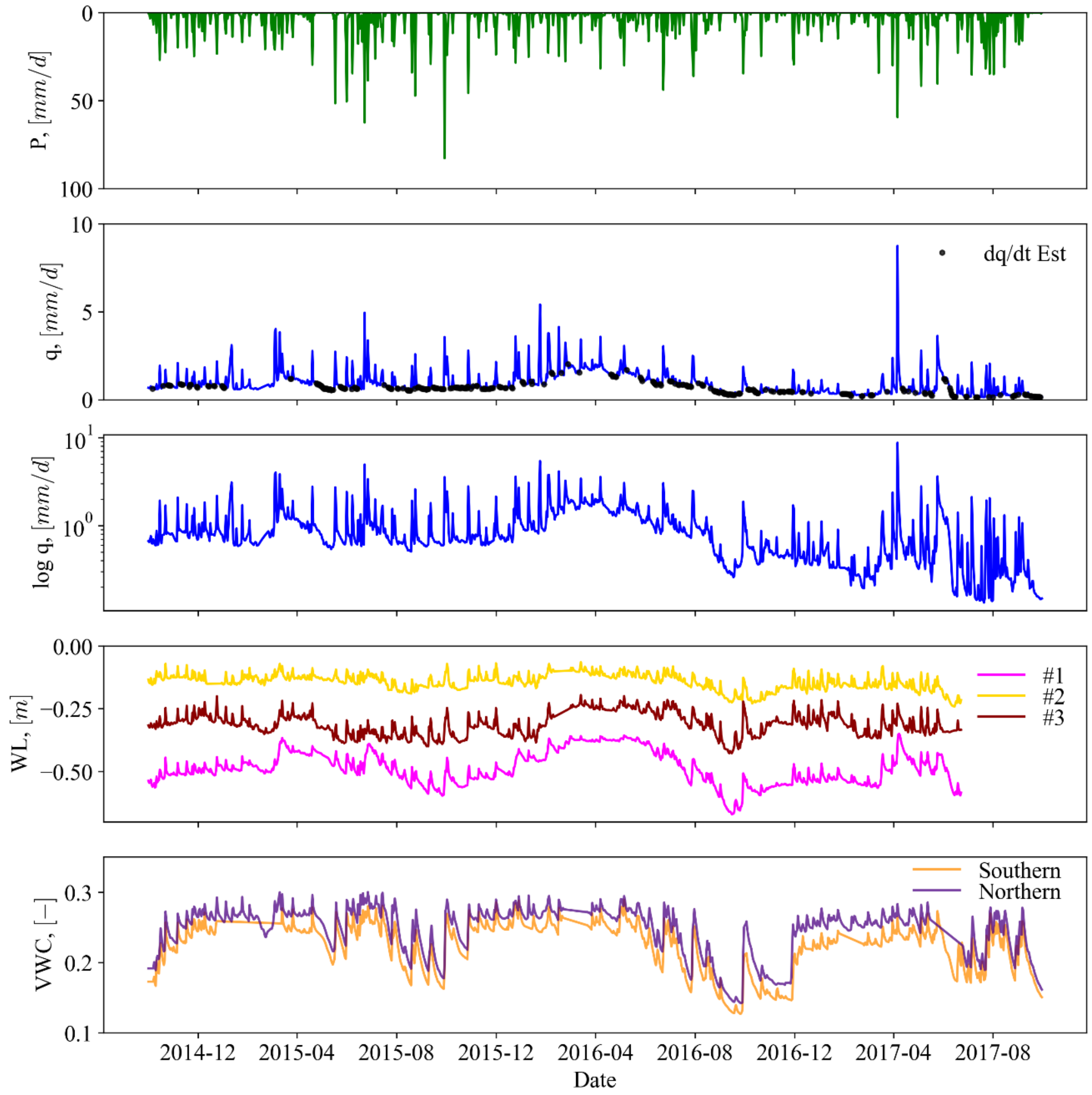

Figure 2.5: Summary of the daily data used in combination with the methods described in the previous section to estimate storage for the catchment as whole, hydraulically coupled and uncoupled portions of the landscape, and individual landscape units. Precipitation (P) and specific discharge (q) are in units of millimeters per day; the logarithmic of the specific discharge (log q) has units of logarithmic millimeters per day; the water level (WL) measured in each riparian well is in meters below the land surface; and the volumetric water content (VWC) is in units of cubic meters per cubic meter and therefore dimensionless. The black points in the second pane are days in which the recession rate from the previous day is estimated. The numbers in the fourth pane correspond to the riparian wells labeled in Figure 2.2, and the labels in the last pane correspond to the relative cardinal direction of the two plots containing volumetric water content probes as shown in Figure 2.2.

Table 2.1: Comparison of the total of the water balance terms for the three years over which daily catchment storage was calculated where P, q, ET, ΔS, and ΔS_{range} stand for the precipitation, specific discharge, actual evapotranspiration, dynamic catchment storage, and range in the dynamic catchment storage, respectively. The last row in the table is the 17-year annual water year average calculated from the same data used to construct Figure 2.1, such that ET, ΔS, and ΔS_{range} were not available (NA).

Year	P [mm]	q [mm]	ET [mm]	ΔS [mm]	ΔS_{range} [mm]
15	1276	352	924	0	261
16	1063	441	916	-293	477
17	1062	198	853	10	201
00' - '17 Average	1152	368	NA	NA	NA

The specific discharge ($q(t)$) time-series used in the water balance is shown in Figure 2.5 both in linear and logarithmic space. $q(t)$ at the Pond Branch Catchment outlet is greater than zero for the entire three-year analysis period, with a minimum value of 0.13 mm/day (0.02 cubic feet per second) recorded on July 21, 2017 and a maximum of 8.74 mm/day (1.32 cubic feet per second) on April 6, 2017. By plotting the $q(t)$ on a logarithmic scale, the separation between the low-frequency baseflow component of $q(t)$ and the high-frequency quickflow component can be more easily seen. Baseflow is generally highest in late winter and spring before leaf-on as seen in all three water years. Baseflow is maintained above a relatively consistent level until August 2016 when it begins to drop off, remaining below average through the 2017 water year. The monthly $q(t)$ shown in Figure 2.1 also shows this behavior, where $q(t)$ is below average from September 2016 through September 2017. In Table 2.1, the annual water year average $q(t)$ for each water year is provided along with 2000 to 2017 average. $q(t)$ for the 2015 water year is approximately average (96% of average), 2016 water year is greater than average (120% of average), and 2017 water year is much less than average (54% of average). Figure 2.1 shows that the 2016 water year had higher than average $q(t)$ from December 2015 to August 2016 resulting in the greater than average overall value. In contrast, $q(t)$ for the 2017 water year was consistently below average for each month producing a deficit for the water year when compared to the 17-year normal.

The scaling factor k used to estimate the actual evapotranspiration ($ET(t)$, shown in Figure 2.6) from potential evapotranspiration ($PET(t)$) was $k = 0.74$. A $k < 1$ suggests that the catchment is water limited at least part of the year, i.e. that there is more energy available to transpire or evaporate water than there is water available at all times. Figure 2.6 shows the seasonal signal in $ET(t)$, which ranges from approximately 0.5 mm/day in winter to 7 mm/day in summer. This seasonality is the result of the seasonal signal in both the incoming radiation as well as the leaf area index, which is expected given that the catchment is dominated by a deciduous forest and is located at approximately 39.5 degrees north latitude. The daily variability in $ET(t)$ is the result of a combination of factors, including the relative humidity, wind speed, and amount of cloud cover. $ET(t)$ ranges from 853 mm in water year 2017 to 924 mm in water year 2015 (Table 2.1). For the 2015 water year, this means that approximately 2.6 times more water leaves the catchment as $ET(t)$ compared to as $q(t)$, or that approximately 72% of precipitation is evapotranspirated.

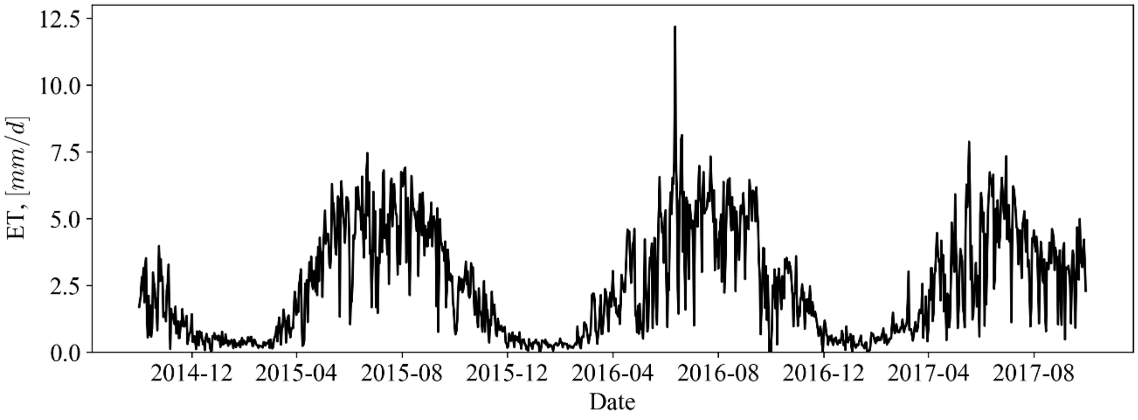

Figure 2.6: Daily actual evapotranspiration (ET) for the Pond Branch Catchment. Actual evapotranspiration was calculated as described in Section 2.3.2 by scaling the potential evapotranspiration estimated from the Penman-Monteith Equation.

The daily catchment scale dynamic storage, $\Delta S(t)$, is shown in the top pane of Figure 2.7. Over the entire water balance the change in $\Delta S(t)$ is equal to -281 mm and the range is equal to 560 mm. The negative sign indicates that $\Delta S(t)$ is 281 mm less on September 30, 2017 at the end of the water balance than it was on October 1, 2014 at the start, meaning that the catchment storage reduced substantially over the three-year study period. The $q(t)$ plotted on a logarithmic scale in Figure 2.5 shows that $q(t)$ is much lower at the end of the water balance than at the beginning, but that $q(t)$ is approximately the same at the beginning and end of the 2015 water year, supporting the assumption that the change in $\Delta S(t)$ is zero over the 2015 water year, but not necessarily over the entire water balance. The change in $\Delta S(t)$ for individual water years is summarized in Table 2.1 along with the range of $\Delta S(t)$. The range and change in $\Delta S(t)$ are similar for the 2015 and 2017 water years even though $\Delta S(t)$ is much lower for the 2017 water year compared to the 2015 water year, as can be seen in Figure 2.7. In contrast, the range and change in $\Delta S(t)$ are larger for the 2016 water year, with the range nearly double that of the other two water years and the change in $\Delta S(t)$ equal to -293 mm (compared to near zero values for the other years). The contrast between the 2016 water year and the 2015 and 2017 water years in terms of the range and change in $\Delta S(t)$ can be seen as the large decrease in $\Delta S(t)$ that occurs over the summer of 2016 in Figure 2.7. In June 2016, $\Delta S(t)$ drops below any value observed in the 2015 water year and continues to generally decrease until a minimum storage is reached in mid-November 2016. This draw-down in storage precedes the lower than average $q(t)$ in the fall of 2016 by approximately two and a half months (Figures 2.5 & 2.7). $\Delta S(t)$ remains below the 2015 water year level for the entirety of the 2017 water year even with above average precipitation for five out of the last seven months of the water year.

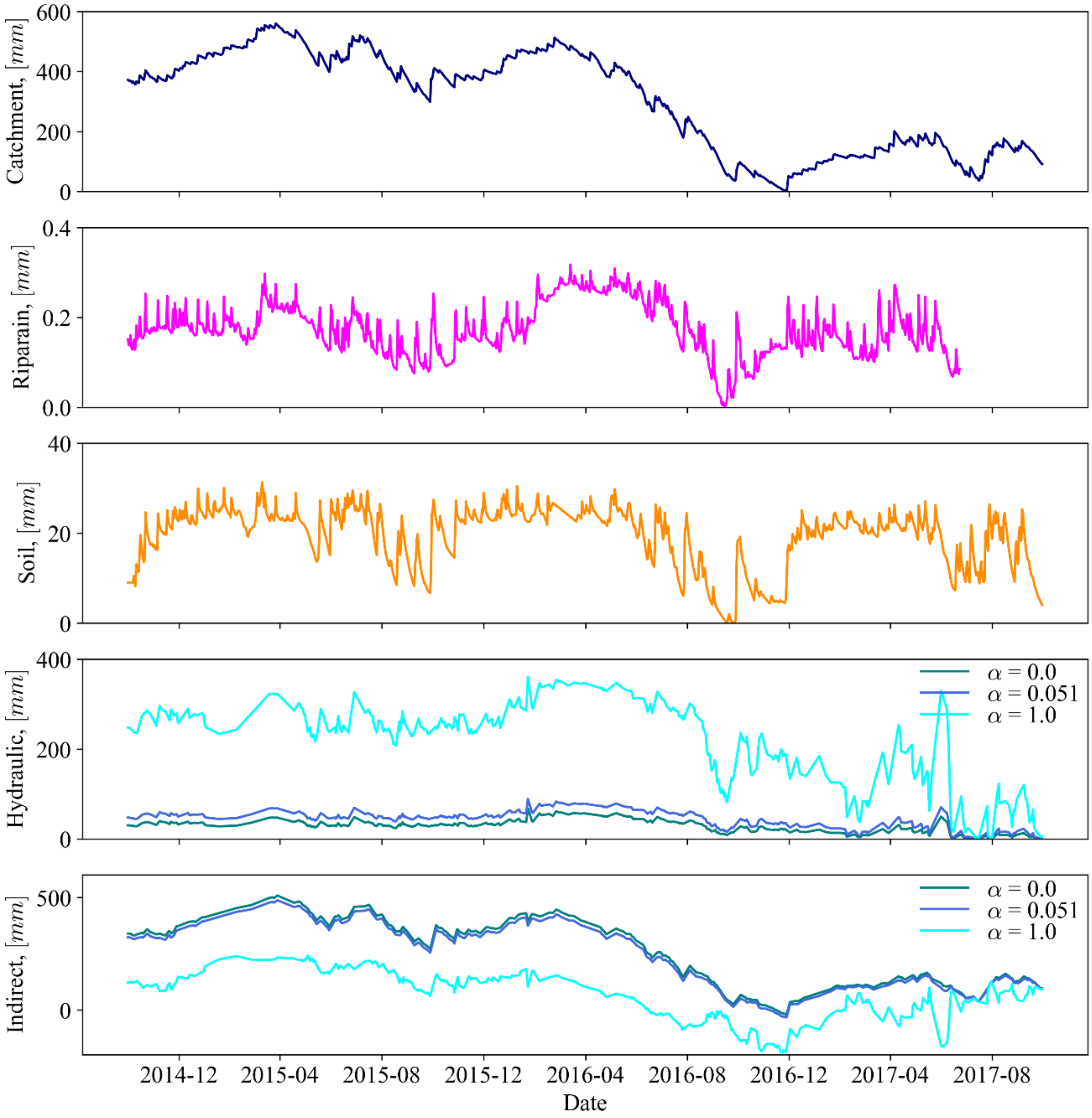

Figure 2.7: Summary of the daily storage time series estimated during this analysis. The alpha values in the last two panes correspond to the ratio of the hydraulic area to the total catchment area that is used to estimate the corresponding storage following the method presented in Section 2.3.5.

2.4.2 Riparian Storage

Daily riparian storage ($\Delta S_R(t)$) is calculated over the same three water years as $\Delta S(t)$ in the previous section and plotted in the second pane of Figure 2.7. Note that $\Delta S_R(t)$ is unavailable for the last three months of the 2017 water year as a result of malfunctioning water level loggers, but the entire 2015 and 2016 water years are available for comparing $\Delta S_R(t)$ to other stores. In order to make $\Delta S_R(t)$ comparable to $\Delta S(t)$, the riparian storage depth (riparian storage volume divided by riparian area) is scaled by the ratio of the riparian area to the Pond Branch Catchment area which is equal to 0.037.

The range for $\Delta S_R(t)$ is 0.24 mm, which is more than three orders of magnitude smaller than the range of 560 mm for $\Delta S(t)$. This range for $\Delta S_R(t)$ means that changes in $\Delta S_R(t)$ would have a small effect on the overall $\Delta S(t)$ and that storage somewhere outside of the riparian area within the catchment must be controlling the variability in $\Delta S(t)$. Individual storm events can significantly increase the $\Delta S_R(t)$ temporarily (see Figure 2.7), especially when storage is low before the precipitation event, resulting in two timescales of response in $\Delta S_R(t)$. Despite the difference in the relative magnitudes of their ranges and their responses to storm events, the low-frequency component of $\Delta S_R(t)$ is similar to the overall trend in $\Delta S(t)$ for the first two years of the time-series. In both $\Delta S(t)$ and $\Delta S_R(t)$ time series, a seasonal signal can be discerned over the 2015 water year, and over the summer of 2016, $\Delta S_R(t)$ decreases in accord with $\Delta S(t)$. However, the agreement between the trends in $\Delta S(t)$ and $\Delta S_R(t)$ ends in September 2016, when $\Delta S_R(t)$ begins to recover following a series of rain events, retuning to near-2015 levels while $\Delta S(t)$ continues to decrease. $\Delta S_R(t)$ also lagged the draw down in $\Delta S(t)$ by the same length of time as $q(t)$, with $\Delta S_R(t)$ levels not dropping below 2015 values until the end of August 2016.

2.4.3 Soil Storage

Daily soil storage ($\Delta S_S(t)$) for the upper 20 cm of the catchment's hillslope soil profile is calculated over the same interval of time as $\Delta S(t)$ using the data in the last pane of Figure 2.5 and is plotted in the third pane of Figure 2.7. Once again, in order to make $\Delta S_S(t)$ comparable to $\Delta S(t)$, the soil storage is scaled by the ratio of the hillslope area to the Pond Branch Catchment area, which is equal to 0.95. The range for $\Delta S_S(t)$ is 31.3 mm, which is more than one order of magnitude smaller than the range for $\Delta S(t)$, but much closer than the range for $\Delta S_R(t)$. This range of 31.3 mm is similar in size to variations in $\Delta S(t)$ that occur on a daily or weekly time-scale. However, the larger scale variability in $\Delta S(t)$ cannot be accounted for by changes in $\Delta S_S(t)$ alone. Assuming that the range of $\Delta S_S(t)$ for the upper 20 cm of soil can be scaled to represent the entire 150 cm soil profile, the range in total soil storage is 235 mm. However, this 235 mm is half of the range of $\Delta S(t)$ and is likely larger than the actual range of soil storage since there is more variability at the soil surface than at depth.

The time series of $\Delta S_S(t)$ is similar to $\Delta S_R(t)$ in that it contains both high and low frequency temporal variability, with individual storm events rapidly increasing storage followed by a long recession back to the lower frequency component. Once again, the seasonal signal in the $\Delta S_S(t)$ is similar to the season signal in $\Delta S(t)$, and the dry down in the summer of 2016 is apparent in $\Delta S_S(t)$, with $\Delta S_S(t)$ dropping below pre-summer 2016 levels for the first time approximately one month after $\Delta S(t)$ declines below previous levels. However, $\Delta S_S(t)$ partially recovers at the end of September 2016, returning to near-2015 levels by the end of November 2016 while $\Delta S(t)$ remains depressed. The responsiveness of $\Delta S_S(t)$ to storm events, its recovery in the fall of 2016, and the difference between the range of the estimated total soil storage (for the 150 cm soil profile) and $\Delta S(t)$ further suggests that $\Delta S(t)$ behavior is controlled by an alternative store or stores within the catchment.

2.4.4 Hydraulic and Indirect Storage

Daily hydraulic ($\Delta S_H(t)$) and indirect storage ($\Delta S_I(t)$) storage are estimated over the same period of time as $\Delta S(t)$ using the methods outlined in Section 2.3.5 (Figure 2.7). The black points plotted on top of discharge in the second pane of Figure 2.5 are the days in which the recession rate ($-dq/dt$) from the previous day is estimated. Given the assumptions made in the methods section, $-dq/dt$ could not be estimated in late winter and early spring of 2015 when it rained almost daily. The individual recession rates from Figure 2.5 are scaled using Equation 2.7 and plotted in Figure 2.8a for each of the three α-values selected. Each gray point represents an individual recession, while the black points are the binned averages, with gray bars representing the standard error. The effect of scaling $-dq/dt$ in terms of reducing scatter can be seen as one moves across the panes in Figure 2.8a, with the least scatter associated with an α of 1.0. The black lines in Figure 2.8a are the estimated sensitivity functions ($g(q)$) with coefficients of determination (R^2) equal to 0.56, 0.64, and 0.74 for an α of 0.0, 0.051, and 1.0, respectively. The highest R^2 value corresponds to an α of 1.0, implying that evapotranspiration removes water from the hydraulic storage across the entire catchment, including from underneath the hillslope.

Figure 2.8b shows the binned recession rates and $g(q)$ on a logarithmic-logarithmic plot. Figure 2.8c shows the residuals between the line of best fit, i.e. $g(q)$, and the binned recession rates on a logarithmic-logarithmic plot. Figure 2.9 shows the resulting storage-discharge relationship for each α and corresponding $g(q)$ on both a linear-linear (left-hand side) and logarithmic-linear plot (right-hand side). The effect of the different α values on $g(q)$ becomes apparent when looking at the storage-discharge relationships. The smaller the α value, the steeper the storage discharge relationship, such that 1 mm/day discharge corresponds to 47 mm, 73 mm, and 345 mm of storage for α of 0.0, 0.051, and 1.0, respectively. A steep storage discharge relationship implies that a small dynamic range in $\Delta S_H(t)$ can produce a wide range of discharges.

The resulting ranges for $\Delta S_H(t)$ over the three-year study period are 68 mm, 89 mm, and 360 mm and for $\Delta S_I(t)$ are 528 mm, 521 mm, and 430 mm, corresponding to an α of 0.0, 0.051, and 1.0, respectively for each store. Again, the difference between the different α values in terms of their effect on the range in $\Delta S_H(t)$ is clear when comparing the range for an α of 0.0 to the of an α of 1.0, with the range of $\Delta S_H(t)$ five-times smaller for the lower α value. In contrast, the ranges for the three $\Delta S_I(t)$ time series are all of similar size, with the smallest range for an α of 1.0. The $\Delta S_H(t)$ with an α of 1.0 is the only estimate of $\Delta S_H(t)$ whose range is similar in size to the range of $\Delta S(t)$, while all of the ranges for $\Delta S_I(t)$ are within a 130 mm of the range for $\Delta S(t)$. $\Delta S_H(t)$ is a component of $\Delta S(t)$ such that the range for $\Delta S_H(t)$ is expected to be less than the range of $\Delta S(t)$, where the difference between the two stores is the $\Delta S_I(t)$ as defined. Since, $\Delta S_I(t)$ is estimated using the time series for $\Delta S(t)$, only $\Delta S_H(t)$ is further compared to $\Delta S(t)$ here to avoid making comparisons between two stores, which by definition, are directly related.

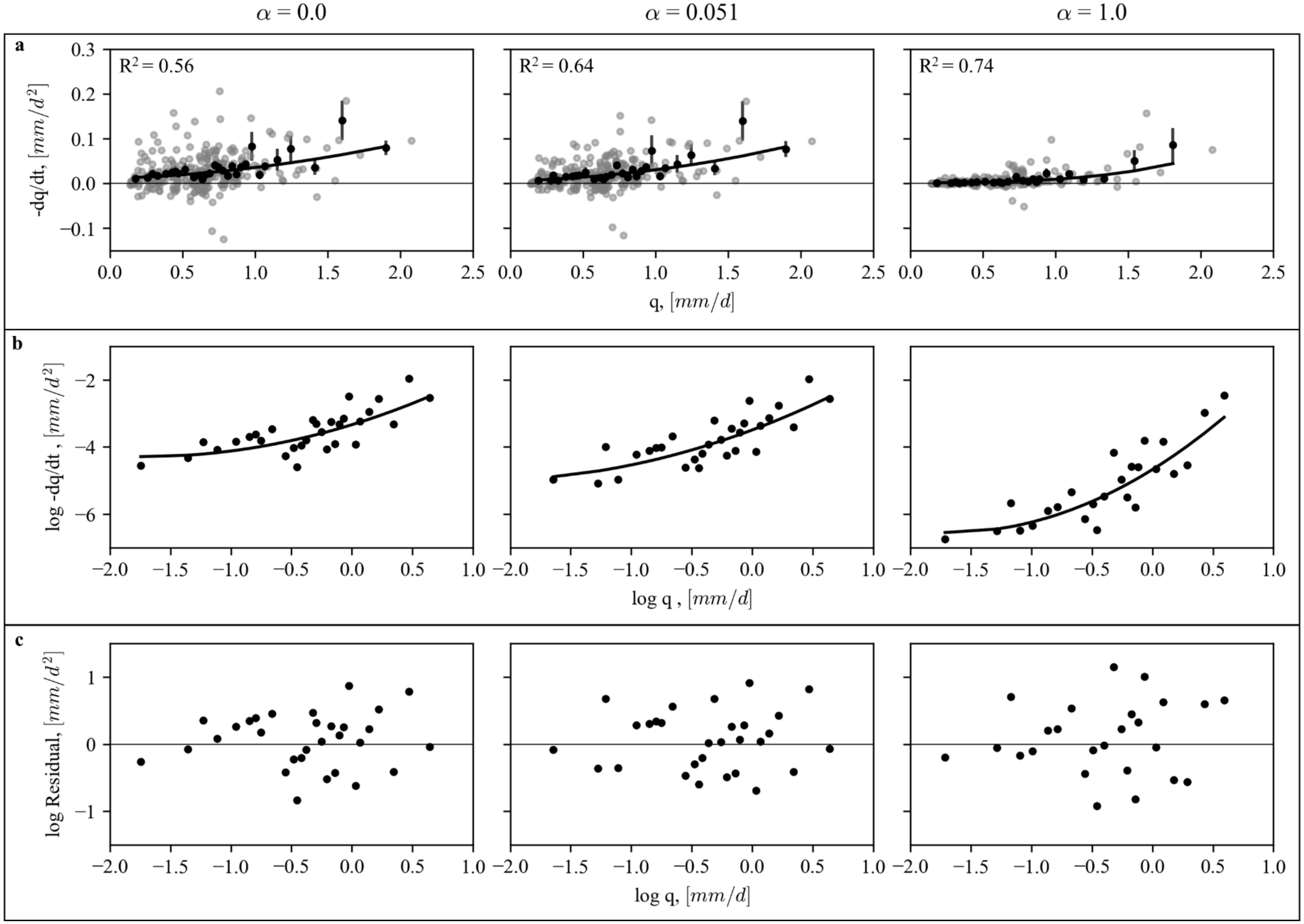

$\alpha = 0.0$
$\alpha = 0.051$
$\alpha = 1.0$
a
$R^2 = 0.56$
$R^2 = 0.64$
$R^2 = 0.74$
-dq/dt, $[mm/d^2]$
0.3
0.2
0.1
0.0
−0.1
0.0
0.5
1.0
1.5
2.0
2.5
q, $[mm/d]$
b
log -dq/dt , $[mm/d^2]$
−2
−4
−6
−2.0
−1.5
−1.0
−0.5
0.0
0.5
1.0
log q , $[mm/d]$
c
log Residual, $[mm/d^2]$
1
0
−1
log q, $[mm/d]$

Figure 2.8: (a) Individual recession rates (-dq/dt) from Figure 2.5 (gray points), binned average recession rates (black points), standard error for the binned averages (black bars), and the line of best fit, i.e. the catchment sensitivity function, (black line) versus the specific discharge (q) for each of the three α-values used to scale the recession rates. The coefficient of determination (R^2) for each line of best fit is shown in the upper left-hand corner. (b) Binned average recession rates (black points) and the line of best fit (black line) versus the specific discharge for each α-value on a logarithmic-logarithmic plot. (c) Residuals between the line of best fit and the binned average recession rates versus the specific discharge for each α-value on a logarithmic-logarithmic plot.

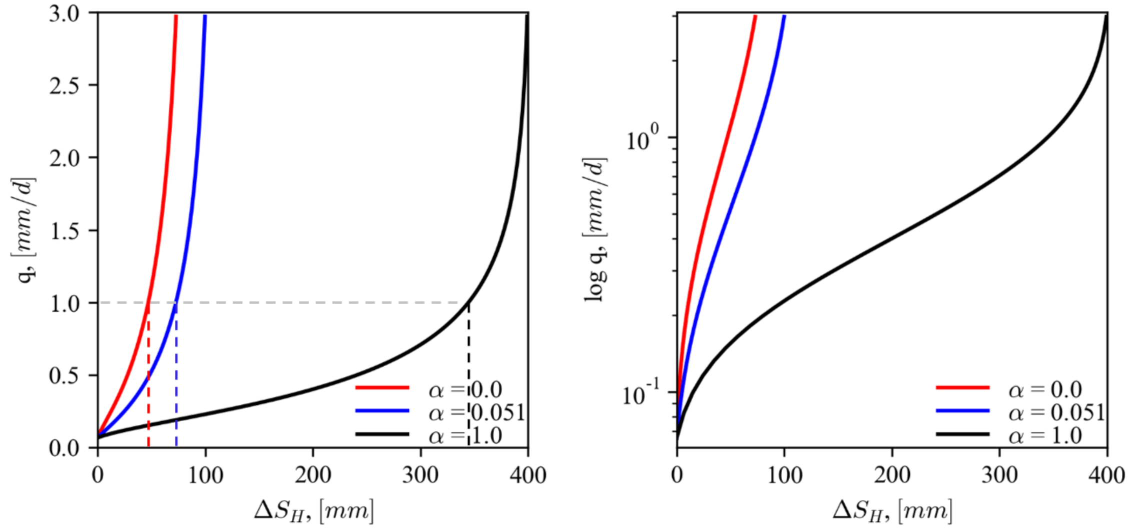

Figure 2.9: Hydraulic storage (ΔS_H) versus specific discharge for Pond Branch (q) for each α-value and corresponding catchment sensitivity function. Discharge is plotted on a linear-axis on the left and on a logarithmic-axis on the right. The dashed lines on the left plot map the relationships between hydraulic storage and 1 mm/day of discharge for each α-value.

All three estimates of $\Delta S_H(t)$ exhibit similar trends where the main difference is the magnitude of each store. In contrast to $\Delta S_S(t)$ and $\Delta S_R(t)$, $\Delta S_H(t)$ does not, in general, appear to have high frequency temporal variability as shown in Figure 2.7. However, this lack of $\Delta S_H(t)$ response to precipitation events is in part due to a limitation in the method which requires that $\Delta S_H(t)$ is only calculated over two consecutive days with no precipitation. There is some agreement between the trends in $\Delta S_H(t)$ and those of $\Delta S(t)$, with high storage in the spring of 2015 and 2016 and a general decline in storage over the summer of 2016. However, the decline in $\Delta S_H(t)$ in summer 2016 lags behind $\Delta S(t)$ by approximately two and a half months, with $\Delta S_H(t)$ not dropping below previously observed levels until August 2016. The lag between $\Delta S(t)$ and $\Delta S_H(t)$ is also observed in $\Delta S_R(t)$ and $q(t)$, but not in $\Delta S_I(t)$ or to as much of an extent in $\Delta S_S(t)$. In addition, $\Delta S_H(t)$ temporarily returns to near pre-summer 2016 levels at the end of September 2016, while $\Delta S(t)$ recovers little. Another interesting feature of $\Delta S_H(t)$ is its rapid increase at the end of May 2017 which does not appear in $\Delta S(t)$, the implications of which will be explored further in the discussion sections that follow.

2.5 Discussion

2.5.1 "Hidden" Storage in the Piedmont Saprolite

In this study, dynamic catchment storage ($\Delta S(t)$) is quantified over a three-year period using the water balance approach described in Section 2.3.2. In plotting this $\Delta S(t)$ versus baseflow discharge for Pond Branch, multiple hysteresis loops reveal a non-monotonic relationship between storage and baseflow discharge, indicating that $\Delta S(t)$ is composed of multiple stores, some of which are not hydraulically coupled to baseflow at all times (Figure 2.10). Note that this baseflow is estimated using a two-parameter recursive digital filter suggested by Eckhardt (2005), where the parameters are selected so that the hydrograph is separated into a baseflow and quickflow component so that baseflow corresponds to the slowly changing component of discharge and quickflow corresponds to the "flashy" or quickly changing component of discharge. Baseflow is plotted against $\Delta S(t)$ since this low temporal frequency component of discharge is often related to the slow drainage of storage within the landscape while the quickflow quantity may be influenced by direct precipitation and overland flow. In Figure 2.10, there are periods when $\Delta S(t)$ and baseflow vary monotonically, such as in parts of the spring and summer of 2016 (light green points), indicating that the component of catchment storage that is draining is hydraulically connect to baseflow. This spring and summer 2016 period correspond to the period when storage and discharge decline below levels not previously observed in the study period. In order to explore the influence of landscape structure on the dynamic catchment storage within deeply weathered, Piedmont catchments as well as the propagation of a drought through catchment storage, individual stores within the catchment are quantified including soil ($\Delta S_S(t)$), riparian ($\Delta S_R(t)$), hydraulic ($\Delta S_H(t)$), and indirect ($\Delta S_I(t)$) storage.

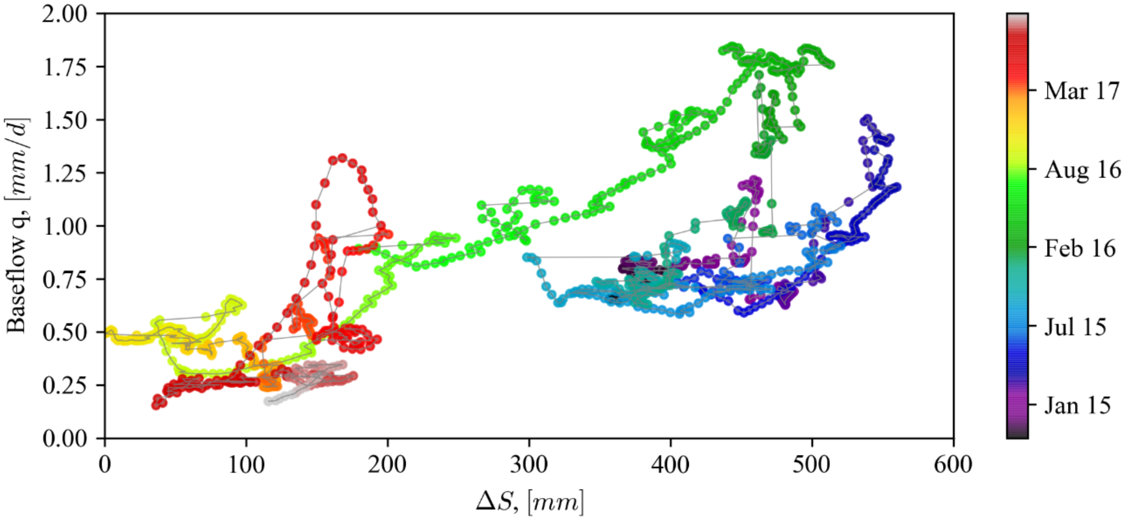

Figure 2.10: Dynamic catchment storage (ΔS) versus the two-week average of baseflow calculated from the Pond Branch specific discharge (q). The color map corresponds to the date of the plotted points which range from October 1, 2014 (black) to September 30, 2017 (light gray). Hysteresis indicates that there are multiple catchment stores, some of which are not hydraulically connected to baseflow at all times.

$\Delta S_S(t)$ and $\Delta S_R(t)$ are directly observable using volumetric water content probes and water level loggers in wells, respectively. Both $\Delta S_S(t)$ and $\Delta S_R(t)$ decline over the summer of 2016, with the drawdown in $\Delta S_S(t)$ preceding $\Delta S_R(t)$ by approximately a month but following $\Delta S(t)$ by a month and a half. However, both $\Delta S_S(t)$ and $\Delta S_R(t)$ partially recover at the end of September 2016 while ΔS remains depressed below pre-summer 2016 levels. The lag between the individual landscape units (soil and riparian) and the catchment storage, the recovery of these units, as well as their relative size, as discussed in the previous section, indicates that the drawdown in catchment storage cannot be explained by the drawdown in storage within these landscape units alone. In fact, storage within the riparian area appears to be an insignificant part of the total catchment storage, in agreement with the findings of Ocampo et al. (2006) in a deeply weathered catchment in Western Australia. Instead, storage within some unobserved part of the landscape must be controlling the overall decline in $\Delta S(t)$, which begins in June 2016 and persists throughout the 2017 water year.

This unobserved portion of storage within the landscape includes water that may be contained within saturated and unsaturated portions of the soil and saprolite underlying the hillslope. However, given that the depth to saprolite is typically 150 cm, it is likely that the majority of the storage variability is in the deeper saprolite. Given a change in catchment dynamic storage of 560 mm and an average specific yield of 21 % for saprolite (Nutter & Otton, 1969), the saturated water level would have to fluctutate by 2.7 m over the water balance to account for the change in $\Delta S(t)$. Sesimic refraction surveys conducted in the spring of 2014 and reported in St Clair et al. (2015), as well as previous research within the catchment (Cleaves et al., 1970), indicate that the saprolite is tens of meters thick, meaning that there is more than enough storage potential within the saprolite to account for the change in $\Delta S(t)$ observed.

In order to quantify the unobserved components of $\Delta S(t)$, including storage within the saprolite, $\Delta S_H(t)$ and $\Delta S_I(t)$ are calculated using the method described in Section 2.3.5. $\Delta S_H(t)$ exhibits a similar trend as observed in $\Delta S_R(t)$, lagging behind the decline in $\Delta S(t)$ below pre-summer 2016 levels by two and a half months and temporarily recovering at the end of September 2016. In contrast, $\Delta S_I(t)$ follows the same trend as $\Delta S(t)$, where storage drops below pre-summer 2016 levels for the first time in June 2016 and reaches a minimum storage in November 2016. This $\Delta S_I(t)$ begins to recover starting in December 2016 while $\Delta S_H(t)$ once again decreases through March 2017. $\Delta S_I(t)$ is the portion of the dynamic catchment storage which is hydraulically disconnected from discharge and may include unsaturated zone storage within the saprolite as well in the soil. The soil storage calculated above is assumed to be representative of only the upper 20 cm of the soil profile, which overlies the saprolite. However, the shorter lag between the drawdown in the soil storage and the catchment storage compared to the riparian or hydraulic storage, suggests that unsaturated zone storage within the saprolite may control the overall decline in the catchment storage that begins in June 2016, since the water content in the unsaturated zone below the soil could decline before the upper 20 cm of the soil, especially given transpiration from the saprolite and soil recharge from precipitation.

The decrease in $\Delta S_H(t)$ below pre-summer 2016 levels in August 2016 can be explained by a draining of the saturated portion of the saprolite which is hydraulically connected to discharge and can only be recharged through the unsaturated zone. The increase in $\Delta S_H(t)$ in September 2016 without a corresponding increase in $\Delta S(t)$ may be the result of the conversion of $\Delta S_I(t)$ held under tension saturation to $\Delta S_H(t)$, which would require little additional recharge but could result in a large change in $\Delta S_H(t)$. The recovery of the soil storage in December 2016 followed by the slow recovery of $\Delta S_I(t)$, while $\Delta S_H(t)$ continues to decline, may indicate that the unsaturated zone in the saprolite is recharging but still below the field capacity required to drain to the saturated zone below. Finally, in March 2017 $\Delta S_H(t)$ begins to recover temporarily before, once again, declining along with $\Delta S_I(t)$ and $\Delta S_S(t)$.

2.5.2 Challenges in Identifying Hydraulic Storage

The interpretations made in the previous section assume that $\Delta S_H(t)$ and thus $\Delta S_I(t)$ can be accurately estimated given the assumptions made in Section 2.3.5. These assumptions include (1) that there is a single storage reservoir controlling the recession rate and thus a single-valued function relating storage to discharge (Kirchner, 2009) and (2) that there exists a single α-value representing the fraction of evapotranspiration ($ET(t)$) whose removal reduces the hydraulic storage. In examining Figure 2.8b, it can be seen that the binned average recession rates do not increase monotonically with discharge, creating scatter around the line of best fit. The non-monotonic relationship of the binned averages is a result of the scatter in the individual recession rates ($-dq/dt$). This scatter could be explained by the presence of multiple stores controlling the recession behavior of the catchment. This would mean that at any given discharge, there are multiple values of $-dq/dt$ that are possible as a result of two or more stores draining. In the Pond Branch Catchment, it appears as though some of the individual recession events are controlled by portions of the landscape which drain rapidly, overprinting the long-term recession of discharge that is controlled by a much more slowly draining storage reservoir. The presence of multiple stores invalidates assumption 1, such that $\Delta S_H(t)$ and $\Delta S_I(t)$ cannot be estimated with confidence.

An additional source of the scatter in $-dq/dt$ shown in Figure 2.8a is from $ET(t)$ which imparts its own recession signal on discharge as water is removed from storage. In order to correct for this $ET(t)$ induced recession, $-dq/dt$ is scaled by $ET(t)$ and the previously described α-value (Equation 2.7). This correction reduces the scatter in $-dq/dt$ as shown in Figure 2.8a when moving across the panes from left to right. However, the α-values selected for this analysis provide a range of possible values but none of them may be the true α-value. Furthermore, the assumption of a single, time-invariant value could not be tested here. It is possible that the α-value may vary in time as water levels within the subsurface rise and fall, allowing more or less of the hydraulically connected area of storage to be accessed by trees transpiring or direct evaporation from the soil surface. Unfortunately, the chosen α-value also has a substantial effect on the estimated time series of $\Delta S_H(t)$, see Figure 2.7, making the uncertainty in its value even more of a problem. Assuming an α-value could be chosen with confidence, additional insights into the interactions between $ET(t)$ and $\Delta S_H(t)$, which may be partially composed of saturated storage tens of meters below the surface in the saprolite, could be gained. To avoid drawing conclusions given an unknown α-value, the general trends in $\Delta S_H(t)$ are considered within this analysis since they are relatively consistent across α-values.

2.5.3 Groundwater Drought in the Deeply Weathered Piedmont

In order to contextualize the draw-down in storage described above in terms of the long-term variability of dynamic catchment storage ($\Delta S(t)$), $\Delta S(t)$ is plotted against the water level observed in a United States Geological Survey (USGS) well located 10.3 kilometers from Pond Branch and installed within the same bedrock unit underlying the study site (top pane of Figure 2.11). In general, there is a good agreement between the trends in the well water level and the $\Delta S(t)$, with the highest storage/water level in February 2016 and the lowest storage/water level in late November 2016. Note once again that $\Delta S(t)$ includes both saturated and unsaturated storage while the well water level reflects only saturated zone storage which may explain some of the discrepancies between the two time series. The agreement between $\Delta S(t)$ and the well indicates that the observed drought is not specific to the catchment but was regional and affected storage across the deeply weathered Piedmont.

Given that the relative range in well water level over the three-year study period covaries with the range of $\Delta S(t)$, the entire 62-year record from the USGS well can be used to provide insights into the drought experienced over the study period (bottom pane of Figure 2.10). Specifically, there are five other periods recorded by the well as dry as fall 2016, suggesting that the observed drawdown is approximately a decadal "groundwater drought." Interestingly, there are many periods in which the water level is higher than anytime observed over the three-year study period, possibly indicating that the observed range in $\Delta S(t)$ may only represent a portion of the total range in storage experienced by the Pond Branch Catchment. In fact, the water level range is only 1.51 m from October 1, 2014 to September 30, 2017 while the range for the 62-year time series is 3.01 meters, which is approximately double. If the range of $\Delta S(t)$ were also doubled, that would mean that the saturated water level within the saprolite would fluctutate by 11.2 m over the 62-year period, using the logic described in Section 2.5.1. Again, given the thickness of the saprolite, it seems plausible that the saturated thickness may fluctuate by up to 11.2 m.

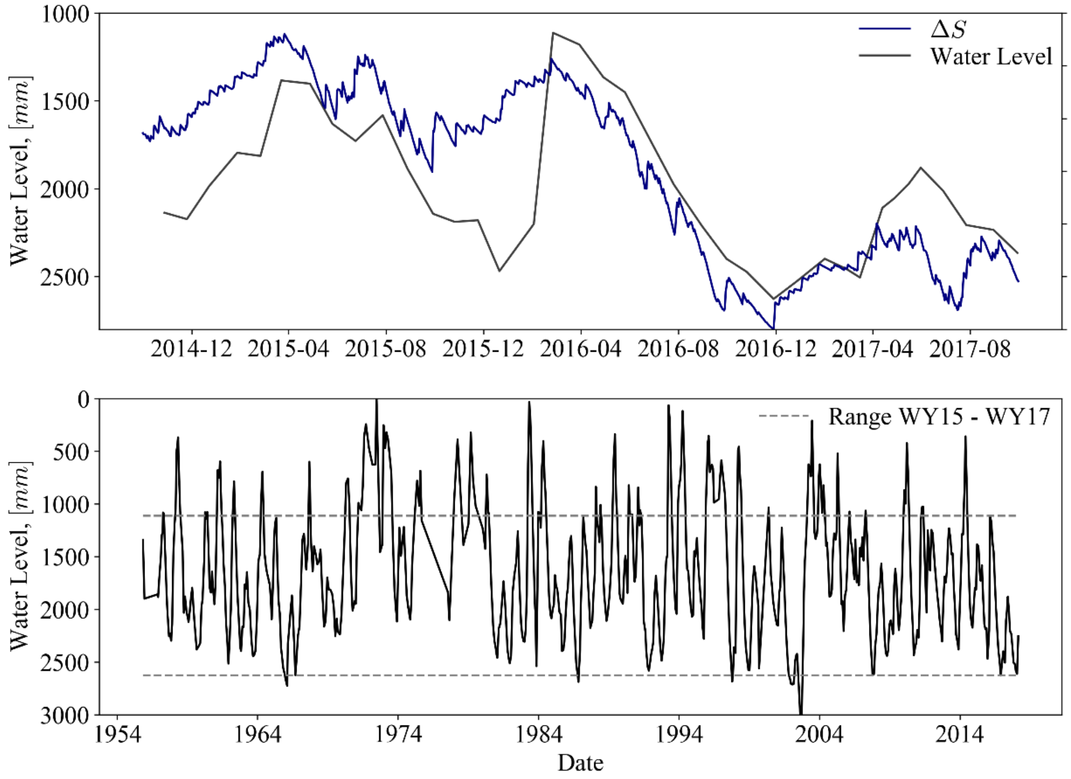

Figure 2.11: The top pane compares the monthly relative water level observed in a USGS well located approximately 10 kilometers from the research site to the calculated daily dynamic catchment storage (ΔS) over the 2015 to 2017 water years. The water level is plotted on the left y-axis and storage on the right y-axis. The bottom pane shows the complete monthly water level record for the USGS well, which extends back 62 years to 1955. The dashed lines are the range in the water level observed over the three years in which storage was calculated.

2.5.4 Drought Propagation through Structured Storage

The propagation of the decadal drought through the individually calculated stores is used to understand the influence of the storage structure on the emergent catchment scale storage and discharge within the deeply weathered Pond Branch Catchment. As shown in

Figure 2.1, the monthly discharge ($q(t)$) drops below average beginning in September 2016 and remains consistently below average through September 2017. This lower than average $q(t)$ in September 2016 follows a month in which there is lower than average precipitation ($P(t)$). However, $\Delta S(t)$ drops below pre-summer 2016 levels for the first time in June of 2016, a month and a half before the lower than average $P(t)$, and remains depressed through September 2017. $\Delta S_I(t)$ follows the same trend at $\Delta S(t)$ while $\Delta S_S(t)$, representing storage in the top 20 cm of the soil, drops below previously observed levels a month later in July 2016. Assuming the $\Delta S_I(t)$ represents the unsaturated zone storage within the soil and saprolite, the decline in $\Delta S_I(t)$ before $\Delta S_S(t)$ could be expected given that $\Delta S_I(t)$ must be recharged by precipitation passing through $\Delta S_S(t)$ and water may be removed from $\Delta S_I(t)$ via transpiration. In late August 2016, $\Delta S_H(t)$, $\Delta S_R(t)$, and $q(t)$ drop below previously observed levels as $\Delta S_H(t)$ drains, potentially from within the saturated saprolite. $\Delta S_I(t)$ begins to recover in December 2016 while $\Delta S_H(t)$ continues to decline through February 2017 until which time $\Delta S_I(t)$ has recovered enough to drain freely to $\Delta S_H(t)$. However, recharge to $\Delta S_H(t)$ once again ceases at the onset of the Spring 2017 growing season, with $\Delta S_H(t)$ and $q(t)$ remaining low despite several months of above average precipitation in spring/summer 2017.

Given the progression of the drought through the individual stores, the conditions leading to the drought can be explained assuming $\Delta S_I(t)$ and $\Delta S_H(t)$ represent the unsaturated and saturated storage within saprolite, respectively. The onset of the drought appears to have occurred as a result of below average precipitation in March and April 2016, during which time $\Delta S_I(t)$ begins a nine-month decline. As a result of reduced $\Delta S_I(t)$, $\Delta S_H(t)$ is not recharged in early summer 2016 despite higher than average precipitation, resulting in the eventual decline in $\Delta S_H(t)$, as well as $q(t)$ and $\Delta S_R(t)$, in late August 2016. Initially $\Delta S(t)$ declines as a result of reduced storage in the unsaturated zone, however, the decline continues as the saturated zone drains without significant recharge, except for a two-month period in Spring 2017.

2.6 Conclusions

In this analysis, data from the Pond Branch Catchment are used to calculate storage for individual landscape units, hydraulically coupled and uncoupled portions of the landscape, and for the catchment as a whole. Storage within the soil ($\Delta S_S(t)$) and riparian ($\Delta S_R(t)$) landscape units is estimated directly from observations, while dynamic catchment ($\Delta S(t)$), hydraulic ($\Delta S_H(t)$), and indirect ($\Delta S_I(t)$) storage are estimated using a combination of water balance models and a modified version of the recession analysis described by Kirchner (2009). For this recession analysis, a new parameter, α, is introduced which represents the ratio of the hydraulic area to the total catchment area. The true α-value, assuming that there is a single value, cannot be determined, still, the trend in $\Delta S_H(t)$ remains the same, regardless of α. Scatter in the recession rates used to determine $\Delta S_H(t)$ suggests that there may not be a single storage-discharge relationship, such that the validity of using this method to estimate $\Delta S_H(t)$, and the meaning of the resulting values of $\Delta S_H(t)$, is uncertain.

During the three-year study period, $\Delta S(t)$ transitioned from near normal to a decadal drought as indicated by a local groundwater well whose record extended back 62 years. The propagation of this drought through individual catchment stores was used to identify the influence of storage structure on the emergent catchment response to precipitation variability. The results suggest that below average precipitation in March and April of 2016, which lead to a deficit in unsaturated zone storage, set the stage for the drought. By mid-spring, the increase in evapotranspiration the corresponds with leaf-on continued to decreased unsaturated zone storage, preventing the saturated zone below from recharging, despite above average precipitation between May and July. Initially, the draw-down in catchment scale storage was from the unsaturated zone storage deficit. However, as the saturated zone continued to drain without recharge, saturated zone storage declined, resulting in the decadal drought observed in the catchment scale storage and discharge. This cascade of events highlights the importance of understanding the role of landscape structure in controlling the emergent catchment scale storage and discharge response to hydroclimatic forcing in deeply weathered landscapes.

Chapter 3

Streamflow Generation in a Forested Piedmont Catchment

3.1 Introduction

In Chapter 2, the influence of landscape structure in controlling the propagation of a drought through individual catchment stores and the resulting effect on the emergent catchment scale storage was studied using data from the Pond Branch Catchment. As described in Chapter 2 Section 2.2, Pond Branch is a small, forested catchment within the Piedmont Physiographic Province of the eastern United States. However, despite being nearly-completely forested, it has been observed that there is a sharp contrast in the time-scales of response in the streamflow, with a high temporal frequency, rapidly responding quickflow component and a low temporal frequency, slowly changing baseflow component. The contrast in the two time-scales of response would be expected if the catchment contained a large impervious area or was otherwise human impacted, but that is not the case for Pond Branch. This unexpected behavior motivates the questions addressed in this chapter, which focuses on understanding the generation of the baseflow and quickflow components of streamflow and how that generation is influenced by Piedmont landscape structure.

More broadly, interest in studying the influence of structure on the baseflow component of discharge is motivated by previous research within the Piedmont Physiographic Province and in other landscapes underlain by deeply weathered bedrock, which suggests saprolite controls the baseflow component of discharge (Bachman et al., 1998; Cleaves et al., 1970; Ocampo et al., 2006). See Chapter 2 Section 2.1 for a detailed description of Piedmont landscape structure. In addition, this saprolite has been identified as a vital reservoir of water in arid and semi-arid mountainous terrain (Holbrook et al., 2014; Riebe et al., 2016), highlighting the importance of understanding its storage and release of water. The previous chapter also discussed the potential of storage within the saprolite to influence dynamic catchment scale storage during a drought. However, up until now, few if any studies have used direct observations of discharge from the hillslope and underlying saprolite in order to relate the quantity of water released from storage to the quantity of streamflow, particularly the baseflow component. Here discharge from two hillslope springs is used to test the hypothesis that the quantity of baseflow can be accounted for by water released from hillslope storage. This hypothesis is not original; however, this may be the first time where it is tested by making direct comparisons between hillslope and baseflow discharge.

Additional interest in studying the generation of the quickflow component of streamflow is motivated by numerous previous studies which relate runoff generation mechanisms and landscape structure to the quickflow response (Dunne & Black, 1970b; Hewlett & Hibbert, 1967; Sidle et al., 2000). Since the 1930s, many runoff generation mechanisms have been proposed including: (1) direct precipitation onto the stream channel (Hursh & Brater, 1941); (2) infiltration excess overland flow, known as Hortonian overland flow (Horton, 1933); (3) subsurface stormflow (Hewlett & Hibbert, 1963; Hursh & Brater, 1941); (4) saturation excess overland flow (Dunne & Black, 1970b); and (5) groundwater ridging (Abdul & Gillham, 1984; Sklash & Farvolden, 1979). In a given catchment with a specific climate and landscape properties, several of these runoff generation mechanisms may be operating over the course of a storm event, thereby, controlling the overall stormflow response (Figure 3.1). In addition, studies have demonstrated that hydrologic connectivity between hillslopes, riparian areas, and stream channels can be an important part of quickflow generation (Jencso et al., 2009; Jencso & McGlynn, 2011; McGlynn et al., 2004).

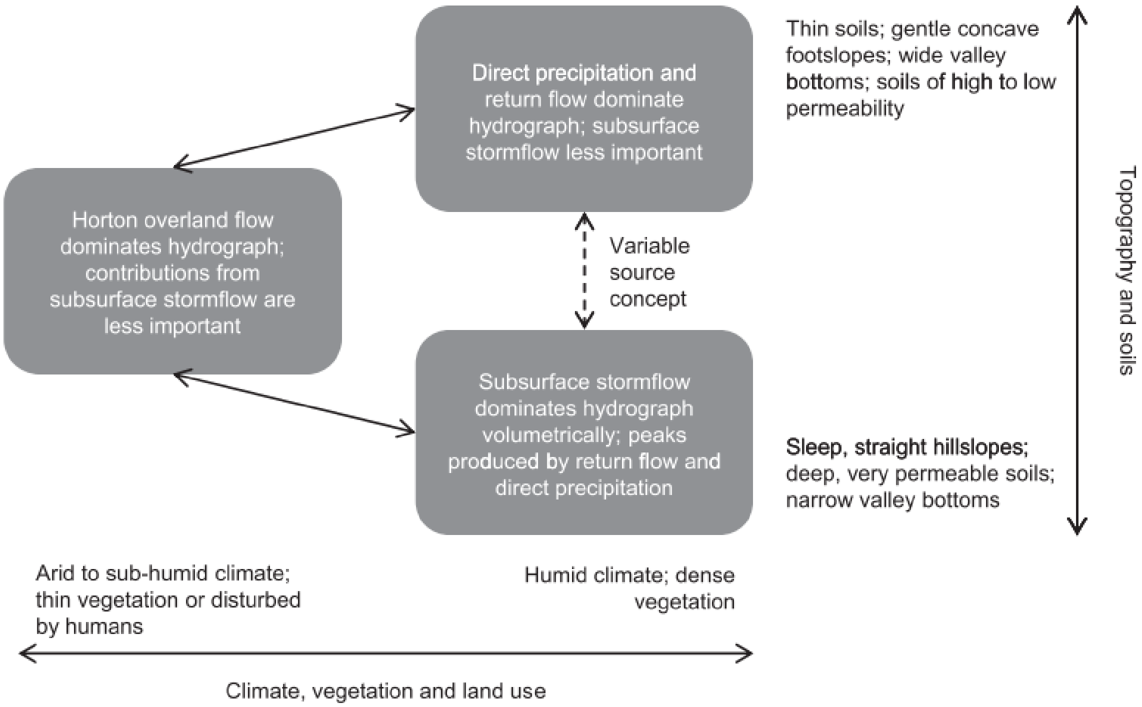
Direct precipitation and return flow dominate hydrograph; subsurface stormflow less important
Horton overland flow dominates hydrograph; contributions from subsurface stormflow are less important
Variable source concept
Subsurface stormflow dominates hydrograph volumetrically; peaks produced by return flow and direct precipitation
Thin soils; gentle concave footslopes; wide valley bottoms; soils of high to low permeability
Sleep, straight hillslopes; deep, very permeable soils; narrow valley bottoms
Topography and soils
Arid to sub-humid climate; thin vegetation or disturbed by humans
Humid climate; dense vegetation
Climate, vegetation and land use

Figure 3.1: Diagram summarizing dominant runoff generation processes as a function of soils, topography, climate, vegetation, and land use from Dunne (1983) and reproduced by Wagener et al. (2007).

However, most of the past work on studying quickflow generation has been conducted in steep watersheds with thin soils overlying impermeable bedrock and narrow valley bottoms with streams tightly coupled to the hillslopes. In contrast, little research on runoff generation mechanisms and hillslope-riparian-stream hydrologic connectivity has been conducted in low-relief watersheds with deeply weathered bedrock and an unconfined stream network coupled to a large riparian area. In fact, Jencso et al. (2009) highlighted this shortcoming within the literature when they made the argument that they could directly compare the behavior of their catchment to the majority of other research catchments since they all shared similar physical attributes, including Maimai, Hubbard Brook, Coweeta, and HJ Andrews. This lack of research in low-relief, deeply weathered catchments, motivates the hypotheses tested within this chapter surrounding the relationship between landscape structure and quickflow generation within the Pond Branch Catchment. These hypotheses are developed in an iterative process which starts by making inferences from the data, conducting a test, analyzing the result, accepting or rejecting the hypothesis, and creating a new hypothesis if needed. The first hypothesis used to start this iterative process is that the quantity of quickflow can be accounted for by the quantity of runoff which could be generated from direct precipitation on to the riparian area.

Data from the Pond Branch Catchment are used throughout this analysis in order to test hypotheses that relate Piedmont landscape structure to streamflow generation. A brief overview of Pond Branch is provided here, however, see Chapter 2 Section 2.2 for additional details. Pond Branch is a 37-hectare catchment located 12 kilometers north of the northern boundary of Baltimore City, Maryland, within the Piedmont Physiographic Province (Figure 3.2). The catchment is almost entirely forested, with only three percent herbaceous vegetation overlying a gas pipeline right-of-way that bisects the catchment (Cleaves et al., 1970). The bedrock is composed of uniform, medium- to coarse-grained biotite-plagioclase-muscovite-quartz schist (Otton et al., 1975), which has weathered in place to form up to 25 m of saprolite under the hillslopes (Cleaves et al., 1970; St Clair et al., 2015). Overlying the saprolite is one to two meters of soil, which grades from channery loam on the ridgetops to silt clay loam and silt loam in the valley bottom (Duncan et al., 2015; NRCS Soil Survey). Elevations range from 132 to 194 m above sea level and slopes range from 0 to 45 degrees, with a mean of seven degrees within the Pond Branch Catchment. For the purposes of this analysis, the landscape is divided into hillslope, riparian, and swale landscape units based partly on the contrast in slope and contributing area. The mean annual temperature is 13 ºC (1981-2010 climate normals at Baltimore Washington International Airport) (NOAA NCEI), the mean annual precipitation is 1064 millimeters (mm) (NOAA NCEI), and the mean annual specific discharge is 368 mm. Instrumentation installed in Pond Branch is described in the next section. Data from this instrumentation network are used to both generate and test hypotheses that relate landscape structure to the generation of streamflow within deeply weathered landscapes.

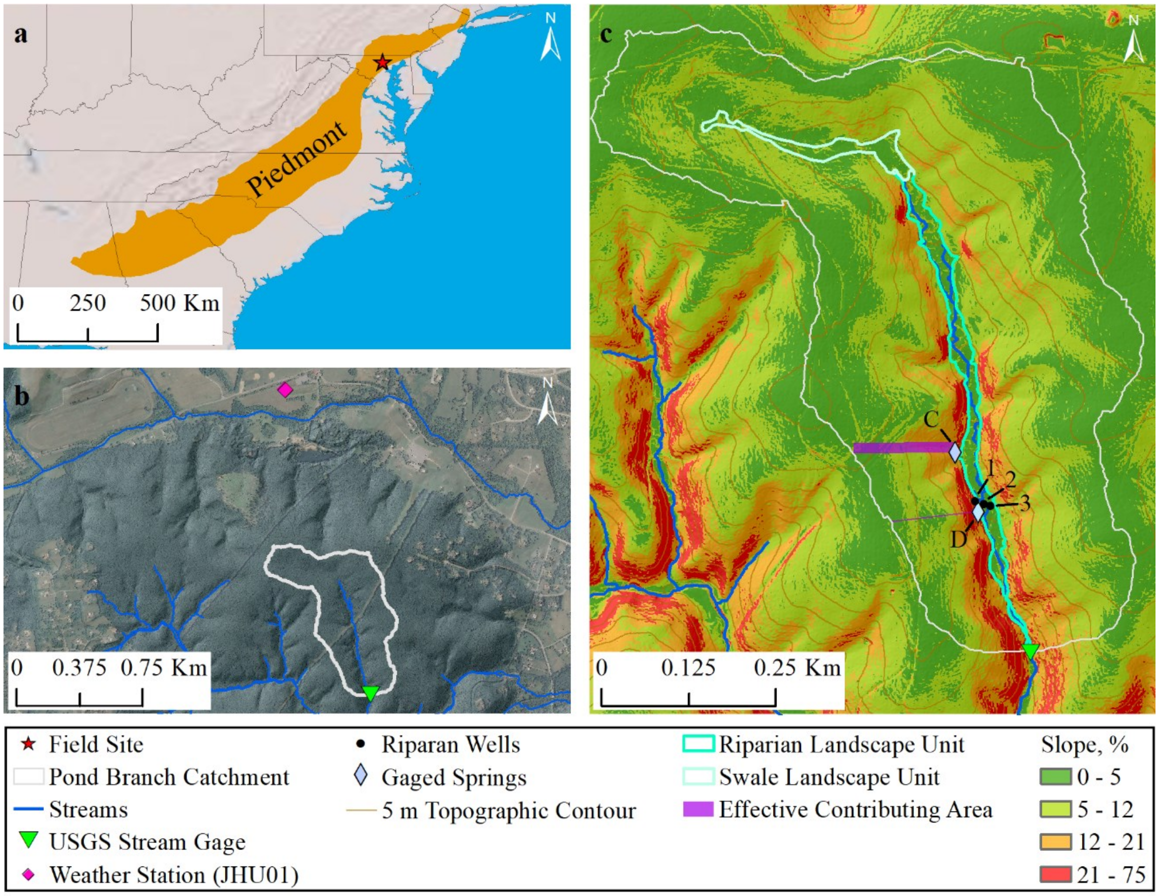
a
N
Piedmont
0 250 500 Km
b
N
0 0.375 0.75 Km
c
N
C
1
2
3
D
0 0.125 0.25 Km
★ Field Site
Pond Branch Catchment
Streams
USGS Stream Gage
Weather Station (JHU01)
● Riparan Wells
Gaged Springs
5 m Topographic Contour
Riparian Landscape Unit
Swale Landscape Unit
Effective Contributing Area
Slope, %
0 - 5
5 - 12
12 - 21
21 - 75

Figure 3.2: (a) A map of the eastern United States with the Piedmont Physiographic Province shaded in orange and the location of the study site (39º 29' 03" N, 76º 41' 17" W) denoted by a red star. (b) Orthoimage of the study site with the location of the Pond Branch Catchment boundary, USGS Stream Gage, and JHU01 Weather Station. This image also shows the dominance of forest cover in the Pond Branch Catchment. (c) Detailed map of the Pond Branch Catchment with instrumentation including the USGS Stream Gage at the outlet, riparian wells, and gaged hillslope springs. The numbers "1," "2," and "3" on the map correspond to the riparian well numbers, while the letters "C" and "D" refer to the convergent and divergent hillslope springs, respectively. The outline of the riparian and swale landscape units are shown, with the remainder of the catchment area defined as the hillslope landscape unit. These units are delineated in part based on the contrast in slope between the steep toe of the hillslope and the relatively flat swale and riparian landscape units. In purple is the estimated effective contributing area for each hillslope spring.

3.2 Methods

3.2.1 Instrumentation & Data Collection

The study site was instrumented in the summer and fall of 2014 in order to supplement the existing Baltimore Ecosystem Study (BES) Long Term Ecological Research Network (LTER) infrastructure. Figure 3.2 shows the location of all instrumentation used to generate data for this analysis, including two United States Geological Survey (USGS) stream gages, two gaged hillslope springs, three riparian wells with pressure transducers, and a weather station (JHU01). Details about the gap-filling technique used to estimate a continuous 15-minute time series of discharge from the USGS Pond Branch gage data, the corrections applied in order to estimate riparian water levels from the pressure transducer data, and the JHU01 weather station used to measure precipitation amount, are described in Section 2.3.1 of Chapter 2. Information about datasets unique to this chapter or modifications made to previously introduced datasets are described in the following paragraphs and sections.

Discharge from two hillslope springs is calculated every 15-minutes between November 2014 and June 2017 using two custom made gages. The two springs are located within a meter upgradient of the break-in-slope at the toe of the western hillslope of the Pond Branch Catchment. The springs are approximately 90 meters (m) apart along a north-south axis within the lower one-third of the catchment. The western most well, Well #1, of the riparian well transect is located approximately 15 m north of the southern-most spring. The northern spring is at the base of a hillslope with concave plan curvature and is referred to as the convergent hillslope spring, while the southern spring is at the base of a hillslope with convex plan curvature and is referred to as the divergent hillslope spring. The words convergent and divergent refer to the topographic surface of the hillslope upgradient of the two springs. Each spring is outfitted with a gage composed of a 45º v-notch weir cut into a five-gallon bucket containing a pressure transducer (Solinst Levelogger) and a staff gage. A plastic barrier is installed on either side of the bucket to redirect all flow through the gage (Figure 3.3a) and then the entire area between the gage and the source of the spring is covered in a plastic tarp to prevent direct precipitation onto the saturated area created by the spring (Figure 3.3b). Water levels are read-off from each staff gage each week, as well as before and after downloading the data from the pressure transducers.

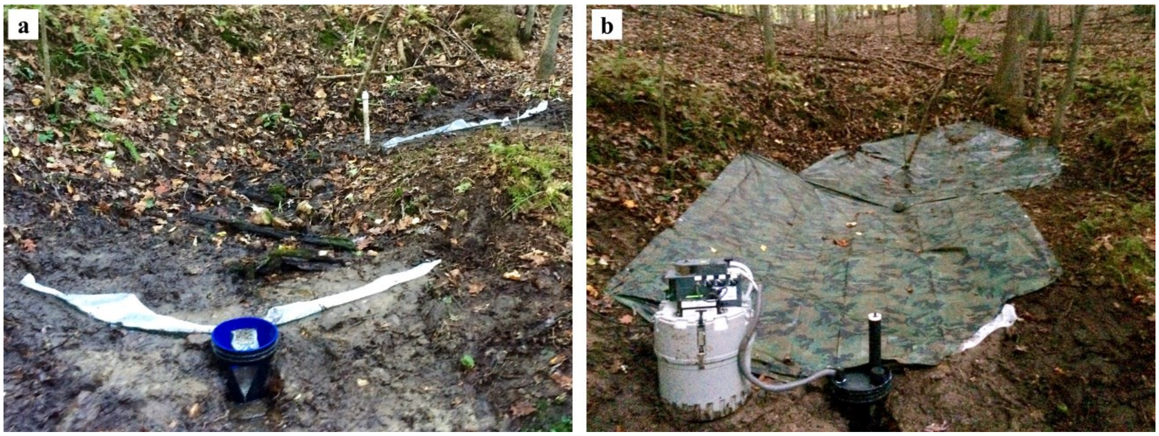

Figure 3.3: (a) Image of the convergent hillslope spring during the construction of its gage. Shown are the plastic barriers used to redirect flow toward the bucket containing a 45º v-notch on the downslope side. (b) Image of the completed convergent hillslope spring gage including the plastic tarp used to prevent direct precipitation on to the saturated area between the gage and the source of the spring. This image was taken at a similar location as the previous one but at a slightly different angle, such that you can see the convergent area upslope of the source of the spring. Note that the instrument in the lower left-hand corner of the image is an autosampler which is used for a different study.

The 15-minute time series of discharge for each spring is calculated by first taking the rolling one-hour averages of the spring's pressure transducer data and the atmospheric pressure measured in the headspace of one of the riparian wells by a Solinst Barologger. The smoothed atmospheric pressure is then subtracted from the spring's smoothed pressure data to get the water level within the gage. A time series of offsets between the water levels recorded from the staff gage and the water levels measured by the pressure transducer is then constructed and used to bring the pressure transducer data into agreement with the manual observations. These adjusted water levels are used along with the weir equation for a 45° v-notch weir (Kulin & Compton, 1975) to calculate the 15-minute discharge time series. Finally, the discharge estimated from the weir equation is compared to manual discharge measurements in order to check the accuracy of the calculated discharge.

The 15-minute time series of riparian water levels described in Section 2.3.1 of Chapter 2 for each of the three wells shown in Figure 3.2 are converted from the depth of water below the land surface to meters above sea level (mASL). In order to convert the water levels to mASL, the relative elevation of the land surface at each well is first determined by constructing a topographic profile from the toe of the hillslope at Well #1 to the left bank of the Pond Branch channel at Well #3. This profile is constructed by laying a tape measure along the ground in a straight line between Well #1 and Well #3 and measuring the relative elevation along the line using a hand level and leveling rod. The relative elevation measured by the topographic profile is converted to mASL using the elevation of Well #1, which is determined in ArcGIS from a 1-m resolution digital elevation model (DEM) and the position of the well measured by a Global Navigation Satellite System (GNSS) device (Trimble Geo 7X). Note that the DEM and GNSS could have been used to construct the entire topographic profile, however, the accuracy of the relative elevation between each well would have been reduced as a result of the uncertainty in the positions measured by the GNSS device as well as the 1-meter resolution of the DEM. Given the elevation of each well in mASL, the depth of the water level below the land surface is converted to the elevation of the water in mASL. The elevation in mASL of water level at each well can then be compared between the wells and to the stage within the Pond Branch channel.

3.2.2 Baseflow Separation

The quantity of streamflow measured at the Pond Branch Catchment outlet is separated into baseflow and quickflow components using a recursive digital filter. The two-parameter filter suggested by Eckhardt (2005) is applied to the smoothed, gap-filled discharge data for Pond Branch to construct a time series of baseflow. The gap-filled discharge data are smoothed by taking a six-hour rolling mean of the 15-minute data prior to conducting the baseflow separation, in order to prevent the digital filter from interpreting diel fluctuations in discharge created by evapotranspiration as storm events. In addition, the digital filter is only applied for the three hours prior to any measurable precipitation (0.254 mm) and the 12 hours after the last measurable precipitation of a storm event to further reduce spurious separations created by instrument noise and diurnal fluctuations. However, this means that all discharge outside of this window is assumed to be baseflow, such that discharge is assumed to be composed only of baseflow 12 hours after the end of a storm. Precipitation amount is measured at the JHU01 weather station as previously described. The two parameters of the digital filter, the recession constant (a) and the maximum baseflow index (BFI_{max}), are selected so that the hydrograph is separated based on the time-scale of response of the discharge, i.e. so that baseflow corresponds to the slowly changing component of discharge and quickflow corresponds to the “flashy” or quickly changing component of discharge. Here an a of 0.999 and a BFI_{max} of 0.85 are used to achieve this separation of time-scales. It should be noted that the quantity of total baseflow estimated using this method represents the lower bound in terms of the amount of stored water released to discharge, since a proportion of the quickflow may be composed of stored, pre-event water that is rapidly liberated during storm events. The quickflow component is calculated by subtracting the baseflow from the 15-minute gap-filled discharge data during the three hours prior and 12 hours after a storm event.

3.2.3 Stream Stage Estimation

The water surface elevation of the Pond Branch stream is estimated at the riparian well transect based on the assumptions that (1) the discharge measured at the Pond Branch Catchment outlet can be scaled by relative catchment areas to give the discharge at the riparian transect, (2) bankfull discharge in the stream approximately corresponds with the 1.5-year recurrence interval event, and (3) that the stage-discharge relationship below bankfull can be approximated by Manning's Equation: $Q = (\sqrt{S_f}/n)AR^{\frac{2}{3}}$ with a constant value of $\sqrt{S_f}/n$. The first step in this analysis is scaling the gap-filled 15-minute time series of discharge measured at the Pond Branch Catchment outlet from October 1, 2000 until September 30, 2017 by the fraction of the total catchment area upstream of the riparian wells. The area upstream of the riparian wells is estimated in ArcGIS using a sink-filled, 1-m resolution DEM to calculate the flow direction and accumulation, a pour point defined at the riparian well transect, and the Watershed Spatial Analyst tool. The resulting area is 80.5% of the entire Pond Branch Catchment area. The scaled discharge is then used to estimate the bankfull discharge by performing a flood frequency analysis using the 17 years of available data and assuming that bankfull occurs at a 1.5-year recurrence interval

(Wolman & Miller, 1960). Given this bankfull discharge (Q) and the bankfull geometry of the channel measured in the field (cross-sectional area (A) and wetted perimeter (R)), Manning's Equation can be rearranged to solve for the friction slope $\left(S_f\right)$ and roughness coefficient (n) as a lumped constant: $\sqrt{S_f}/n$. The 1.5-year discharge was estimated to be $Q = 0.0821$ $\mathrm{m^3s^{-1}}$, and the cross-section geometry gives $A = 0.480$ $\mathrm{m^2}$ and $R = 0.226$ m, thus $\sqrt{S_f}/n = 0.461$. This value for $\sqrt{S_f}/n$ is then substituted back into Manning's Equation along with the scaled discharge in order to estimate the stage at each moment in time. Note that the channel's cross-section is assumed to be a trapezoid and that any stage estimates which exceed the bankfull depth are inaccurate since the geometry of the flow domain is no longer trapezoidal. Finally, the stage is adjusted using the elevation of the bottom of the channel from the riparian well topographic profile so that its units are meters above sea level.

3.3 Results

The 15-minute time series of precipitation, discharge, and water levels described or estimated in Section 3.2 are displayed in Figure 3.4. All discharge values, including hillslope spring discharge, are normalized by the Pond Branch Catchment area and reported in millimeters per day on the primary y-axis. The spring discharge is also reported on the secondary y-axis in cubic meters per day for clarity.

In the top pane of Figure 3.4, precipitation amount measured by the JHU01 weather station is shown. The intensity in the precipitation exhibits a seasonal signal with higher intensity events in April through October and lower intensity events in November through March. This intensity signal is expected given that precipitation in the warm season is generated by short duration convective storms, while precipitation in the colder months is often associated with long duration low pressure systems. The periods with the highest intensity precipitation generally coincide with the greatest peak quickflow generation as can be seen in panes two and three of Figure 3.4.

In contrast, baseflow does not appear to be related to precipitation intensity, and is generally highest from mid-January through mid-April. Both baseflow and hillslope spring discharge do respond to storm events though, and also exhibit similar longer-term trends in discharge as shown by the weekly averages of the time series. Note that the ground areas where the springs emerge are covered in a tarp to prevent direct precipitation on to the saturated area between the source of the spring and the gage. The rapid component of spring response to storms is therefore a result of either subsurface storm flow, a transient mound of water created at the toe of the hillslope, or some other mechanism not related to saturation or infiltration excess overland flow. Both the largest recorded baseflow and convergent spring discharge occurs on April 6, 2017, while the divergent spring only exhibits a moderate increase in discharge. The largest divergent spring discharge occurs on August 24, 2015, with discharge from the convergent spring also corresponding to one of the largest values and baseflow exhibiting a moderate response. Note that this August storm had the second highest precipitation intensity of any event recorded over the three-year study period and generated significant quickflow. At a longer time scale, there also appears to be a relationship between baseflow and spring discharge with the weekly averages showing similar seasonal trends. For example, the highest baseflow and spring discharge generally occurs in mid-January through mid-April while the lowest generally occurs in late summer and fall. Over the entire three-year study period, baseflow and convergent spring discharge are always greater than zero, while there is a three-week period in late-September and early-October 2016 when the average weekly discharge for the divergent spring is zero. This no flow period for the divergent spring corresponds to the drought period identified in Chapter 2, and indicates that portions of the hillslope disconnect during drought conditions.

The seasonal signal observed in the spring and baseflow discharge is also present in the riparian well water levels; however, the seasonal range in water levels is larger for Wells #1 and #3 than Well #2, with the largest range observed in Well #1. Specifically, the range for Well #1 is approximately double the range of Well #2. The difference in range between Well #2 and #3 appears to result from Well #3 drying down over the summer while water levels in Well #2 remain more consistent. Both Well #2 and #3 are located in the center of the riparian area, Well #3 is positioned between the left bank of Pond Branch and a hollow which separates the hillslope from this well, and Well #2 is located between the right bank of Pond Branch and the hillslope. Notice that the water level in Well #1 is always higher than the water level in Well #2, indicating that flow is from the hillslope toward the riparian area. In addition, the water level in Well #2 and Well #3 is higher than the stage in the channel except for four events, such that hydraulic gradient is almost always from the riparian area toward the channel. Note that the stage for these four events is inaccurate since the level is above the bankfull height and that the flow direction might not reverse in these instances.

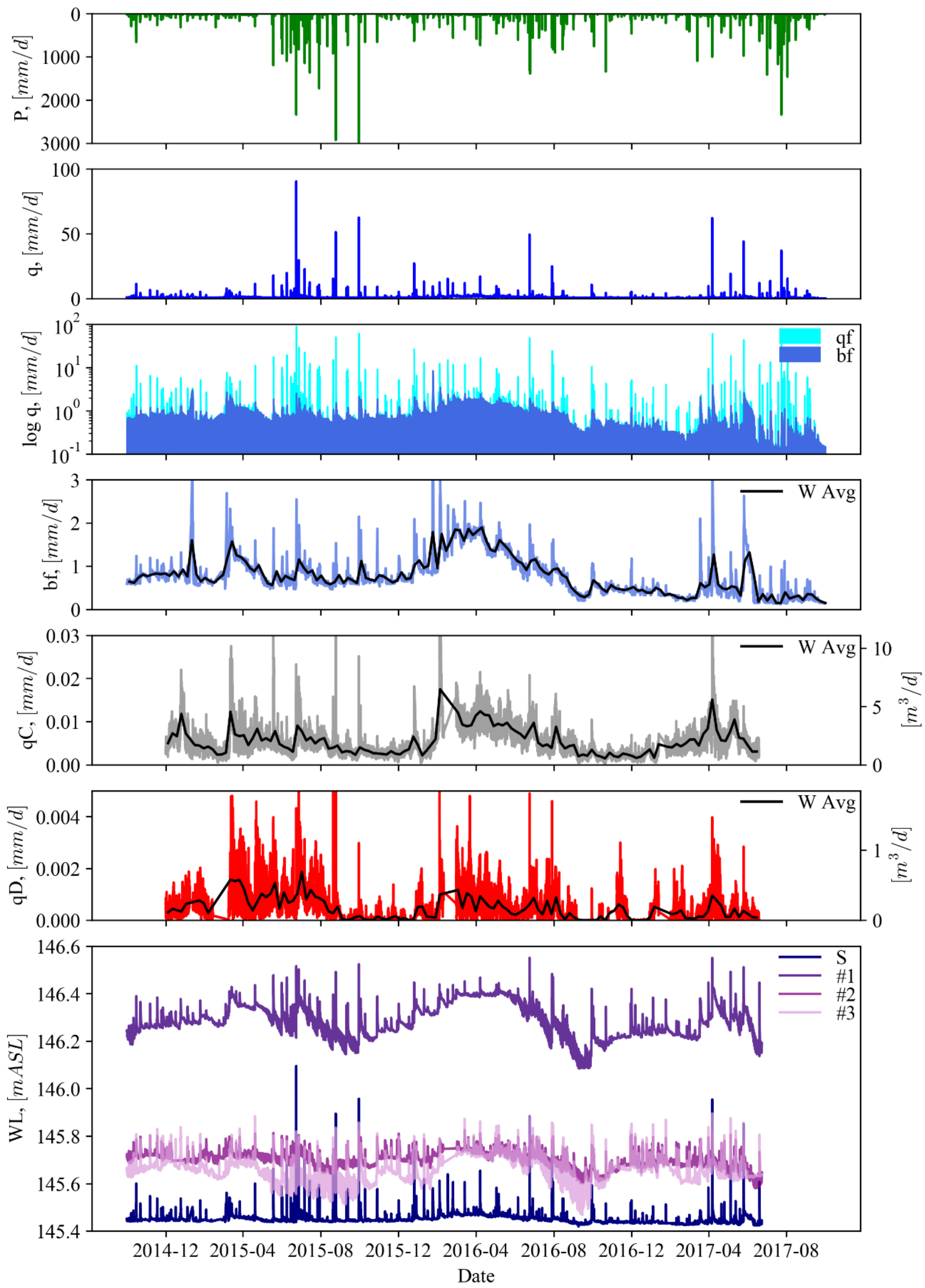

Figure 3.4: Summary of the 15-minute time series that are used in this analysis to study streamflow generation within the Pond Branch Catchment. Precipitation (P), Pond Branch discharge (q), Pond Branch

baseflow (bf), convergent hillslope spring discharge (qC), and divergent hillslope spring discharge (qD) are in units of millimeters per day (mm/d) on the primary y-axis; the logarithmic of Pond Branch discharge (log q) has units of logarithmic mm/d; and the water level (WL) measured in each riparian well and in the Pond Branch channel is in meters above sea level (mASL). Note that all discharge is normalized by the Pond Branch Catchment area but that the discharge for the hillslope springs is included in cubic meters per day on the secondary y-axis for clarity. Pane three shows the results of the baseflow separation of the Pond Branch discharge on a logarithmic scale, with baseflow (bf) in sky blue and quickflow (qf) in cyan. In panes four through six, the largest discharge events are truncated as a result of scaling the y-axis in order to show the variability in the weekly average of the 15-minute time series (solid black line). The numbers in pane seven correspond to the riparian wells labeled in Figure 3.2, while the letter "S" denotes the Pond Branch stage estimate from Section 3.2.3.

3.4 Inferences about Process

3.4.1 Baseflow as Hillslope Storage Release at the Valley Margin

In the previous section, the time series of baseflow and hillslope spring discharge is qualitatively compared to each other and it is found that there are many similarities between the spring discharge and the baseflow both at the high frequency, event scale, and the low frequency, weekly average scale. Even during the drought discussed in Chapter 2, both baseflow and the convergent spring discharge were greater than zero. In addition, the potential of the saprolite underlying the hillslope to act as a large reservoir for hydraulically connected storage is discussed in Chapter 2. Given the potential of the hillslope to store large quantities of water, the position of the springs at the toe of the hillslope, and the observed similarities between baseflow and spring discharge, the hypothesis that the quantity of baseflow can be accounted for by water related from the hillslope landscape unit is tested, where the spring discharge is assumed to be a proxy for hillslope storage.

Note that the alternative hypothesis is that storage within the riparian area or in a portion of the hillslope disconnected from the springs, can account for the quantity of baseflow.

Abductive reasoning can be used to test this hypothesis by determining the contributing area of the spring necessary to account for baseflow, and comparing this area to observations in the field. The first step in this analysis, is to plot the weekly average baseflow for Pond Branch ($Q_{BF}(t)$) against the weekly average discharge for each hillslope spring ($Q_{spring}(t)$) and fit linear regressions to the data. The weekly averages are used as opposed to the 15-minute data in order to reduce scatter in the relationship which might arise from time-lags between spring discharge and baseflow or from evapotranspiration-induced diel cycles in baseflow. The slope of the linear regression (m) represents the ratio of the contributing area of the spring (A_{spring}) to the area contributing to baseflow, which is assumed to be the total hillslope area of the catchment (A_{hill}). The hillslope area is calculated by subtracting the area of the riparian and swale landscape units from the total catchment area; where the area of the riparian and swale landscape units are estimated using ArcGIS to manually demarcate the boundary between the hillslope and these other two units based on the contrast in the slope and contributing area (see Chapter 2, Section 2.2 for additional details). For clarity, the relationship between $Q_{spring}(t)$, $Q_{BF}(t)$, m, and the ratio of A_{spring} to A_{hill} can be expressed as follows:

$$Q_{spring}(t) = mQ_{BF}(t) = \frac{A_{spring}}{A_{hill}} Q_{BF}(t) \tag{3.1}$$

Given m for each linear regression and A_{hill}, which is equal to 0.351 square kilometers, A_{spring} for each spring can be estimated. A_{spring} can then divided by the respective hillslope length (L_{hill}) in order to calculate the effective contributing width of the spring (W_{spring}). The L_{hill} for each spring is determined using ArcGIS to calculate the length of a line drawn perpendicular to the topographic contours from the spring to the approximate drainage divide at the top of the ridge. Finally, W_{spring} can be compared to the width of surface convergence above each spring that is observed within the field. If the width estimated from the regression analysis is similar to the observed width, then the quantity of baseflow can be reasonably explained as water released from hillslope storage via hillslope seeps and springs. This result would also support the hypothesis that the gaged springs are not unique features but are instead the surface expression of exfiltration that occurs all along the valley margin at the toe of the hillslope. Alternatively, if W_{spring} is much smaller than the observed width, then baseflow cannot be accounted for by the release of hillslope storage through the springs, suggesting that baseflow is sourced either from the hillslope but that exfiltration is predominately along deeper flow pathways or is from storage in the riparian area. Finally, if W_{spring} is much larger than the observed width, baseflow can be explained by the release of hillslope storage via the springs. However, this result implies that the springs are not representative of exfiltration along the valley margin but are instead unique features, which may be the product of the subsurface convergence of flow pathways.

The results of this analysis are summarized in Figure 3.5 and Table 3.1. Figure 3.5 shows the plot of the weekly average discharge for the convergent and divergent hillslope spring verses the weekly average baseflow, along with the linear regression (black line). The slope of the linear regression (m) for each spring is summarized in Table 3.1, along with the corresponding coefficient of determination (R^2) and significance level (p-value). The calculated p-values for both springs indicate that there is a significant relationship ($p<0.01$) between spring discharge and baseflow. The higher R^2 between the baseflow and the convergent spring discharge may in part be due to the low signal to noise ratio of the divergent spring discharge, which introduces scatter in the relationship between the divergent spring discharge and the baseflow. Following the procedure outlined above, the contributing area of the spring (A_{spring}) and the effective contributing width of the spring (W_{spring}) are calculated and summarized in Table 3.1. The effective contributing area of each spring is shown in Figure 3.2c by creating a rectangle with width W_{spring} and length L_{hill}. Notice that as would be expected, the effective contributing area of the divergent hillslope spring is much smaller than the effective contributing area of the convergent hillslope spring. The W_{spring} for both the convergent and divergent springs agree with the observed widths of surface convergence above each spring within a factor of two. Therefore, the hypothesis that the quantity of baseflow can be explained as water released from hillslope storage is supported by this analysis. This result further highlights the importance of studying storage within the deeply weathered Piedmont as discussed in Chapter 2, since baseflow makes up a significant proportion of the total discharge from the Pond Branch Catchment.

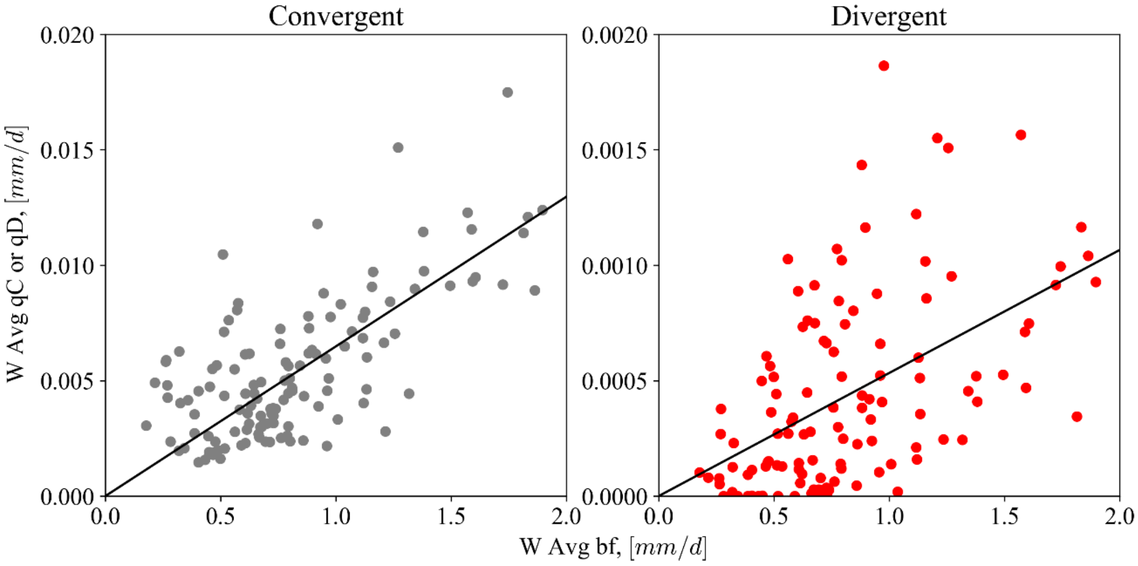

Figure 3.5: Plot of the weekly average (W Avg) discharge for the convergent (qC) and divergent (qD) hillslope spring verses the weekly average baseflow (bf), with linear regression (black line). The slope of each linear regression represents the ratio of the contributing area of the spring to the area contributing to baseflow. See Table 3.1 for the numerical results of the regressions.

Table 3.1: Summary of the slope (m), coefficient of determination (R^2), and significance level (p-value) for the linear regression shown in Figure 3.5 for each hillslope spring. The slope of the linear regression is multiplied by the area contributing to baseflow, which is assumed to be the hillslope area, to calculate the corresponding contributing area of the spring (A_{spring}). A_{spring} is divided by the hillslope length (L_{hill}) in order to calculate the effective contributing width of the spring (W_{spring}). The 99% confidence interval is included for both A_{spring} and W_{spring} as a measure of the bounds within which the observed contributing width must fall within in order to validate the hypothesis that water released from hillslope storage controls the baseflow component of discharge.

Spring	m [-]	R^2 [-]	p-value [-]	A_{spring} [m^2]	W_{spring} [m]	L_{hill} [m]
Convergent	0.00648	0.47	4.8E-24	2278.8 ± 472.5	15.43 ± 3.2	147.7
Divergent	0.00053	0.26	3.8E-09	187.3 ± 76.6	1.49 ± 0.61	125.7

3.4.2 Quickflow as Riparian Runoff

In contrast to the baseflow component of discharge which covaries with spring discharge, the quickflow component of discharge appears to covary with precipitation as discussed in Section 3.3. Specifically, the largest quickflow quantity is produced during the most intense precipitation events; however, quickflow may also vary with precipitation amount since many of the events with the highest 15-minute precipitation intensity also produce the most precipitation over a storm. Quickflow quantity would be expected to vary with precipitation intensity assuming that quickflow is generated in a process such as infiltration excess overland flow. Alternatively, quickflow quantity would vary with precipitation amount if quickflow is generated in a process such as saturation excess overland flow. In the Pond Branch Catchment, the anastomosing stream network is surrounded by the riparian landscape unit where water tables are generally within a meter of the surface and many areas remain saturated throughout the year. The presence of shallow water tables and surface saturated areas suggest that quickflow may be generated from saturation excess overland flow or groundwater ridging from this riparian landscape unit. Given the potential of the riparian area to generate quickflow, the hypothesis that the quantity of quickflow generated can be explained as direct precipitation on to the riparian area is tested. In addition, the quantity of quickflow that could be generated from direct precipitation onto the riparian plus swale area is estimated since the swale is hydrogeomorphically similar to the riparian area, except that it is unchanneled. The alternative hypothesis is that quickflow is generated from the hillslope.

In order to test this hypothesis, the quantity of quickflow ($Q_{QF}(t)$) estimated from the baseflow separation in Section 3.2.2 is compared to the quantity of runoff that could be generated by direct precipitation ($P(t)$) on to the riparian area (A_{rip}) alone and by $P(t)$ onto the A_{rip} plus the swale area (A_{swale}). This hypothesis can be expressed as follows:

$$P(t) \times A_{rip} = Q_{QF}(t) \qquad (3.2)$$

or

$$P(t) \times \ (A_{rip} + A_{swale}) = Q_{QF}(t) \tag{3.3}$$

A_{Rip} and A_{Swale} are estimated using ArcGIS to manually delineate these two areas based in part on the contrast in the slope and contributing area of these two units from the surrounding hillslope landscape unit (see Chapter 2, Section 2.2 for additional details). The left and right-hand sides of Equations 3.2 and 3.3 can be compared by plotting the cumulative sums as well as by calculating the totals over a given period of time.

Figure 3.6 shows the cumulative sum of quickflow and the cumulative sum of runoff that may be generated from precipitation on to the riparian area (3.7% of the catchment area) or the riparian plus swale area (5.1% of the catchment area). The cumulative quickflow is bounded by the other two cumulative estimates, indicating that the quantity of quickflow can be accounted for by direct precipitation on to the riparian area, plus a portion of the swale. Notice that prior to March 2014 the amount of quickflow generated is slightly less than the amount that could be produced by runoff from the total riparian area, meaning that only a portion of the riparian area is needed to explain the quantity of quickflow during that period. Over the entire time series, 91.5% of the quickflow quantity can be explained by direct precipitation on to the riparian area alone. The remaining 8.5% of quickflow is less than the amount that would be generated by direct precipitation on to the swale if it were fully contributing. In summary, the quantity of runoff that may be produced by the riparian area plus a portion of the swale can account for the quickflow quantity. However, the mechanism with which this runoff may be generated cannot be determined without additional information. For example, quickflow may be generated from saturation excess overland flow, groundwater ridging, or even from lateral subsurface stormflow.

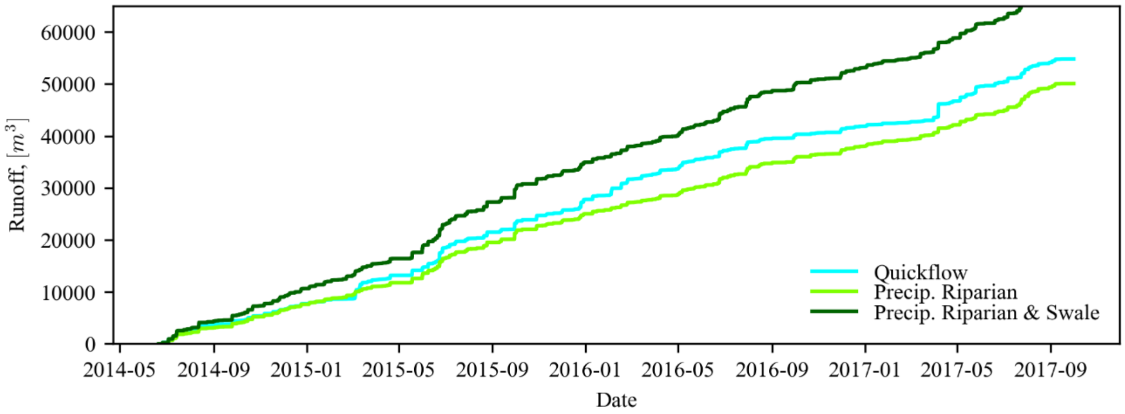

Figure 3.6: Comparison of the cumulative quickflow discharge estimated from baseflow separation and the cumulative runoff which may be generated from direct precipitation on to the riparian area or the riparian plus swale areas. Notice that the quickflow is bounded by the other two cumulative runoff estimates.

3.4.3 Water Table Response to Storm Events

The previous section highlighted the potential of the riparian area to generate quickflow, however, the mechanism or mechanisms with which this quickflow may be generated cannot be discerned without additional information. Here, data from the riparian well transect described in Section 3.2.1 and the stage of Pond Branch calculated in Section 3.2.3 are used to estimate the water table that extends from the toe of the hillslope, across the riparian area and Pond Branch channel. Figure 3.7 shows the location of this transect relative to the location of the demarcation between the hillslope and riparian landscape units as well as to the location of the Pond Branch channel. The presence of Skunk Cabbage (*Symplocarpus foetidus)* below the toe of the hillslope suggests that this area is at or near full saturation for a significant portion of the year, since Skunk Cabbage only grows under these wetness conditions (Fernald, 1950). The response of the water table to individual precipitation events is examined in order to identify how runoff may be generated from the riparian area. Specifically, the hypothesis that groundwater ridging generates quickflow will be explored by looking for a rapid increase in the water table on either side of the Pond Branch channel before an increase in the stage. Alternatively, the intersection of the water table with the surface could indicate that saturation excess overland flow likely generates runoff.

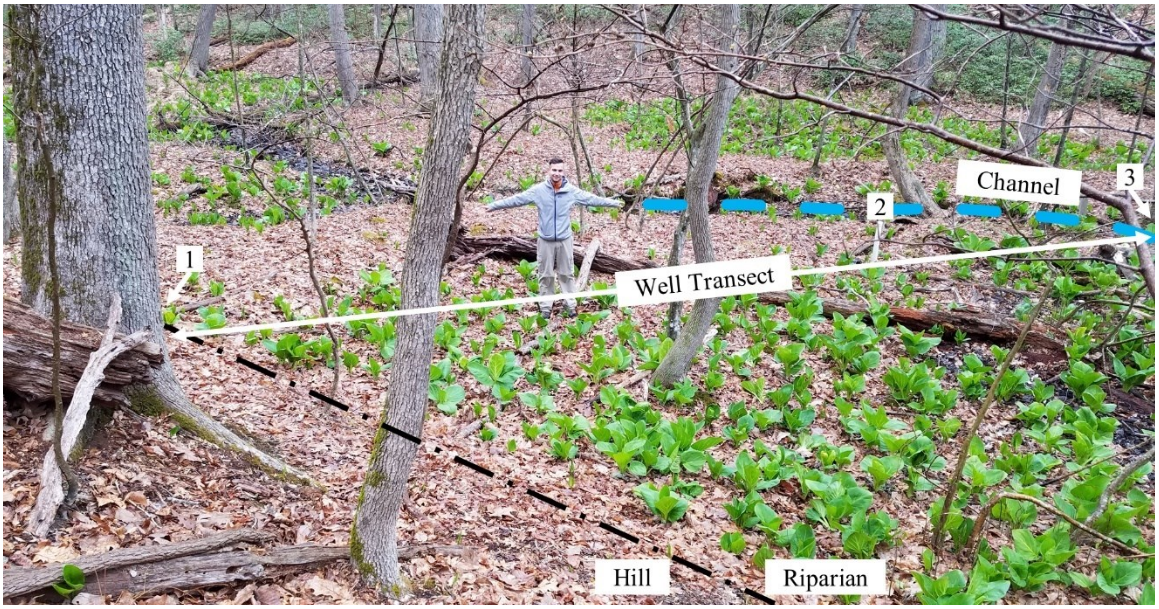

Figure 3.7: Annotated image of a portion of the riparian well transect within the Pond Branch Catchment. The numbers correspond to the well identification numbers. Well #1 is behind the tree in this image, upslope of the break in slope (black dashed line) that divides the hillslope (labeled "Hill") and the riparian landscape units. Well #2 can be seen in this image and is located within five meters of the right bank of the main channel of Pond Branch (labeled "Channel" and shown as a blue dashed line). Well #3 is out of the frame to the right, approximately 2.5 meters from the left bank of Pond Branch. The green leafy plant growing between the break in slope and Well #2 is a patch of *Symplocarpus foetidus* (commonly known as Skunk Cabbage), which only grows in soils at or near full saturation.

The water table from the toe of the hillslope at Well #1 to the left bank of Pond Branch at Well #3 is plotted repeatedly over the course of a storm event for multiple events in order to develop a general understanding of the water table response. Figure 3.8 shows the water table response at four timesteps over two precipitation events. The four selected timesteps are for before the precipitation starts (before), on the rising limb of the hydrograph (mid-event), at the peak stage in the channel (event), and on the falling limb of the hydrograph (post-event). The water table depicted in Figure 3.8a is for a storm on 6/27/15 when catchment storage is high, while Figure 3.8b is for a storm on 11/29/16 when catchment storage is low (see Chapter 2 for more information on the storage state at these times).

In Figure 3.8a, the before event water table is within 10 centimeters (cm) of the surface from approximately 1 meter (m) to 8 m on the transect, which corresponds to the location of the Skunk Cabbage shown in Figure 3.7. At the mid-event time, the water table across the transect has increased such that the water table is just at or below the surface from 1 m to 8 m along the transect and the water levels in Well #2 and #3 are near their maximum levels for the storm. However, the stage has only moderately increased. At the peak of the storm, when the stage in the channel is its highest, the water level at Well #1 has increased such that the water table is at the surface from 1 m to 8 m along the transect. Post-event, the water level in Wells #1 and #3 drop significantly while the water level in Well #2 remains elevated.

In Figure 3.8b, the water table from 1 m to 8 m along the transect is still only 20 cm below the surface before the storm event, despite the fact that the date depicted corresponds almost exactly to the lowest catchment storage observed over the 2015 to 2017 water years. As expected, the stage before the storm event is lower than in Figure 3.8a given the drier conditions. At the mid-event timestep, water levels have increased across the transect, with Well #2 near its maximum level, however, the stage in the channel has only increased slightly. At the peak, when stage is the highest, the well at the toe of the hillslope has increased such that the water table is intersecting the ground surface from 6.5

m to 8 m along the transect. Post-event water levels drop across the transect, remaining the most elevated at Well #2.

In studying the two storms presented in Figure 3.8, as well as numerous other storms under different wetness conditions, precipitation intensities, precipitation amounts, and during both the growing and non-growing season, it appears as though the water table along this transect responds similarly to precipitation events across a range of conditions. In general, the water level before the storm event is determined by the storage state of the catchment as well as the time of the year, since water levels in the riparian area, particularly in those portions disconnected from the hillslope, are drawn down by transpiration in the growing season. At the onset of the storm event the water table rapidly increases, particularly in Well #2, and to a lesser extent in Well #3, however, this increase in water level on either side of the channel does not correspond to the peak stage of the event. Instead, the peak stage occurs once the water level at the toe of the hillslope reaches its maximum level and an area of saturation forms downslope of this toe within the riparian area. Following the storm, the water level in Well #2 remains elevated near its maximum level, despite a significant drop in the stage. These results suggest that groundwater ridging on either side of the channel is not the dominant mechanism of quickflow generation since the peak stage is not reached until the toe of the hillslope reaches its maximum level and since the water level in Well #2 remains near its maximum level post-event despite the stage dropping significantly. Instead, the hillslope seems to control quickflow generation either through subsurface storm flow or by creating saturated zones at the edge of the riparian area where saturation excess overland flow is generated or through some combination of these mechanisms. Additional information is needed in order to determine which mechanism or mechanisms may be generating quickflow, however, the hypothesis that groundwater ridging dominates the quickflow response appears to be unsupported by the evidence.

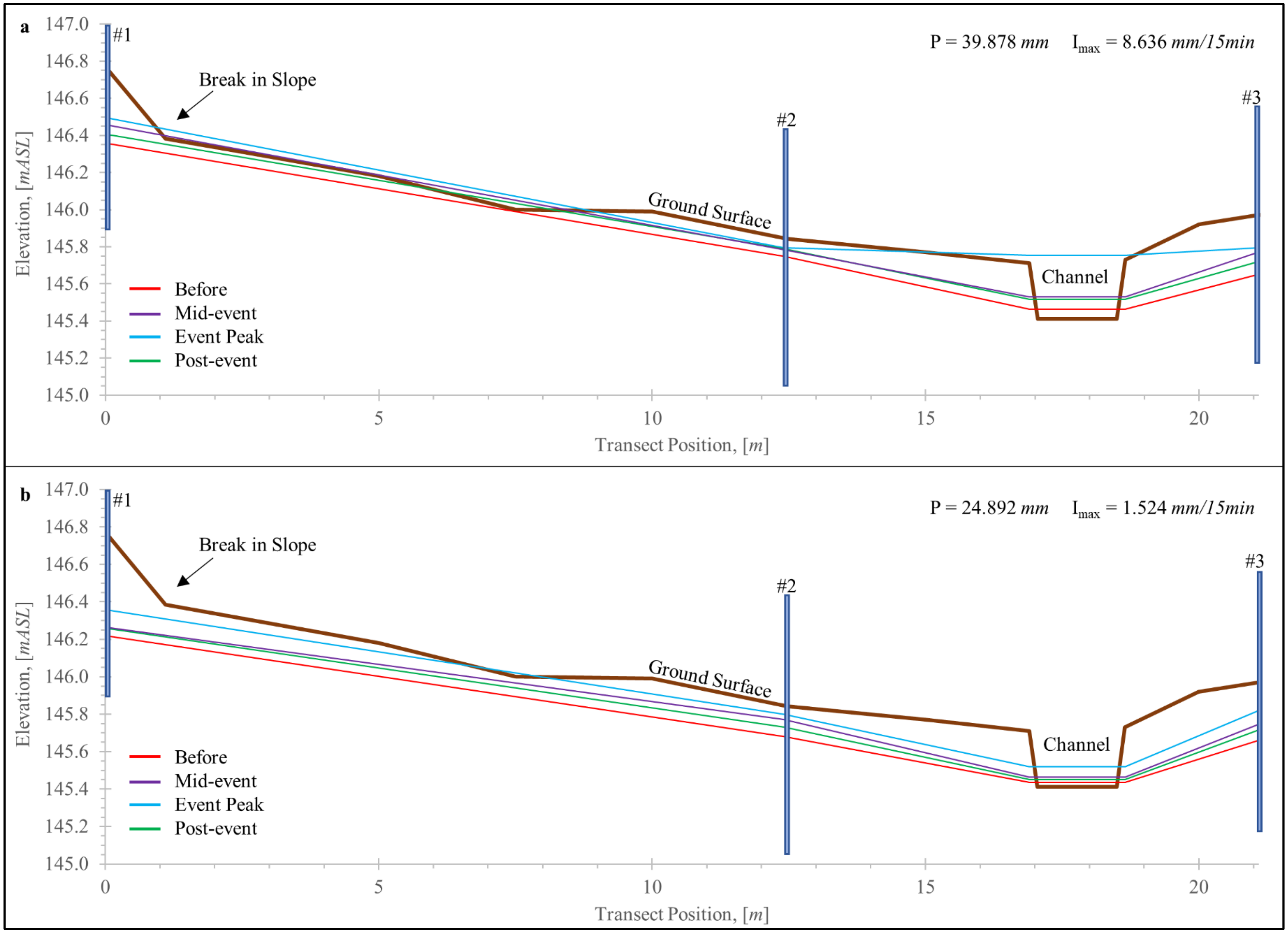
a
P = 39.878 mm
I_{max} = 8.636 mm/15min
#1
#2
#3
Break in Slope
Ground Surface
Channel
Before
Mid-event
Event Peak
Post-event
Elevation, [mASL]
147.0
146.8
146.6
146.4
146.2
146.0
145.8
145.6
145.4
145.2
145.0
0
5
10
15
20
Transect Position, [m]
b
P = 24.892 mm
I_{max} = 1.524 mm/15min
#1
#2
#3
Break in Slope
Ground Surface
Channel
Before
Mid-event
Event Peak
Post-event
Elevation, [mASL]
147.0
146.8
146.6
146.4
146.2
146.0
145.8
145.6
145.4
145.2
145.0
0
5
10
15
20
Transect Position, [m]

Figure 3.8: The topographic profile of the riparian well transect (brown line), with the water table at four time steps over the course of a storm event (before, mid-event, event peak, and post-event). The break in slope denotes the boundary between the hillslope and riparian landscape units with the toe of the hillslope to the left of the break and the riparian unit to the right. The total precipitation amount (P) and maximum precipitation intensity (I_{max}) for each storm is shown in the upper right-hand corner of each plot. (a) The water table response for a storm event on June 27, 2015 with wet antecedent conditions. (b) The water table response for a storm event on November 29, 2016 with dry antecedent conditions.

3.4.4 Hillslope Response to Storm Events

The importance of the hillslope in generating quickflow is discussed in the previous section, however, the mechanism by which the hillslope may influence quickflow generation is not immediately apparent given the riparian water table data alone. Here, the 15-minute time series of discharge from the convergent and divergent hillslope springs is used to further investigate how runoff may be generated in the Pond Branch Catchment. As discussed in the results section, both hillslope springs respond to precipitation events despite their gages being protected by tarps, suggesting that the increased discharge is the result of subsurface stormflow. Still, it is unclear whether this increased discharge from the hillslope makes up a significant proportion of quickflow or whether the increased water levels within the hillslope generate quickflow by creating a zone of a saturation at the toe of the hillslope which produces saturation excess overland flow.

In order to test how the hillslope influences quickflow generation, the volume of discharge produced by each hillslope spring over a storm event is normalized by the contributing area of the spring calculated in Section 3.4.1, scaled by the total hillslope area, and compared to the volume of baseflow and quickflow produced over the same period. By normalizing and scaling each spring's discharge, it is possible to estimate how much hillslope discharge could be produced if all the hillslopes in the catchment responded similarly to the hillslope draining to each spring. This hillslope discharge can then be compared to the baseflow and quickflow quantities to determine if the hillslope discharge from subsurface stormflow alone can account for the quickflow response or if another mechanism, such as saturation excess overland flow, dominates quickflow generation. Multiple storm events over a range of conditions are studied using this approach in order to develop a general understanding of the hillslope response to precipitation events. Here a storm event consists of any measurable precipitation that falls within 12 hours of the last measurable precipitation, such that all storms are at least 12 hours long and separated from all other storms by 12 or more hours. This 12-hour window is chosen since the discharge in the Pond Branch Catchment recesses rapidly back to baseflow following the end of a storm event and is the same window used for the baseflow separation.

The result of analyzing a single storm event to determine if quickflow can be accounted for by discharge from the hillslope is shown in Figure 3.9. During this storm event 566 cubic meters (m^3) of baseflow and 1433 m^3 of quickflow is produced over a period of 19 hours and 15 minutes. The estimated hillslope discharge based on the scaled convergent and divergent spring discharge is 758 m^3 and 700. m^3, respectively. Both hillslope discharge estimates are able to account for the entire volume of baseflow, however, only 13% and 9% of the quickflow volume can be accounted for by the remaining hillslope discharge estimated from the convergent and divergent spring, respectively. In all of storm events studied, the estimated hillslope discharge is at most only able to explain a small percentage of the total quickflow. In fact, in the majority of events the hillslope discharge cannot account for the observed increase in baseflow, which suggests that the temporary increase in baseflow must be the result of the riparian or swale landscape units draining. Since the quantity of quickflow cannot be accounted for by increased hillslope discharge as measured by the hillslope springs, it appears as though subsurface storm flow from the hillslope does not dominate the quickflow response. Instead, the increased water level at the toe of the hillslope seems to control the formation of a saturated zone which produces quickflow via saturation excess overland flow. Note that given the position of the springs a few meters upslope of the toe of the hillslope, it is possible that a mound of water forms at the toe as a result of the tension saturated zone rapidly saturating causing some return flow, however, additional information is needed in order to explore this possible mechanism.

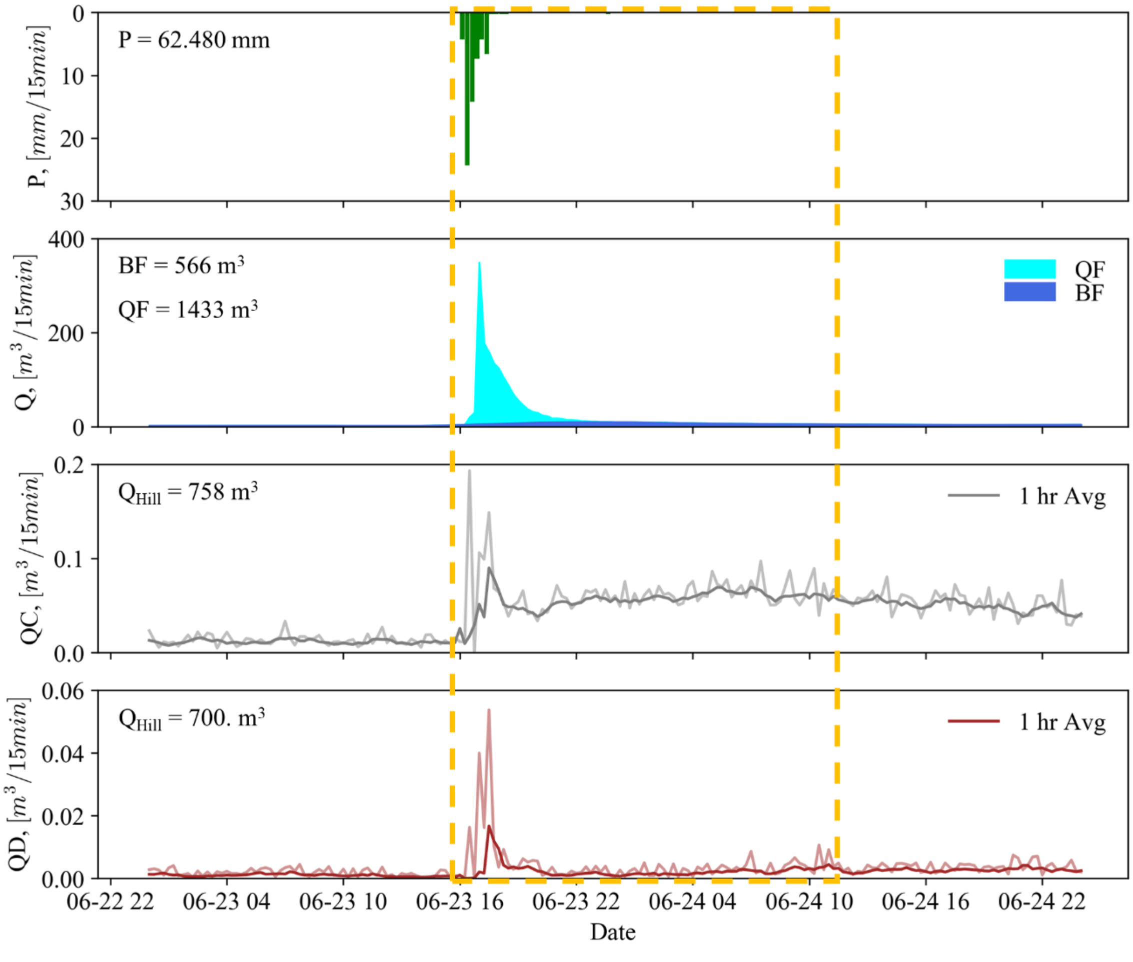

Figure 3.9: Analysis of a storm event that occurred on June 23, 2015 to determine if the quantity of hillslope discharge estimated by scaling the spring discharge can account for the quantity of quickflow. Precipitation

(P), Pond Branch Discharge (Q), convergent spring discharge (QC), and divergent spring discharge (QD) are plotted over a two-day period. Discharge is separated into quickflow (QF) and baseflow (BF) components using baseflow separation as described in Section 3.2.2. The one-hour average (1 hr Avg) of QC and QD is used to calculate the hillslope discharge (Q_{Hill}) though the unsmoothed data produce similar results. The orange dashed-box shows the interval over which the cumulative sum of P, BF, QF, and Q_{Hil} is calculated with values reported in the upper left-hand corner of each corresponding pane. For this storm, all baseflow can be accounted for by hillslope discharge but only a small proportion of the quickflow can be explained.

3.5 Discussion

The results of the analysis presented in Section 3.4.1 suggest that the quantity of baseflow can be accounted for by the release of water from hillslope storage. This conclusion assumes that the hillslope springs are not outliers in terms of discharge but are instead representative of drainage from across hillslopes. This assumption is supported by observations in the field which suggest that discharge occurs all along the toe of the hillslope and that small-scale topographic convergence upslope of the divergent spring captures subsurface flow pathways, creating a spring where hillslope drainage would otherwise occur at the toe. In the Pond Branch Catchment, Cleaves et al. (1970) similarly concluded the hillslope storage, particularly within the saprolite, sustains the baseflow component of discharge, though their conclusions were not supported directly by measurements of hillslope discharge as is the case here. More broadly, Bachman et al. (1998) found that compared to other physiographic provinces within the Chesapeake Bay which are underlain by crystalline and siliciclastic rocks, the Piedmont has a higher baseflow index, which they attributed to the potential of the saprolite to act as an unconsolidated-rock aquifer. Many studies have pointed to saprolite as a vital storage reservoir (Holbrook et al., 2014; Riebe et al., 2016). However, few (if any) studies until now have used direct observations of discharge from the hillslope to test whether baseflow could be accounted for by water released from hillslope storage underlain by this saprolite.

In Section 3.4.2 through 3.4.4 the generation of the quickflow component of discharge is explored, leading to the conclusion that the quickflow quantity can be accounted for by runoff from the riparian area plus a portion of the swale area, and that this runoff generation appears to be controlled by the interaction between the hillslope and riparian area. Specifically, a rapid increase in water level at the toe of the hillslope, raises the water table along the riparian-hillslope boundary, creating a zone of surface saturation where saturation excess overland flow can occur. Note that this mechanism is only observed along a single well transect. However, interestingly, the presence of Skunk Cabbage (*Symplocarpus foetidus*) along the hillslope-riparian boundary in many locations within the catchment suggests that the hillslope's control on the local saturated extent and resulting saturation excess overland flow is not unique to the transect. Additionally, the presence of side channels at the toe of the hillslope throughout much of the catchment seems to support this mechanism as well, whereby the channels are a product of the overland flow downcutting into the riparian soils over time, however, this is just speculation.

Previous studies have highlighted the importance of hillslope-riparian-stream connectivity in influencing the quickflow component of discharge (Jencso et al., 2009; Jencso & McGlynn, 2011; McGlynn et al., 2004; Ocampo et al., 2006). Jencso et al. (2009) concluded that the hillslope water table and its connectivity with the stream network drives runoff generation, while Ocampo et al. (2006) suggested that the perched groundwater within the riparian area and lower poritions of the hillslope drives the runoff response. In contrast, in the Pond Branch Catchment, it appears as though the importance of the hillslope-riparian connectivity is not the direct contribution of hillslope groundwater to runoff, but instead the influence of the hillslope in creating saturated zones at the toe of the hillslope within the riparain area which generates saturation excess overland flow.

The results of this analysis, including the role of different landscape units in controlling the baseflow and quickflow components of streamflow, are presented in a perceptual hydrologic model (Figure 3.10). A perceptual model summarizes one's perceptions of the flow pathways of water through a catchment and how those flow pathways change from between storm events to during an event (Beven, 2012). The structure of the landscape can be incorporated into this type of model along with the results of previous analyses in order to provide a framework for future hypothesis testing. Here subsurface structural data include the depth of soil from the Natural Resources Conservation Service (NRCS) Soil Survey and the approximate depth of the unweathered bedrock inferred from seismic refraction geophysics conducted in April 2014 and reported in St Clair et al. (2015). Figure 3.10 is meant to be representative of both the structure, flow pathways, and mechanisms of streamflow generation throughout the Pond Branch Catchment, however, the location of the water table, zones of surface saturation, springs, and stream channel do vary across the catchment and are therefore approximate in this figure.

The top portion of Figure 3.10 illustrates the landscape structure of the catchment and shows the theorized location of the hillslope water table under normal conditions in the spring and fall as well as under drought conditions. Note that the exact position of the water table is unknown but that the relative range is based on the catchment storage ranges described in Chapter 2, Section 2.4.1. The bottom two boxes show the flow pathways and water table dynamics inferred from the data presented in Figure 3.4 and from the conclusions drawn in the previous sections. In between storm events, the hillslope drains via springs and seepage along the toe of the hillslope to side channels and the riparian area where it maintains baseflow. During the summer time, evapotranspiration induces diurnal cycles in the hillslope and riparian water levels which propagate through to stream discharge. During storm events, increased water levels at the toe of the hillslope raise the water table at the riparian-hillslope boundary, creating saturated zones that produce saturation excess overland flow.

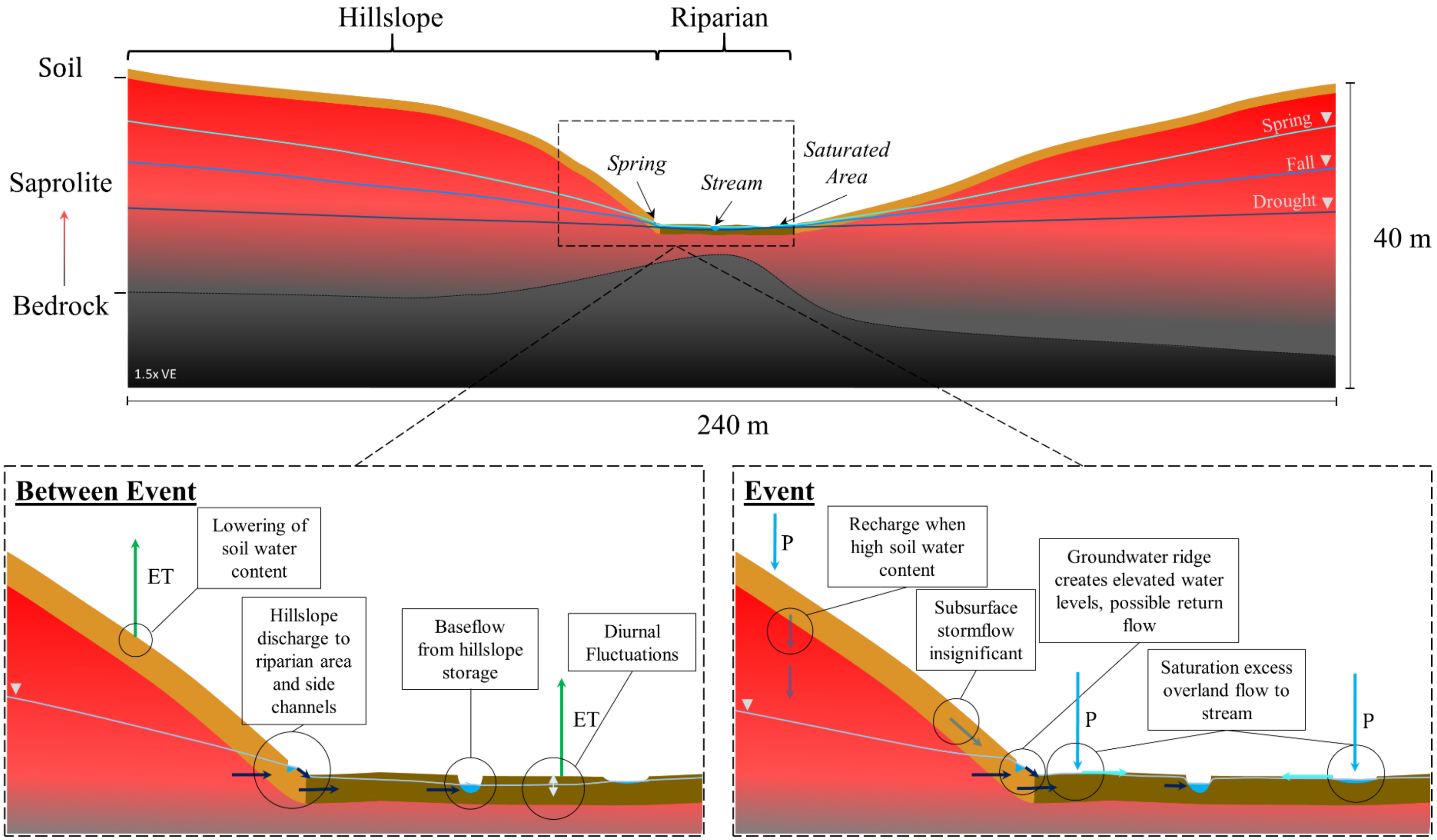
Hillslope
Riparian
Soil
Saprolite
Bedrock
Spring
Stream
Saturated Area
Spring
Fall
Drought
40 m
240 m
1.5x VE
Between Event
Lowering of soil water content
ET
Hillslope discharge to riparian area and side channels
Baseflow from hillslope storage
Diurnal Fluctuations
ET
Event
P
Recharge when high soil water content
Subsurface stormflow insignificant
Groundwater ridge creates elevated water levels, possible return flow
Saturation excess overland flow to stream
P
P

Figure 3.10: Perceptual hydrologic model of the Pond Branch Catchment. The top portion of the figure shows the structure of the landscape including the location of the hillslope and riparian landscape units and its relationship to hydrologic features. The locations of the pictured water tables are approximate but are based on the dynamic range in catchment storage. Note that a vertical exaggeration (VE) of 1.5 is used for this figure. The bottom two boxes show the between event and event response of flow pathways. Between events, hillslope storage sustains baseflow and evapotranspiration (ET) induces diurnal fluctuations in riparian water levels. During precipitation (P) events, water levels at the toe of the hillslope rapidly rise, causing the water table at the hillslope-riparian interface to intersect the surface, creating an area of saturation which generates saturation excess overland flow. This saturation excess overland flow dominates the quickflow component of discharge.

3.6 Conclusions

The goal of this chapter was to study the influence of landscape structure on streamflow generation within the deeply weathered, Pond Branch Catchment of the Piedmont Physiographic Province. Streamflow in the Pond Branch Catchment exhibits two distinct time-scales of response, a slowly changing baseflow component and a rapidly responding quickflow component. These two components of streamflow, baseflow and quickflow, are studied independently in order to unravel the influence of structure on each component. This research is motivated by studies within the Piedmont which have suggested that storage within the saprolite controls the baseflow component of discharge (Bachman et al. 1998; Cleaves et al. 1970), and by the lack of research on runoff generation mechanisms in low-relief, deeply weathered catchments. Here a variety of hydrometric data including precipitation, catchment discharge, hillslope spring discharge, and riparian water levels are used to (1) test whether the quantity of baseflow can be accounted for by discharge from hillslope storage and (2) identify the mechanisms that generate quickflow.

As a first step, baseflow separation is used to construct time series of baseflow and quickflow which can then be compared to the available hydrometric data to draw conclusions. Direct observations of discharge from the hillslope, i.e. from hillslope springs, along with abductive reasoning confirms that the quantity of baseflow can be accounted for by water released from hillslope storage. Multiple mechanisms of runoff generation are explored during this analysis, however, riparian water levels together with spring discharge measurements suggest that quickflow is generated from saturation excess overland flow from zones of saturation at the riparian-hillslope boundary. The zones of saturation appear to form as a result of a rapid increase in the water table driven by increased water levels at the toe of the hillslope. A proportion of quickflow may be composed of return flow from the toe of the hillslope though additional modeling is necessary to confirm this hypothesis. Finally, the results of this analysis are summarized within a perceptual hydrologic model in order show the relationship between flow pathways and landscape structure and to provide a framework for future hypothesis testing.

Chapter 4

Transport Modeling to Elucidate Runoff Generation Mechanisms in a Forested Piedmont Catchment

4.1 Introduction

Many of the foundational theories describing the process of runoff generation, including infiltration excess overland flow (Horton, 1933), saturation excess overland flow (Dunne & Black, 1970a, 1970b), and lateral preferential flow (Mosley, 1979), were developed using estimates of the relative quantities of water produced during a storm event. However, in the late 1960s catchment studies began to use environmental tracers to quantify the composition of water (e.g. Pinder & Jones, 1969), resulting in a revolution in the understanding of runoff generation mechanisms over the last several decades (Beven, 2012; Klaus & McDonnell, 2013). In their 1969 study, Pinder & Jones used the concentrations of a tracer in precipitation and in pre-event water stored in a catchment in order to solve a two-component mixing model and quantify the relative contributions of pre-event water and event precipitation in streamflow. Chemical hydrograph separations of this kind revealed a high contribution of pre-event water in streamflow during a storm event, contrary to the widely-held notion at the time, which assumed that storm event hydrographs were dominated by event precipitation.

The runoff mechanisms proposed to explain the rapidly responding and recessing component of discharge during and immediately following a precipitation event, i.e. quickflow, had to be reconsidered in order to account for the newly discovered phenomenon “that the stream hydrograph responds within minutes to hours of the precipitation input, but the water comprising the hydrograph is often months to years old” (McDonnell et al., 2010). However, this seemingly paradoxical finding can be explained by considering the difference between the flow velocity of water and the celerity of the system, i.e. the velocity with which a pressure wave is propagated through the saturated zone of a watershed. This pressure wave is the result of recharge due to precipitation during an event and causes water stored in a catchment to be rapidly delivered to the stream channel. For example, in the process of groundwater ridging, the tension saturated zone above the water table is rapidly converted to atmospheric pressure by the addition of a small amount of infiltrated water, causing a mound of water to form, which increases hydraulic gradients and drives stored, pre-event water toward channels or seeps (Abdul & Gillham, 1984; Sklash & Farvolden, 1979). The potential of pre-event water to dominate streamflow during storm events has made tracers essential tools in hydrologic studies focused on understanding the complex ways in which landscape structure, runoff generation mechanisms, and flow pathways interact to produce the integrated catchment response represented by stream discharge.

Commonly used environmental tracers include the stable isotopes of oxygen and hydrogen. Naturally occurring oxygen is composed of three stable isotopes: oxygen-16 (^{16}O), oxygen-17 (^{17}O), and oxygen-18 (^{18}O), while hydrogen is composed of two stable isotopes: protium (^{1}H) and deuterium (^{2}H). The relative ratio of each element's isotopes in the precipitation produced during a particular storm event is distinct and is introduced over the entire catchment, therefore, making it possible to "fingerprint" individual storm events and study runoff generation on scales ranging from individual hillslopes to entire watersheds (Kendall & McDonnell, 2006). Unlike many chemical tracers, water isotopes introduced in meteoric waters are relatively conservative and retain their distinctive composition until mixed with water in the landscape (Kendall & McDonnell, 2006).

Environmental tracers can be used to quantify event and pre-event water for individual events. An alternative approach is to use time series of environmental tracers to model transport through a catchment by parameterizing transit time distributions (TTDs). The TTD is the probability density function (PDF) of the ages of the water exiting a control volume (CV) at a specific point in time, i.e. the catchment outlet. The transit time, or age of water, is the amount of time it takes for a given molecule or parcel of water to travel from input into a given CV to output across the system boundary. This CV can be any landscape unit of interest including hillslopes, riparian areas, hyporheic zones of streams (Haggerty, 2002), or catchments as a whole (McGuire & McDonnell, 2006). The distribution of ages of a water sample taken at a fixed point in the landscape is controlled by the spatial distribution of inputs into the CV contributing to the sampling point as well as the physical processes which control the velocities of the individual water molecules that make up the sample (McDonnell et al., 2010). As a result, TTDs can be used as a tool to identify the dominate hydrologic processes, i.e. partitioning, runoff generation, etc., within a landscape unit or an entire catchment (McDonnell et al., 2010).

These TTDs, along with the hydrologic processes they represent, are often estimated using time-invariant (TIV) and steady state assumptions. However, it can be shown that actual catchment TTDs vary with time, showing substantial variation at time scales on the order of days to years as a result of changes in storage or antecedent conditions (McDonnell et al., 2010). Past modeling approaches have sought to overcome this challenge by identifying periods when flow through the system is relatively constant or by assuming TIV TTDs for different flow components and allowing the relative contributions from each component to vary (Roa-García & Weiler, 2010). However, recent advances in transport theory overcome the fundamental theoretical difficulties in accounting for the time-varying (TV) dynamics of hydrologic systems and avoid coupling transport with a hydrologic model (Botter et al., 2011; Harman, 2015; van der Velde et al., 2012).

4.2 Hypothesis Testing Using rSAS

In this work, an approach for modeling lumped solute transport is used that addresses many of the limitations of using time-invariant (TIV) transit time distributions (TTDs). This approach is employed to test hypotheses and relate runoff generation mechanisms to the composition of streamflow. The selected method of representing lumped solute transport, known as the rank StorAge Selection (rSAS) theoretical framework, is that which was presented in Harman (2015). The rSAS approach decomposes a control volume's (CV's) TTD into a part that depends on the time variability and partitioning of hydrologic inputs and a part that depends on the way water of a given age is sampled by the fluxes leaving the CV (Harman, 2015). This age sampling is defined by a cumulative distribution function (CDF) of the age-rank storage ($S_T(T,t)$), known as the rSAS function ($\Omega(S_T,t)$) (Harman, 2015). $S_T(T,t)$ is defined as the volume of water younger than age T at time t, such that a conservation law for this quantity in a catchment can be written as:

$$\frac{\partial S_T}{\partial t}+\frac{\partial S_T}{\partial T}=P(t)-q(t)\overleftarrow{P}_q(T,t)+ET(t)\overleftarrow{P}_{ET}(T,t) \qquad (4.1)$$

where $P(t)$ is precipitation, $q(t)$ is specific discharge, $ET(t)$ is actual evapotranspiration, and $\overleftarrow{P}_q(T,t)$ and $\overleftarrow{P}_{ET}(T,t)$ are the cumulative TTDs for q and ET, respectively (Harman, 2015). By definition and based on a simple mass balance of storage, $\overleftarrow{P}(T,t)$ for a given flux is equal to $\Omega(S_T,t)$ under a change of variable (Harman, 2015). Equation 4.1 can be solved using parameterized $\Omega(S_T,t)$ and estimated hydrologic fluxes (P, q, ET) in order to calculate the time-variable (TV) $\overleftarrow{P}(T,t)$ for each flux out of the catchment (Harman, 2015).

Figure 4.1 illustrates the basic operation of the rSAS modeling framework. In this framework, rainfall is assumed to be age zero when it enters a CV of interest, such as a catchment, and then ages as a function of time elapsed. The distribution of the ages of water selected from the outflow of the CV is determined by the parameterized rSAS CDF, $\Omega(S_T,t)$. At any given time, the proportion of ages selected by the $\Omega(S_T,t)$ determines the $\overleftarrow{P}(T,t)$, such that the TIV $\Omega(S_T,t)$ can be used to estimate the TV $\overleftarrow{P}(T,t)$. Each flux out of a CV has its own $\Omega(S_T,t)$, who's CDF and parameter set are theorized to be controlled by the hydrologic processes, i.e. partitioning, runoff generation mechanisms, etc., which control the composition of the flux. In Harman (2015), a uniform distribution for the $\Omega(S_T,t)$ of ET ($\Omega_{ET}(S_T,t)$) and a gamma distribution for the $\Omega(S_T,t)$ of q ($\Omega_q(S_T,t)$) are chosen to represent each flux. The use of a uniform distribution for $\Omega_{ET}(S_T,t)$, which uniformly selects from an S_T of zero to a maximum S_T (S_{Tmax}), is based on the assumption that the root zone contains the youngest water in the age-rank storage and that water is selected without bias from this zone (Harman, 2015). A gamma distribution is chosen for $\Omega_q(S_T, t)$, with shape parameter α_q and scale parameter θ_q, given its ability to reproduced the $1/f$ spectral filtering of white noise from precipitation (Harman, 2015; Kirchner et al., 2000). The parameters of these two distributions (S_{Tmax}, α_q, θ_q) in Harman (2015) are optimized to match the observed tracer concentration before being interrogated in order to relate their values to physical storage quantities.

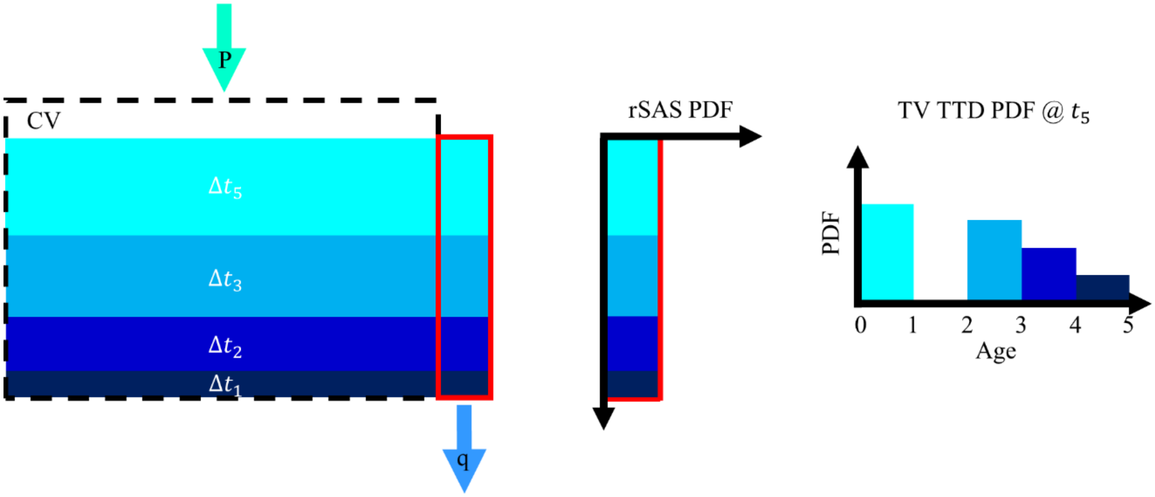

Figure 4.1: Diagram illustrating the basic concepts of the rank StorAge Selection (rSAS) theoretical framework and the relationship between a rSAS function's probability density function (PDF) and the corresponding time-variable (TV) transit time distribution (TTD). Precipitation (P) enters a control volume (CV) with age zero and then ages as a function of the time (t) elapsed. The water stored in a given CV is ranked by age (shown here conceptually), with the younger water (Δt_5) stacked over the older (Δt_1). Note that Δt_4 is missing from the control volume, indicating that there was no precipitation during that interval. The rSAS function's PDF, here a uniform distribution, specifies the proportion of water of a given age selected from the CV by discharge (q). At each time step, the rSAS PDF determines the TTD, here shown for t_5, where t_5 is the time at the end of Δt_5.

Here, the rSAS framework is used for hypothesis testing by translating competing runoff generation mechanisms into $\Omega(S_T, t)$ distributions based on the physical selection process of a mechanism and then calibrating the resulting distributions to reproduce tracer transport at the catchment scale. The transport modeling results are compared to tracer data in order to gain insights and determine if the hypothesis is plausible. This framework of hypothesis testing and gaining insights into catchment processes by comparing modeled predictions to observations is similar to the model-data learning approach discussed in Thompson et al. (2013). In this regard, the flexibility of rSAS allows a more rigorous testing of qualitative insights about a physical process by transferring those insights to a testable mathematical model with physically meaningful parameters.

In Chapter 3, the change in the water level in or flux from different landscape units is used to test competing runoff generation mechanisms. However, confidence in the results from this approach alone is limited given the potential for both the movement of parcels of water as well as the propagation of a pressure wave through the saturated zone to impact water levels and fluxes. Here, an additional layer of information is added, i.e. the isotopic composition of precipitation and streamflow, which is used as a part of the aforementioned hypothesis testing framework in order to continue the investigation of the previous chapter and examine the conclusions drawn from the hydrometric data alone. Specifically, competing hypotheses are tested regarding how quickflow is generated. The two hypotheses both relate to the source of saturation excess overland flow and particularly whether it is (1) dominated by direct precipitation or (2) composed of both stored pre-event water from return flow and direct precipitation. Data from the Pond Branch Catchment including time series of P, q, and ET introduced in the previous chapters are combined with new stable water isotope data for P and q in order to test these hypotheses using the rSAS framework.

4.3 Methods

4.3.1 Instrumentation & Data Collection

A complete overview of the Pond Branch field site is provided in Chapter 2 Section 2.2, however, a brief description is included here for convenience of the reader. Pond Branch is a 37-hectare catchment located 12 kilometers north of the northern boundary of Baltimore City, Maryland, within the Piedmont Physiographic Province of the eastern United States (Figure 4.2). As is common in the Piedmont, the parent bedrock, Loch Raven Schist (Otton et al., 1975), has weathered in place to form up to 25 meters (m) of saprolite under the hillslopes (Cleaves et al., 1970). This saprolite is mantled in one to two meters of soil, which grades form channery loam on the ridges to silt clay loam and silt loam in the valley bottom (Duncan et al., 2015; NRCS Soil Survey). The land cover is 97% deciduous forest and 3% herbaceous vegetation (Cleaves et al., 1970). Elevations range from 132 m to 194 m above sea level and slopes range from 0 to 45 degrees, with a mean of 7 degrees. The contrast in slope and contributing area are used to delineate three landscape units: hillslope, riparian, and swale. The mean annual temperature is 13 ºC based on 1981-2010 climate normals at Baltimore Washington International Airport (NOAA NCEI), the mean annual precipitation is 1064 millimeters (mm) (NOAA NCEI), and the mean annual specific discharge is 368 mm. Streamflow is perennial at the catchment outlet except in exceptional drought conditions and is also characterized by two distinct time scales of response, a rapidly responding quickflow component and a slowly changing baseflow component.

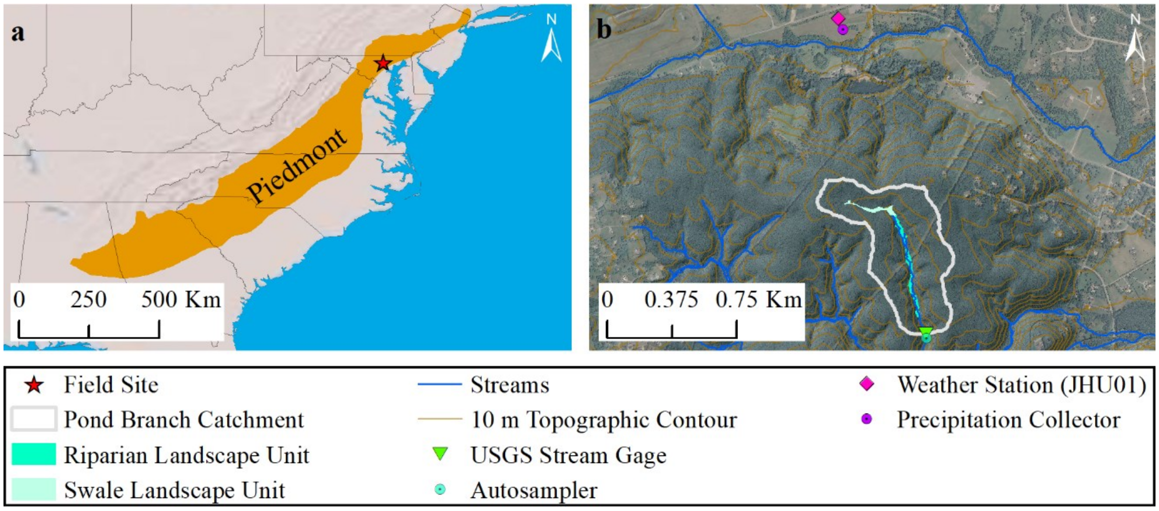
a
N
Piedmont
0 250 500 Km
b
N
0 0.375 0.75 Km
Field Site
Pond Branch Catchment
Riparian Landscape Unit
Swale Landscape Unit
Streams
10 m Topographic Contour
USGS Stream Gage
Autosampler
Weather Station (JHU01)
Precipitation Collector

Figure 4.2: (a) A map of the eastern United States showing the location of the field site (39º 29’ 03” N, 76º 41’ 17” W) relative to state boundaries and the Piedmont Physiographic Province. (b) Detailed map of the field site showing the location of the Pond Branch Catchment boundary, defined landscape units, streams, and all instrumentation used in this chapter. The riparian and swale landscape units are shaded in greenish-blue, with the remainder of the catchment area defined as the hillslope landscape unit. These units are delineated in part based on the contrast in slope between the steep toe of the hillslope and the relatively flat swale and riparian landscape units. A USGS stream gage and an autosampler used to collect 12-hourly water samples are co-located at the catchment outlet, while a precipitation collector used to collect bulk weekly precipitation samples is co-located with the JHU01 weather station. This orthoimage highlights the dominance of forest cover within the Pond Branch Catchment.

The Pond Branch Catchment instrumentation is described in Chapter 2 Section 2.3.1 and Chapter 3 Section 3.2.1 Previously described instrumentation that is used in this analysis is shown in Figure 4.2, which includes the United States Geological Survey (USGS) stream gage located at the Pond Branch outlet and the JHU01 weather station located one kilometer north of the Pond Branch Catchment boundary. Discharge data from the USGS stream gage are gap-filled in order to construct a continuous 15-minute time series of discharge as described in Chapter 2 Section 2.3.1. In Chapter 3 Section 3.2.2, a recursive digital filter (Eckhardt, 2005), is applied to these gap-filled discharge data in order to separate the discharge based on the time-scales of response, i.e. into quickflow and baseflow components. Precipitation amount is measured by a tipping-bucket rain gage at the JHU01 weather station and assumed to be representative of the precipitation amount over the entire Pond Branch Catchment. Potential evapotranspiration is determined in Chapter 2 Section 2.3.2 using the Penman-Monteith Equation and, in part, data from the JHU01 weather station. This potential evapotranspiration estimate is scaled in order to calculate the actual evapotranspiration, where the scale factor is chosen in order to close the water balance over the 2015 water year as described in Chapter 2 Section 2.3.2.

Beginning in January 2014, a broad sampling design is implemented at the study site, which includes the weekly water sampling of six surface water locations, weekly bulk precipitation samples, and 12-hourly water samples from the Pond Branch outlet. As a part of this design, additional instrumentation including a specialized precipitation sampler and a 24-bottle autosampler (Teledyne ISCO compact portable sampler) is deployed at the JHU01 weather station and Pond Branch outlet, respectively (Figure 4.2). The precipitation collector is designed and built to minimize the surface area of the sample exposed to the atmosphere in order to prevent evaporation and the resulting fractionation of the sample following a similar design by Gröning et al. (2012). Since January 4, 2014, bulk weekly precipitation samples have been collected. These samples are collected in a one-dram glass vial with a polyseal cap, parafilmed, and refrigerated until analysis. 12-hourly water samples have been collected from the outlet of the Pond Branch Watershed since June 27th, 2014 using the aforementioned autosampler. Each bottle in the autosampler is pre-filled with one centimeter of mineral oil to prevent evaporation of the sample prior to collection. Once in the lab, the 12-hourly samples are processed using a separatory funnel and coffee filters to remove the mineral oil before preserving an aliquot in the same manner as the precipitation sample. The 12-hourly samples are collected at 3:00 am and 3:00 pm Eastern Standard Time (EST) in order to test against and represent any variability in the composition of the streamflow that may result from diurnal cycling. All water samples are analyzed using a Los Gatos Research Off-Axis Integrated Cavity Output Spectroscopy (LGR OA-ICOS) system for their $^{18}O/^{16}O$ ratios following filtration with a 0.45 micrometer membrane filter. These ratios (R) are reported in delta-notation ($\delta^{18}O$) in units of per mil (‰) according to Vienna Standard Mean Ocean Water (VSMOW), which is defined by the relation: $\delta^{18}O = \left(\frac{R_{sample} - R_{standard}}{R_{standard}}\right) \times 10^3$ ‰ (Faure & Mensing, 2005). Note that a positive value for $\delta^{18}O$ indicates that the sample is enriched in the heavy isotope relative to VSMOW while a negative delta value indicates the sample is depleted in the heavy isotope relative to VSMOW (Faure & Mensing, 2005).

Finally, all of the flux data described above—including discharge, baseflow, quickflow, precipitation, and evapotranspiration—are resampled to a 6-hourly timestep so that observations overlap with the 12-hourly streamflow isotope time series. The 15-minute time series of discharge, baseflow, quickflow, and precipitation are summed over a 6-hour period to get the total flux at 3:00 am, 9:00 am, 3:00 pm, and 9:00 pm EST. The daily evapotranspiration is downscaled by assuming evapotranspiration is zero over the 6-hour intervals which end at 3:00 am and 9:00 am and that the daily evapotranspiration can be divided equally among the remaining two intervals. This method of estimating the 6-hourly evapotranspiration is an approximation, however, given the lack of higher temporal resolution data, which could be used to estimate sub-daily evapotranspiration from the Penman-Monteith Equation, this approximation is selected as the most appropriate compromise between accuracy (using actual daylight hours) and convenience (using a constant interval over time).

4.3.2 rSAS Modeling of Saturation Excess Overland Flow

In order to use the rank StorAge Selection (rSAS) framework to test hypotheses about quickflow generation, the rSAS function for discharge $\Omega_q(S_T, t)$ is first decomposed into its quickflow $\Omega_{qf}(S_T, t)$ and baseflow $\Omega_{bf}(S_T, t)$ components, so that the hydrologic processes which are hypothesized to influence the form of each component's $\Omega(S_T, t)$ can be studied individually. This decomposition results in a new governing conservation law:

$$\frac{\partial S_T}{\partial t} + \frac{\partial S_T}{\partial T} = P(t) - qf(t)\,\Omega_{qf}(S_T, t) + bf(t)\,\Omega_{bf}(S_T, t) + ET(t)\,\Omega_{ET}(S_T, t) \qquad (4.2)$$

where $qf(t)$ is quickflow, $bf(t)$ is baseflow, and the remaining terms are previously defined; note that the cumulative transit time distributions (TTDs) in Equation 4.1 are also replaced by the rSAS functions here. Given this decomposition, the form of the cumulative distribution function (CDF) of $\Omega_{qf}(S_T, t)$ and its parameter set can be specified based on each hypothesis described in Section 4.2. The CDFs and parameters of $\Omega_{bf}(S_T, t)$ and $\Omega_{ET}(S_T, t)$ must also be defined in order to solve Equation 4.2, however, the focus of this chapter is on the generation of quickflow so the functional form of $\Omega_{bf}(S_T, t)$ and $\Omega_{ET}(S_T, t)$ remain fixed for each quickflow hypothesis, while their parameters are optimized.

The specified CDFs of $\Omega_{qf}(S_T, t)$, $\Omega_{bf}(S_T, t)$, and $\Omega_{ET}(S_T, t)$; the 6-hourly hydrologic fluxes described in the previous section; and Equation 4.2, are used to estimate time-varying (TV) transit time distributions (TTDs) for each flux (Harman, 2015). These TV TTDs are then convolved with precipitation δ^{18}O time series, assuming each precipitation event has the same composition as the bulk weekly sample, in order to estimate a 6-hourly time series of modeled streamflow δ^{18}O (Harman, 2015). The modeled δ^{18}O is then compared to the observed 12-hourly δ^{18}O data for streamflow and the parameters of the original $\Omega(S_T, t)$ can be adjusted to optimize the modeled data to the observed tracer data, or left fixed in order to test the ability of the hypothesized runoff generation mechanism to capture the composition of the streamflow. Here a modified version of the Kling-Gupta Efficiency (KGE) is used to measure the goodness-of-fit between the predicted and modeled tracer time series and to optimize select parameters (Kling et al., 2012). The KGE decomposes the mean squared error into correlation, bias, and variability terms so that the relative importance of these different components on the goodness-of-fit can be identified independently (Kling et al., 2012). The ability of each hypothesized runoff generation mechanism and resulting $\Omega_{qf}(S_T, t)$ to capture the variability in the isotopic composition of the streamflow is examined qualitatively in order to draw inferences about process.

4.3.2.1 Direct Precipitation

The first hypothesis tested using the framework described above is that quickflow is generated through saturation excess overland flow and is primarily composed of precipitation. This hypothesis is based on the results of Chapter 3, which suggest that the water level at the toe of the hillslope rises rapidly during a precipitation event, forming a saturated area at the riparian-hillslope boundary where quickflow may be produced as saturation excess overland flow from direct precipitation. Quickflow that is composed largely of direct precipitation will have an isotopic signature that is similar to the isotopic composition of the event water, i.e. of event precipitation. In order to represent this process and test the defined hypothesis, a uniform distribution which selects from an S_T of 0.0 millimeters (mm) to a maximum S_T (S_{Tmax}) of 0.254 mm is chosen for $\Omega_{qf}(S_T, t)$. The value of S_{Tmax} is the resolution of the tipping-bucket rain gage used to measure precipitation, such that $\Omega_{qf}(S_T, t)$ uniformly selects the youngest water in the age-rank storage to compose quickflow (Figure 4.3a). This uniform distribution of $\Omega_{qf}(S_T, t)$ approximates a Dirac delta function since the age-rank storage interval, over which the distribution selects water from storage, is infinitesimally small compared to the overall age-rank storage of the catchment.

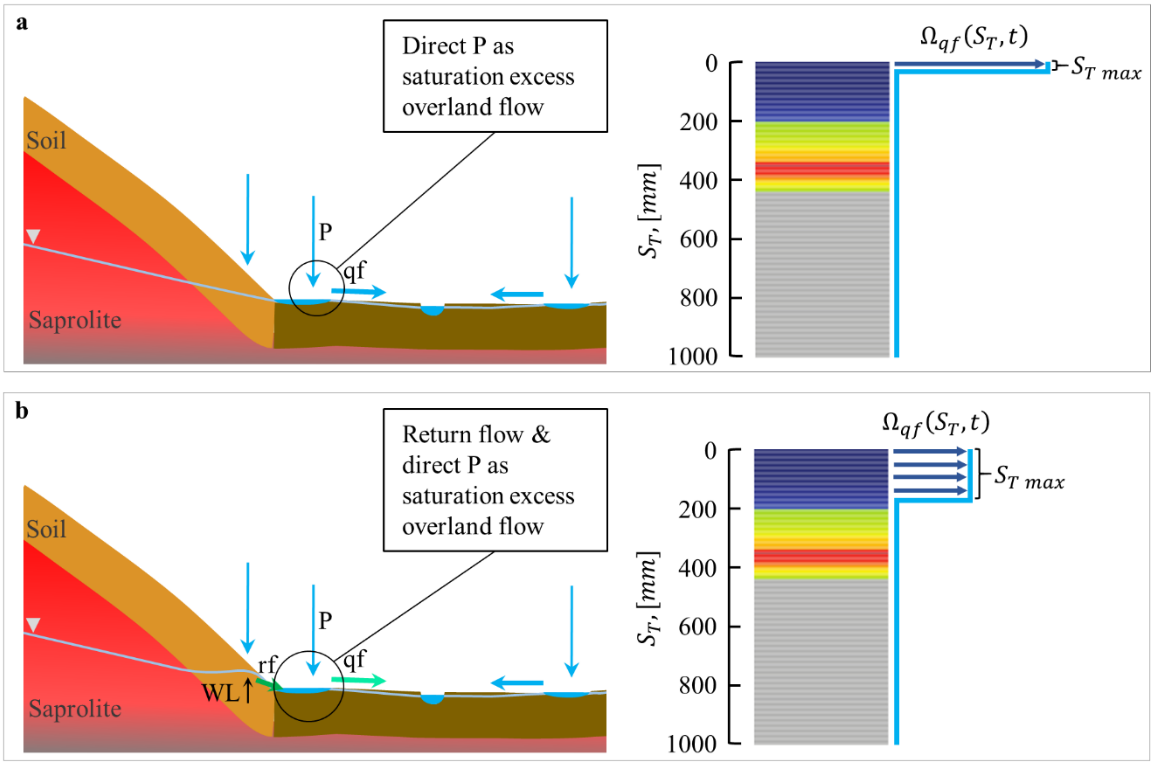
a
Direct P as saturation excess overland flow
Soil
Saprolite
P
qf
$\Omega_{qf}(S_T,t)$
$S_{T\,max}$
0
200
400
600
800
1000
S_T, [mm]
b
Return flow & direct P as saturation excess overland flow
Soil
Saprolite
P
rf
qf
WL↑
$\Omega_{qf}(S_T,t)$
$S_{T\,max}$
0
200
400
600
800
1000
S_T, [mm]

Figure 4.3: A figure showing the relationship between the hypothesized quickflow generation mechanism and the choice of the corresponding rank StorAge Selection (rSAS) function for quickflow ($\Omega_{qf}(S_T, t)$). The perceptual model of each runoff generation process is shown on the left and the corresponding $\Omega_{qf}(S_T, t)$, which selects from the age-rank storage column, is shown on the right. P, qf, rf, and WL stand for precipitation, quickflow, return flow, and water level, respectively. A uniform distribution is chosen to

represent the selection of water from the age-rank storage column, with different maximum age-rank storage (S_{Tmax}) for each hypothesis. (a) This panel corresponds to the hypothesis that quickflow is generated from saturation excess overland flow, which is produced from direct precipitation. For this hypothesis an S_{Tmax} of 0.245 mm is chosen to represent the selection of the very youngest water within the age-rank storage column. (b) This panel corresponds to the hypothesis that quickflow is generated from saturation excess overland flow, which is composed of both direct precipitation and return flow from the toe of the hillslope. Here the S_{Tmax} parameter of $\Omega_{qf}(S_T, t)$ is optimized in order to represent the selection of water from the tension saturated zone at the toe of the hillslope and from the youngest water in storage.

Before testing whether the hypothesized quickflow generation mechanism is able to capture the observed isotopic composition in the streamflow, the distributions of $\Omega_{bf}(S_T, t)$ and $\Omega_{ET}(S_T, t)$ must be defined. As in Harman (2015), a uniform distribution, which selects from an S_T of zero to S_{Tmax} is chosen to represent the unbiased sampling of water from the root zone. A gamma distribution is chosen for $\Omega_{bf}(S_T, t)$, with shape parameter α_{bf} and scale parameter θ_{bf}. The gamma distribution is selected for baseflow given its ability to reproduce the approximate $1/f$ spectral filtering observed in other catchments (Harman, 2015; Kirchner et al., 2000) and the fact that a gamma $\Omega(S_T, t)$ can sample across the entire range of age-rank storage, including the very oldest water. The parameters of $\Omega_{ET}(S_T, t)$ and $\Omega_{bf}(S_T, t)$ are not chosen *a priori* as they were for $\Omega_{qf}(S_T, t)$, but are instead optimized using the stable water isotope data. The resulting optimized parameters are then evaluated in terms of their physical meaning in order to potentially gain insights into the processes that govern the selection of water from storage by evapotranspiration and baseflow.

4.3.2.2 Return Flow and Direct Precipitation

The second hypothesis tested is that quickflow is generated through saturation excess overland flow which is composed of both return flow and direct precipitation. Significant quantities of return flow could be produced from the toe of the hillslope, even in the absence of subsurface stormflow farther up the hillslope, from a mechanism similar to groundwater ridging. In groundwater ridging, the tension saturated zone above the water table is rapidly converted to atmospheric pressure as a result of the addition of a small quantity of water. This rapidly raises the water table, creating a large potential gradient driving water toward the stream. Under this mechanism, quickflow from saturation excess overland flow would contain both pre-event, i.e. return flow, and event water. In order to test this hypothesis, a uniform distribution is once again chosen to represent this runoff generation process, however, the S_{Tmax} parameter of $\Omega_{qf}(S_T, t)$ is not fixed as before but is instead optimized along with the parameters of $\Omega_{ET}(S_T, t)$ and $\Omega_{bf}(S_T, t)$. The uniform distribution is chosen in order to represent the unbiased selection of water from both the tension saturated zone and the youngest water in the age-ranked storage (Figure 4.3b). The optimized S_{Tmax} parameter of $\Omega_{qf}(S_T, t)$ can then be compared to expected changes in water level that might result from groundwater ridging in order to see if the value is physically reasonable. The modeled $\delta^{18}O$ of streamflow is compared to the observed $\delta^{18}O$ of streamflow in order to test the ability of the model and underlying hypothesis to capture the quickflow generation process and resulting composition of the streamflow.

A caveat about the above model representation of the selection of water from the tension saturated zone is that the thickness of the zone is fixed by S_{Tmax} and therefore assumed to be constant over time. In reality, however, the thickness of the tension saturated zone is likely to vary as a result of antecedent conditions, which control the pre-storm position of the water table relative to the surface and to soil horizons that may have different pore size distributions. In order to explore the potential time-variability in the selection process that is not captured by a fixed S_{Tmax}, a range of S_{Tmax} values are selected given the optimized result, and used to predict the δ^{18}O of streamflow. By identifying times when one S_{Tmax} value does better than another at capturing the isotopic composition of the streamflow, one is able to gain insights into what antecedent conditions might influence the time-variability in the selection of water from the tension-saturated zone.

4.4 Results

The 6-hourly hydrologic fluxes described in Section 4.3 are shown in Figure 4.4, along with the bulk weekly delta-O-18 ($\delta^{18}O$) of precipitation and the 12-hourly $\delta^{18}O$ of discharge at the Pond Branch Catchment outlet. Only two years of data are shown in Figure 4.4 despite the availability of four years of precipitation and discharge samples because of delays in processing the most recent samples, i.e. a backlog in the analysis of the samples for their stable water isotope ratios. The time series plots in Figure 4.4 start on September 1, 2014 and extend until August 31, 2016, with the water year from October 1, 2014 to September 30, 2015 used to scale the potential evapotranspiration in order to estimate the actual evapotranspiration. Precipitation and discharge, including the quickflow and baseflow components, are discussed in detail in Chapter 3 Section 3.3 while the evapotranspiration flux is discussed in Chapter 2 Section 2.4.1.

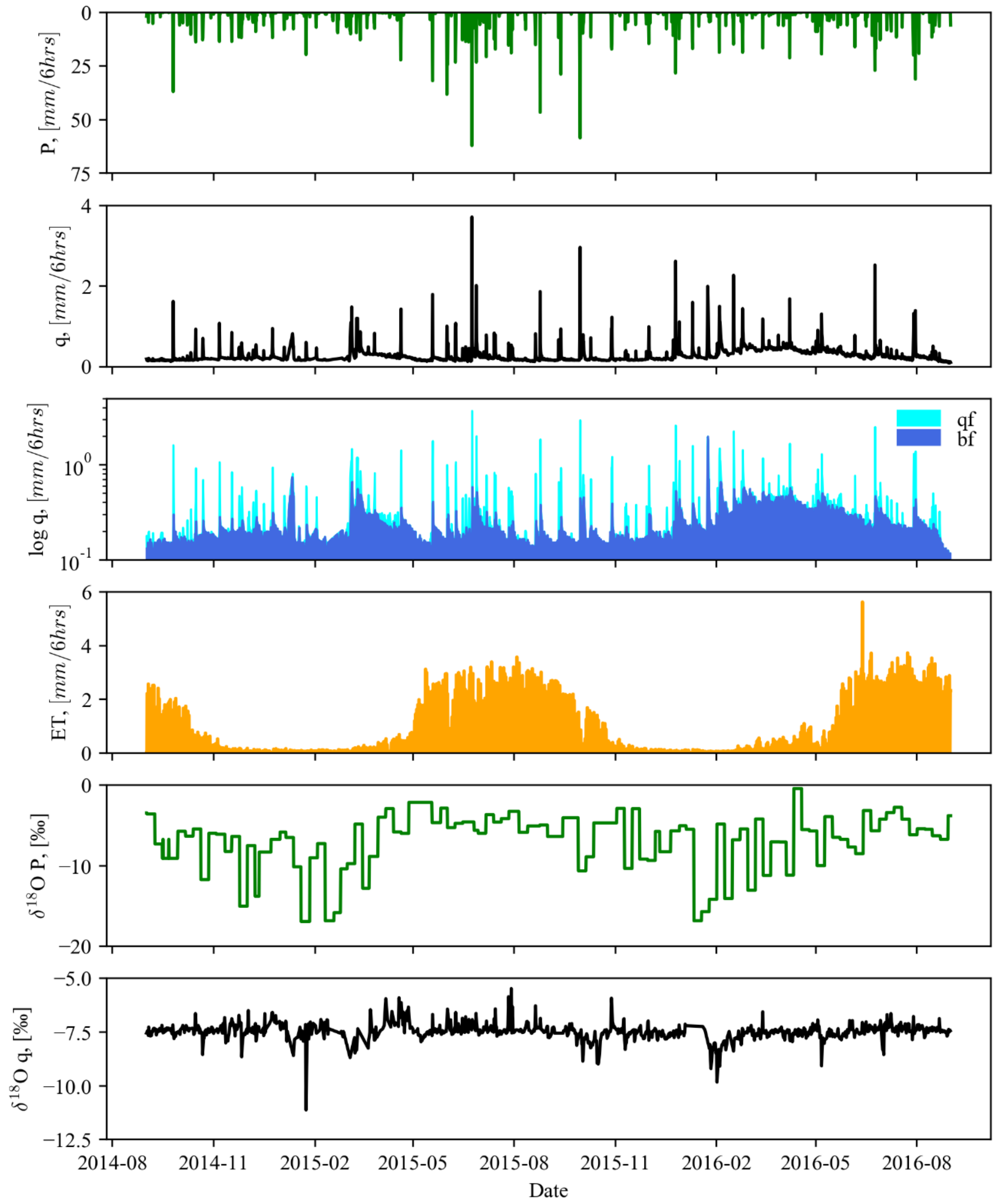

Figure 4.4: Summary of all of the time series used in this chapter. Precipitation (P), specific discharge (q), and actual evapotranspiration (ET) are in units of millimeters per six hours (mm/6hrs); the logarithmic of the specific discharge (log q) has units of logarithmic mm/6hrs; and the delta-O-18 ($\delta^{18}O$) of P and q are in unites of per mil (‰) relative to Vienna Standard Mean Ocean Water (VSMOW). In pane three the logarithmic of the specific discharge is separated into its baseflow (bf) and quickflow (qf) components using baseflow

separation. The $\delta^{18}O$ of P is determined from bulk weekly samples while the $\delta^{18}O$ of q is from 12-hourly grab samples. Notice that the y-axes for $\delta^{18}O$ of P and q are not the same.

New to this dissertation are the time series of the stable water isotope ratios for precipitation and discharge. The $\delta^{18}O$ of precipitation varies between -0.45 ‰ and -16.69 ‰ with the most negative $\delta^{18}O$ values occurring in winter and the most positive $\delta^{18}O$ values in summer, as expected. The $\delta^{18}O$ of precipitation in the winter can vary greatly from week to week, with a range that is similar to the entire annual range. This variability in $\delta^{18}O$ in the winter is likely due, at least in part, to the type of the precipitation and air temperature, with cold snow events having the most negative $\delta^{18}O$ values and warmer rain events having more positive $\delta^{18}O$ values. The $\delta^{18}O$ of discharge varies between -5.49 ‰ and -11.14 ‰ with the most negative value in winter and the most positive value in summer. However, the overall seasonal trend observed in $\delta^{18}O$ of precipitation does not appear in the $\delta^{18}O$ of discharge, with the background $\delta^{18}O$ of discharge remaining relatively constant around -7.5 ‰.

The $\delta^{18}O$ of precipitation has a range of 16.5 ‰, while the $\delta^{18}O$ of discharge has a range of 5.65 ‰. A somewhat smaller range in $\delta^{18}O$ of discharge is expected given that streamflow is composed of a mixture of water with a variety of $\delta^{18}O$ values, and, in fact, this dampening in the variability of the isotopic composition of the precipitation is the behavior that the rank StorAge Selection (rSAS) functions attempt to replicate. In this regard, it is useful to recognize that because the quickflow quantity is often an order of magnitude greater than baseflow, one should expect the range of the $\delta^{18}O$ of precipitation and discharge to be nearly identical if the composition of quickflow was heavily dominated by event precipitation. In fact, however, this is not the case. This is an important result that is discussed further below.

4.4.1 Direct Precipitation

The contrast in the ranges $\delta^{18}O$ of precipitation and discharge suggest that quickflow is not heavily dominated by direct precipitation. This deduction is tested more rigorously using the rSAS framework. Specifically, a uniform distribution which selects from an age-rank storage S_T of 0.0 mm to 0.254 mm is used to test the hypothesis that quickflow is generated from saturation excess overland flow that is dominated by direct precipitation. The predicted $\delta^{18}O$ of discharge for this hypothesis is shown in the top panes of Figures 4.5 and 4.6 along with the observed $\delta^{18}O$ of discharge. The corresponding optimized parameters of the rSAS functions for baseflow and evapotranspiration are shown in Table 4.1, as well as the modified Kling-Gupta Efficiency (KGE).

As can be seen in Figures 4.5 and 4.6, the model overpredicts the variability in the isotopic composition of the streamflow. The range of the modeled $\delta^{18}O$ of discharge is 10.95 ‰, which is approximately double the range of the observed $\delta^{18}O$ of discharge. However, the isotopic composition of discharge does deviate from the baseflow composition during most storm events, suggesting that quickflow is partly composed of direct precipitation or coincidentally of water from a store with the same distinct isotopic composition. In any case, however, the change in the direction of the deviation from the background isotopic composition from event to event supports the conclusion that quickflow is in part composed of direct precipitation. The dramatic over prediction in the variability of the $\delta^{18}O$ of discharge, however, indicates that quickflow also includes previously stored, pre-event water that is liberated during and immediately after storm events. Evidence from the previous chapter suggests that this pre-event water is likely return flow from the toe of the hillslope.

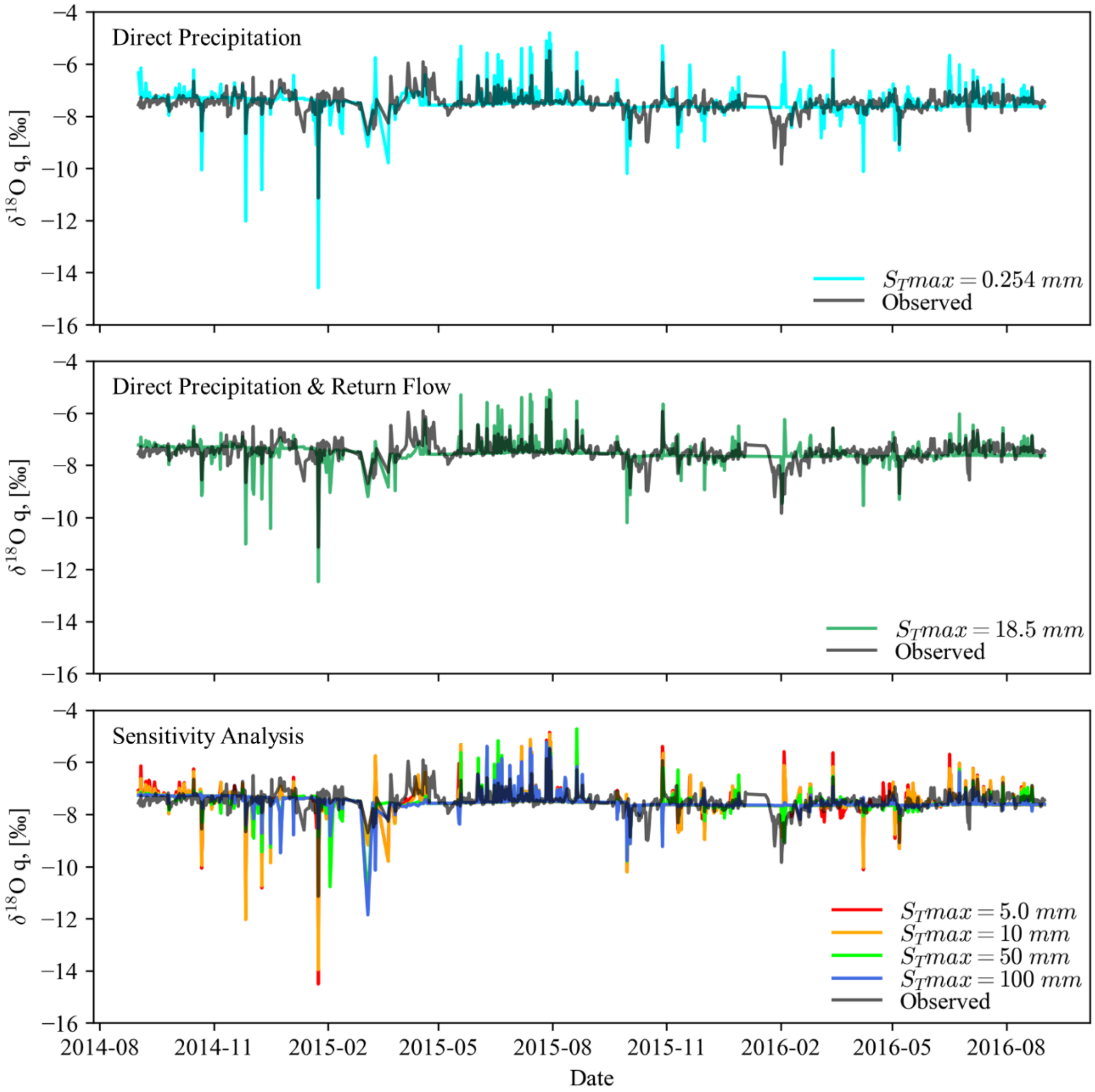

Figure 4.5: The predicted δ^{18}O of discharge (q) in per mil (‰) for different values of the maximum age-rank storage (S_{Tmax}) or the rank StorAge Selection (rSAS) function for quickflow, along with the observed δ^{18}O of Pond Branch discharge. The first pane, with an S_{Tmax} of 0.254 mm, corresponds to the hypothesis that quickflow is dominated by direct precipitation. The second pane, with an optimized S_{Tmax} of 18.5 mm, corresponds to the hypothesis that quickflow is composed of both direct precipitation and return flow. The last pane shows the results of a sensitivity analysis in which S_{Tmax} is varied between 5.0 mm and 100 mm.

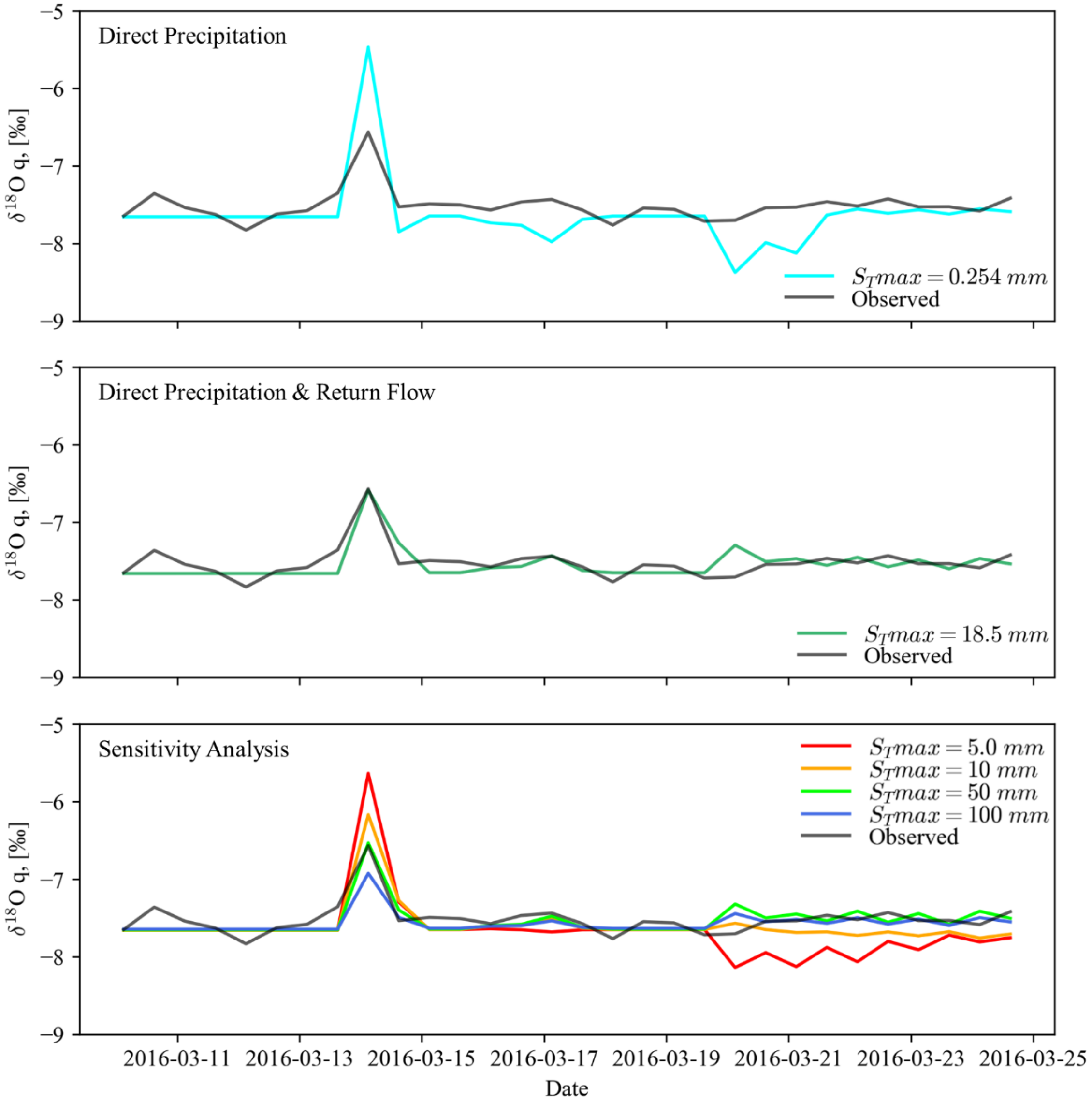

Figure 4.6: A two-week window of the results presented in Figure 5. The y-axis is rescaled to a narrower range in order to compare the predicted δ^{18}O of discharge (q) in per mil (‰) for different values of the maximum age-rank storage (S_{Tmax}) to the observed δ^{18}O of Pond Branch discharge. The first two panes correspond to separate quickflow generation hypotheses while the last pane shows the results of a sensitivity analysis.

Table 4.1: Summary of the optimized or selected parameters for each hypothesis and corresponding set of rank StorAge Selection (rSAS) functions, as well as the resulting modified Kling-Gupta Efficiency (KGE). The maximum age-rank storage (S_{Tmax}) for quickflow (qf) is chosen *a priori* for the direct precipitation hypothesis and optimized for the hypothesis that quickflow is composed of both return flow and direct precipitation. For baseflow (bf), a gamma distribution is chosen for the rSAS function with shape parameter

α_{bf} and scale parameter θ_{bf}. The mean μ_{bf} of the gamma distribution is the product of α_{bf} and θ_{bf}. For evapotranspiration (ET), a uniform distribution is chosen and the S_{Tmax} parameter is optimized. S_{Tmax}, θ_{bf}, and μ_{bf} are in units of millimeters (mm) of storage.

Hypothesis	**$S_{Tmax,\,qf}$ [mm]**	**α_{bf} [-]**	**θ_{bf} [mm]**	**μ_{bf} [mm]**	**$S_{Tmax,\,ET}$ [mm]**	**KGE**
Direct	0.254	1.26	2110	2669	43.2	0.38
Return & Direct	18.5	1.32	1601	2118	22.1	0.48

4.4.2 Return Flow and Direct Precipitation

To model the hypothesis that quickflow is composed of both direct precipitation and return flow, the maximum age-rank storage S_{Tmax} of the rSAS distribution for quickflow is optimized along with the parameters of the rSAS distributions for baseflow and evapotranspiration. The resulting optimized parameter set is shown in Table 4.1, with an S_{Tmax} of 18.5 mm for quickflow. By dividing this 18.5 mm by the specific yield of the soil at the riparian hillslope interface, the thickness of the tension saturated zone, which is theorized to contribute to quickflow, can be estimated. Given a specific yield of 0.29 (Loheide et al., 2005), the theoretical thickness of the tension saturated zone is approximately 64 mm, which is physically plausible given the change in the water level at the toe of the hillslope observed in the previous chapter. Before drawing any other inferences about the optimized parameters or placing too much confidence in this value, however, it is important to explore the fit between the model and the observed stable water isotope composition of discharge.

As reported in Table 4.1, the goodness-of-fit metric, the KGE, is higher than with the previous hypothesis but still not close to unity, which would indicate a perfect fit. In the second panes of Figures 4.5 and 4.6, the predicted $\delta^{18}O$ of discharge is shown along with the observed $\delta^{18}O$ of discharge. From Figure 4.5, it can be seen that this model, with its corresponding hypothesis, predicts the observed $\delta^{18}O$ of discharge better than the previous hypothesis, with a predicted range of 7.36 ‰ compared to an observed range of 5.65 ‰. For the particular two-week period shown in Figure 4.6, the model with the optimized S_{Tmax} of 18.5 mm predicts the observed $\delta^{18}O$ of discharge almost exactly, supporting the hypothesis that quickflow is composed of both direct precipitation and return flow. The lack of a perfect fit (low KGE) is evident, however, when the entire time series is examined, as facilitated by the second pane of Figure 4.5. From these results, one can see that the model results often over predict as well as under predict the variability in the isotopic composition of the streamflow. This does not necessarily disprove the proposed hypothesis, but it does highlight model imperfections. For example, one known flow in the model structure used to represent the hypothesis is that the S_{Tmax} is fixed in time. In reality, the theorized thickness of the tension saturated zone, which is conceptually represented by S_{Tmax}, likely varies with antecedent conditions.

In order to explore the potential of the proposed hypothesis and the corresponding rSAS distributions to predict the observed time series of stable water isotope composition of discharge, the S_{Tmax} parameter is varied between 5 mm and 100 mm. The bottom panes of Figures 4.5 and 6, show the result of varying this S_{Tmax} parameter. Not surprisingly, there are some events where an S_{Tmax} value either greater or less than 18.5 mm produces a better fit. Interestingly, it appears as though the predicted $\delta^{18}O$ of discharge is highly sensitive to small changes in the S_{Tmax} value when it is less than 18.5 mm and relatively insensitive to changes when the S_{Tmax} value is greater than 18.5 mm. In Figure 4.6, the S_{Tmax} of 18.5 mm and 50 mm produces a similar fit to the observed $\delta^{18}O$ of discharge, while an S_{Tmax} of 10 mm is offset by a similar amount as an S_{Tmax} of 100 mm, at least for the event on March 14, 2016. This contrast in the sensitivity of the predicted $\delta^{18}O$ of discharge to values of S_{Tmax} on either side of the optimized value is unsurprising given the storm to storm variability in the isotopic composition of precipitation events which have a greater influence on the smaller S_{Tmax} values. It does suggest, however, that a time-variable S_{Tmax} parameter may vary anywhere between approximately 10 mm and 100 mm, or approximately 34.5 mm and 345 mm of theoretical tension saturated zone, respectively. Given the relative changes in the water level at the toe of the hillslope from storm to storm this range of values for S_{Tmax} seems reasonable.

Further information on antecedent conditions would be needed in order to explore what conditions lead to smaller or larger S_{Tmax} values. Nonetheless, these initial results support the hypothesis that quickflow is composed of both direct precipitation and return flow, with the added caveat that the relative proportion of direct precipitation and return flow varies in time. Given the uncertainty in the precise value of S_{Tmax}, and the likelihood that it varies in time, no further inferences are made on the basis of the other optimized parameter values shown in Table 4.1.

4.5 Discussion

4.5.1 Stable Water Isotope Data

The stable water isotope compositions of precipitation and discharge are critically important data for testing each hypothesis, and it is therefore important to evaluate the confidence in each measurement. In this regard, both the precipitation collector and automated sampler used to collect streamflow were designed and operated to minimize evaporation and exchange of the collected sample with moisture in the air, which might have otherwise resulted in fractionation of the samples before analysis. All samples are preserved in glass vials with a specialized cap that minimizes head space and gaseous exchange with outside air. The LGR OA-ICOS system used to analyze the liquid water samples, has a reported precision of 0.08 ‰ for δ^{18}O (one standard deviation), while the average measured standard deviation for the δ^{18}O of all analyzed discharge samples is 0.07 ‰. Many storm events, including the March 14, 2016 event shown in Figure 4.6, produced a deviation from the baseline δ^{18}O of discharge of 1 ‰ or more, while many of the smaller variations, including the ones immediately following the March 14, 2016 event are not significant. In general, a relatively high confidence can be placed on the accuracy and precision of the precipitation and discharge stable water isotope time series given the care taken in collecting and analyzing the samples.

Potentially more problematic are the assumptions made in using the δ^{18}O of precipitation to predict the δ^{18}O of discharge. One concern is that the precipitation collector is located within a field, while the Pond Branch Catchment is almost completely forested. It is known that re-evaporation of precipitation within the forest canopy can result in the fractionation of the precipitation before it reaches the forest floor as throughfall. In two separate experiments, Allen et al. (2015) found that the δ^{18}O of throughfall is on average, 0.3 ‰ to 0.7 ‰ higher than precipitation. This enrichment (higher delta-values) of throughfall compared to precipitation would likely be most pronounced in the growing season when tree leaves provide a large surface area for re-evaporation. As a result of throughfall enrichment, the direct precipitation that partially composes quickflow would also be enriched, suggesting that the optimized maximum age-rank storage S_{Tmax} may be biased small, since additional storage would need to be sampled by the rSAS function for quickflow in order to account for the more positive precipitation. In addition, it is assumed that the bulk weekly δ^{18}O of precipitation can be used to represent the isotopic composition of individual storm events. Given the variability of precipitation events from week to week, it is however possible, and perhaps likely, that individual storms have considerable variability in their isotopic composition. The use of the bulk precipitation would dampen the effects of individual storm variability on the predicted δ^{18}O of discharge, which, interestingly, could again have the effect that the optimized S_{Tmax} may be biased small. Since a larger than modeled S_{Tmax} would only strength the argument that quickflow is composed of significant quantities of stored pre-event water, the implications of both of these assumptions further support the conclusions drawn in the previous section—namely, that return flow is an important component of quickflow.

4.5.2 Return Flow

The results of Section 4.4, suggest that quickflow is generated from saturation excess overland flow which is composed of both direct precipitation and return flow, where the proportions of direct precipitation and return flow vary in time. Dunne & Black (1970) first described the process of saturation excess overland flow within the hydrologic literature during an investigation of runoff production within the Sleepers River Experimental Watershed of Vermont. In their investigation, they similarly attributed a portion of quickflow generated to return flow. For the return flow described in Dunne & Black (1970), however, the flow was attributed to the water table rising above the surface within the center of an area of convergence at the head of the stream channel. In contrast, in the Pond Branch Catchment, return flow appears to be generated as a result of the groundwater ridging mechanism proposed by Abdul & Gillham (1984), where the tension saturated zone above the water table is rapidly converted to atmospheric pressure as a result of the introduction of a small amount of infiltrated water from above. This groundwater ridging occurs at the hillslope-riparian interface, causing return flow to emerge at the toe of the hillslope where a zone of saturation forms as a result of the water table rising to the surface.

In the Coastal Plain of Virginia, Eshleman et al. (1993) similarly found that runoff is generated from saturation excess overland flow, which is composed of both direct precipitation and return flow. However, the soils in their catchment are too coarse for a thick tension-saturated zone to develop, and they therefore attribute the return flow to a combination of subsurface storm flow and exfiltrating event precipitation (Eshleman et al., 1993). Eshleman et al. (1993) also observed that the proportion of direct precipitation in quickflow is controlled by the precipitation intensity and not by antecedent conditions, with the maximum 24-hour rainfall intensity explaining 96% of the total variation in the peak new water contribution from direct precipitation. They attributed this result to the increased spatial extent of saturated area within the riparian zone. This finding is especially interesting when considered through the rSAS modeling framework because the higher proportion of direct precipitation during more intense precipitation events would translate into a smaller S_{Tmax} parameter for quickflow, since the youngest water in storage would be selected. In the Pond Branch Catchment, it is not immediately clear whether S_{Tmax} would vary with precipitation intensity since the spatial extend of the saturated area seems to be controlled, in part, by return flow from the hillslope. However, in future work, the

S_{Tmax} parameter could be varied as function of precipitation intensity in order to test this hypothesis.

4.6 Conclusions

The fundamental goal of the work described in this chapter is to study the influence of landscape structure on the generation of the quickflow component of streamflow within the deeply weathered, Pond Branch Catchment. The findings of this work also rely on results of the previous chapter, and particularly on the suggestion from the prior work that quickflow is generated from saturation excess overland flow that occurs, in part, at the riparian-hillslope boundary as a result of a rapid increase in the water table at the toe of the hillslope. With the prior results alone, however, it is not possible to determine whether quickflow is dominated by direct precipitation or return flow. In the work described in this chapter, stable water isotope data and the rank StorAge Selection (rSAS) modeling framework are used to test whether direct precipitation dominates quickflow in the Pond Branch Catchment or whether quickflow at this location is composed of both direct precipitation and return flow.

The modeling results support the second hypothesis that quickflow is composed of both direct precipitation and return flow, with the added caveat that the proportion of each component is likely time-variable. The potential time-variability in the proportions of return flow and direct precipitation that compose quickflow is unsurprising. For example, the quantity of return flow may vary as a result of the thickness of the tension saturated zone, which would change based on antecedent storage conditions. In the Virginia Coastal Plain, Eshleman et al (1993) observed that the proportion of quickflow composed of direct precipitation varies as a result of precipitation intensity. The influence of precipitation and antecedent conditions on quickflow generation, namely on the proportions of direct precipitation and return flow are the subject of future work. The results of this study highlight the importance of landscape structure in controlling runoff generation in the Pond Branch Catchment, with the hillslope and riparian landscape units interacting in order to produce saturation excess overland flow which is composed of both direct precipitation and return flow.

Chapter 5

Conclusion

5.1 Summary

The forested Pond Branch Catchment of northern Maryland was used to test hypotheses relating Piedmont landscape structure to catchment storage and streamflow generation. This research was motivated, in part, by a rich history of runoff generation studies in high relief landscapes with thin soils overlying an assumed impermeable bedrock (e.g. Jencso et al., (2009), McDonnell (1990), Sklash et al. (1986), and Tromp-van Meerveld & McDonnell (2006)), and the lack of similar research in deeply weathered landscapes like the Piedmont Physiographic Province of the eastern United States. In addition, previous research within the Piedmont highlighted the potential of the deeply weathered bedrock to store large quantities of water (e.g. Bachman et al. (1998) and Cleaves et al. (1970)), however, these investigations did not link direct observations of hillslope discharge to storage in the weathered bedrock. Over a four-year period, a multitude of data were collected from the Pond Branch Catchment across a range of spatial and temporal scales, including hydrometric, meteorological, and stable water isotope data. These data were used in combination with recession analysis, water balance models, and the rank StorAge Selection (rSAS) modeling framework to test hypotheses driven by direct observations made within the landscape.

5.1.1 Key Findings

In the effort described in Chapter 2, storage was calculated for individual landscape units, hydraulically coupled and uncoupled portions of the landscape, and for the Pond Branch Catchment as a whole. During the three-year study period, from October 1, 2014 to September 30, 2017, catchment scale storage transitioned from near normal to a decadal drought, leading to a 13-month period of below average stream discharge. By examining the propagation of this drought through the individually calculated stores, it was determined that below average precipitation in March and April of 2016 set the stage for the period of below average discharge that began five months later. The below average precipitation in Spring 2016, before leaf on, initiated a nine month decline in the unsaturated zone storage. As a result of the unsaturated zone storage deficit, and despite higher than average precipitation from May through July, the hydraulically connected, saturated zone storage was not recharged in late spring and summer, resulting in the period of below average discharge. By examining the propagation of the drought through individual storages, instead of relying on a lumped estimate of catchment scale storage, the conditions that lead to the drought were identified. This study thus highlights the importance of storage structure in controlling the emergent response of a deeply weathered catchment to hydroclimatic variability.

In the third chapter, discharge and water level measurements were used to test hypotheses relating landscape structure to streamflow generation within the Pond Branch Catchment. Measurements of discharge from hillslope springs were used, in part, to test and prove that the baseflow component of discharge could be accounted on the basis of water released from storage within the hillslope and underlying saprolite. A variety of runoff generation mechanisms were tested in an iterative process in order to identify the mechanisms that produce the quickflow component of streamflow. Riparian water levels and spring discharge measurements indicated that quickflow was generated as a result of a rapid increase in the water level at the toe of the hillslope, which caused the water table at the riparian-hillslope interface to rise to the surface, forming an area of saturation where saturation excess overland flow was produced. Without information on the composition of the quickflow, however, it was not possible to determine whether direct precipitation dominated the overland flow or whether return flow from stored, pre-event water was also a significant component. The results of this study shed light on the role of Piedmont landscape structure in controlling both the baseflow and quickflow components of streamflow.

The fourth chapter incorporated environmental tracer data and the rank StorAge Selection (rSAS) modeling framework to test the prior results (i.e., those reported in Chapter 3) and to further explore the influence of landscape structure on the generation of the quickflow component of streamflow. Individual hypotheses about how specific runoff generation mechanisms select water from storage were transformed into quantitative rSAS models to make predictions about the composition of streamflow which could then be compared to the observed compositions. The results indicated that quickflow was composed of both direct precipitation and stored, pre-event water. The modeling results further suggested that the relative proportions of each component of quickflow change over time. In combination with the earlier results discussed in Chapter 3—i.e., that the pre-event water was likely return flow from the hillslope which was rapidly liberated in a process such as groundwater ridging—the new results support the conclusion that quickflow was generated, at least in part, at the hillslope-riparian interface as a result of groundwater ridging at the toe of the hillslope, which raised the water table, forming an area of saturation where overland flow was produced to combine with that from direct precipitation. This demonstrated interaction between the hillslope and riparian landscape units highlights the importance of the landscape structure in controlling runoff generation and the resulting composition of streamflow.

5.1.2 Limitations

In any study there are countless limitations, and especially so for those which use natural environmental data and attemp to transfer knowledge from one place to an entire region based on landscape structure. Here, the Pond Branch Catchment is studied as an example of a Piedmont catchment; however, not all Piedmont catchments are structured exactly the same as Pond Branch, and this can of course result in differences in storage structure and streamflow generation. Nonetheless, the knowledge generated from the study of the individual landscape components of Pond Branch, can be transferred to other catchments with similar landscape features. At a minimum, this work has clearly proven that certain realizations of a catchment's response to precipitation can be ruled out based on a fundamental understanding of how streamflow is generated.

In terms of the specific conclusions drawn about Pond Branch, there are also a number of limitations deriving from the availability and accuracy of the data. For example, in Pond Branch, data from a single riparian well transect and two hillslope springs are used to test competing runoff generation hypotheses, but there is not sufficient data to conclusively demonstrate that the response of the selected springs and riparian wells are representative of the entire catchment. There is, however, some corroborating evidence for representativeness, such as the link between saturated areas and vegetation and the presence of channels at the toe of the hillslope indicating flow convergence. For the work described in Chapter 2, one important limitation is the lack of a groundwater well at the site. In absence of this, hydraulically coupled storage was estimated using a recession analysis that relied on the assumption that there is a single reservoir controlling the streamflow recession. The scatter in the calculated individual recession rates suggests that there are multiple stores draining, each with their own storage discharge relationship. This suggests that the assumption was incorrect and that the estimate of hydraulic storage may therefore be mis-estimated. Numerous other limitations and sources of uncertainty could also be discussed in relation to simplifying assumptions about the known complexity of the real world. It is for this reason that care was taken in this dissertation to use multiple lines of evidence as a means of validating conclusions to the fullest extent possible.

5.1.3 Broader Impacts

The results of this dissertation have the potential for broader impacts based on (1) the knowledge gained of the Pond Branch Catchment and (2) the general understanding of storage and streamflow generation in deeply weathered landscapes. As previously discussed, Pond Branch has been studied since the 1960's (e.g. Cleaves et al. 1970) with recent research associated with the Baltimore Ecosystem Study and the Johns Hopkins University (JHU) Landscape Hydrology Lab (LHL). The data and results of this dissertation add to the collective knowledge of the Pond Branch Catchment and serve as a foundation for future hydrologic research by members of the JHU LHL as well as collaborators. Furthermore, the results of previous investigations at Pond Branch, such as those presented in Duncan et al. (2015) can be reexamined in light of the understanding of flow pathways gained within this dissertation. Specifically, in revisiting Duncan et al. (2015) it appears as though the seasonality of nitrate export that they observed can be accounted for by the perceptual hydrologic model developed as a part of this dissertation, without the need for the complex biogeochemical reactions that they invoke.

At a broader scale, the results of this dissertation add to the understanding of how landscape structure controls storage and streamflow generation in deeply weathered catchments, such as those found within the Chesapeake Bay Watershed. Understanding the storage and release of water from the landscape is fundamental to predicting the movement of solutes such as nitrate, which may be of primary concern in catchments with impaired surface waters. This knowledge can be used in two ways: (1) by informing best management practices (BMPs) and (2) by incorporating streamflow generation mechanisms into transport models to make better predictions.

The results of Chapter 3 indicate that baseflow is composed of water released at the valley margin from the storage within the hillslope, while the results of Chapter 2 indicate that the hydraulic storage, i.e. the part of storage within the hillslope that is hydraulically connected to baseflow, is recharged only during times when the unsaturated zone storage is high. This unsaturated zone storage is highest in early spring before leaf-on, therefore, in order to prevent nitrate from leaching into the hydraulic storage reservoir and ultimately discharging as baseflow, fertilizer application should be avoided in early spring. Furthermore, the results from Chapter 4, suggest that fertilizer application should be avoided altogether in the riparian area of catchments as well as in adjacent locations where there is a strong contrast in slope. In these areas, saturation excess overland flow may directly transport both solutes and particulate matter, including phosphate, to streams during storm events. Extending existing riparian buffer zones or fencing in pastures to include groundwater exfiltration zones adjacent to riparian areas could help reduce the amount of nitrate and phosphate transported to streams during storm events.

In Chapter 4, various perceptual models of runoff generation mechanisms were transformed into transport models using the rank StorAge Selection (rSAS) framework. It was shown that transport could not be predicted accurately without an understanding of how quickflow was being generated. To accurately predict the transport of nutrients, which may behave non-conservatively, it is important to first accurately capture the transport of water by incorporating understanding of the flow pathways within the structured landscape. The results from this dissertation can be used to inform the selection of model structures used to simulate water and nutrient transport based on the understanding of how water moves through deeply weathered catchments. Specifically, the potential of both direct precipitation and stored pre-event water to compose quickflow may be important when modeling nutrient loading during large storm events. In addition, the ability of storage within the hillslope and underlying saprolite to account for baseflow suggests that this storage reservoir may result in a long lag-time between the implementation of a BMP and an improvement in water quality. Inclusion of this consideration is therefore important for any transport model that attempts to represent time periods of remediation for any deeply weathered landscape.

5.2 Future Research

Based on the work presented herein, future research is recommended that aims to further substantiate the conclusions drawn, as well as incorporates additional data to better define the influence of storm characteristics and antecedent conditions on quickflow generation. In this regard, delays in processing a backlog of samples of the bulk weekly precipitation and the 12-hourly Pond Branch discharge prevented the use of more than two years of stable water isotope data in this analysis. Analyses from these additional two years of data are already planned and will be used to further the comparison of the results of the rank StorAge Selection (rSAS) model to the observed streamflow composition and thus further test and refine the conclusions presented in Chapter 4. In particular, these data will allow exploration of the time-variability in the size of the store from which quickflow is selected (i.e. in the size of the maximum age-rank storage S_{Tmax}), through an exercise that explores adjustments of S_{Tmax} on the basis of a metric of the antecedent wetness and a measure of precipitation intensity. The goal will be to determine the factors that control the time-variability in the relative proportions of direct precipitation and return flow in quickflow. Finally, the perceptual model of streamflow generation for Pond Branch will be compared to perceptual models developed by other researchers who study deeply weathered landscapes. In the latter regard a future “synthesis paper” is already planned as future work.

Bibliography

Abdul, A. S., & Gillham, R. W. (1984). Laboratory studies of the effects of the capillary fringe on streamflow generation. *Water Resources Research*, *20*(6), 691–698. https://doi.org/10.1029/WR020i006p00691

Allen, S. T., Keim, R. F., & McDonnell, J. J. (2015). Spatial patterns of throughfall isotopic composition at the event and seasonal timescales. *Journal of Hydrology*, *522*, 58–66. https://doi.org/10.1016/j.jhydrol.2014.12.029

Anderson, M. G., & Burt, T. P. (1978). The Role of Topography in Controlling Throughflow Generation. *Earth Surface Processes*, *3*, 331–344.

Bachman Lindsey, B., Brakebill, J., Powars, D., L. (1998). Ground-Water Discharge and Base-Flow Nitrate Loads of Nontidal Streams, and Their Relation to a Hydrogeomorphic Classification of the Chesapeake Bay Watershed, Middle Atlantic Coast. *Water-Resources Investigations Report*, (98–4059), 1–71. Retrieved from http://pubs.usgs.gov/wri/wri98-4059/%5Cnfile:///C:/Users/Qian/Documents/Mendeley Desktop/Bachman et al., 1998.pdf

Beven, K. (2012). *Rainfall-Runoff Modelling The Primer* (Second). Hoboken, NJ: John Wiley & Sons.

Botter, G., Bertuzzo, E., & Rinaldo, A. (2011). Catchment residence and travel time distributions: The master equation. *Geophysical Research Letters*, *38*. https://doi.org/10.1029/2011GL047666

Brutsaert, W. (2005). *Hydrology: An Introduction*. New York: Cambridge University Press.

Cleaves, E. T., Godfrey, A. E., & Bricker, O. P. (1970). Geochemical balance of a small watershed and its geomorphic implications. *Geological Society of America Bulletin*, *81*(10), 3015–3032. https://doi.org/10.1130/0016-7606(1970)81

Dingman, S. L. (2008). *Physical Hydrology* (Second). Long Grove, IL: Waveland Press, Inc.

Dowd, J., Wenner, D., & Carpenter, M. (1993). Piedmont Geohydrology: Implications for Flow and Transport. In K. J. Hatcher (Ed.), *1993 Georgia Water Resources Conference* (pp. 194–195). Athens, Georgia. Retrieved from http://smartech.gatech.edu/handle/1853/32143

Dralle, D., Hahm, W. J., Rempe, D., Karst, N., Dietrich, W., & Thompson, S. (2018). Quantification of the seasonal hillslope water storage that does not drives treamflow. *Hydrological Processes*, 1–38. https://doi.org/10.1002/adsc.201

Duncan, J. M., Groffman, P. M., & Band, L. E. (2013). Towards closing the watershed nitrogen budget: Spatial and temporal scaling of denitrification. *Journal of Geophysical Research: Biogeosciences*, *118*, 1105–1119.

https://doi.org/10.1002/jgrg.20090

Duncan, J. M., Band, L. E., Groffman, P. M., & Bernhardt, E. S. (2015). Mechanisms driving the seasonality of catchment scale nitrate export: Evidence for riparian ecohydrologic controls. *Water Resources Research*, *51*(6), 3982–3997. https://doi.org/10.1002/2015WR016937

Dunne, T. (1983). Relation of field studies and modeling in the prediction of storm runoff. *Journal of Hydrology*, *65*(1–3), 25–48. https://doi.org/10.1016/0022-1694(83)90209-3

Dunne, T., & Black, R. D. (1970a). An Experimental Investigation of Runoff Production in Permeable Soils. *Water Resources Research*, *6*(2), 478–490. https://doi.org/10.1029/WR006i002p00478

Dunne, T., & Black, R. D. (1970b). Partial Area Contributions to Storm Runoff in a Small New England Watershed. *Water Resources Research*, *6*(5), 1296–1311. https://doi.org/10.1029/WR006i005p01296

Eckhardt, K. (2005). How to construct recursive digital filters for baseflow separation. *Hydrological Processes*, *19*(2), 507–515. https://doi.org/10.1002/hyp.5675

Eshleman, K. N., Pollard, J. S., & O'Brien, A. K. (1993). Determination of contributing areas for saturation overland flow from chemical hydrograph separations. *Water Resources Research*, *29*(10), 3577–3587. https://doi.org/10.1029/93WR01811

Faure, G., & Mensing, T. M. (2005). *Isotopes: Priciples and Applications*. *Isotopes Principles and Applications* (Vol. Tenth). Retrieved from http://books.google.com/books?id=tlMSAQAAIAAJ&pgis=1

Fernald, M. L. (1950). *Gray's Manual of Botany* (Eighth (Ce). American Book Company.

Groffman P., D. Dillon. 2010. Soil moisture and temperature along an urban to rural gradient at the Baltimore Ecosystem Study 2011- present. Environmental Data Initiative. https://doi.org/10.6073/pasta/0c31398165617ca92265496082f0a5ac. Dataset accessed 7/03/2018.

Groffman, P. M., Law, N. L., Belt, K. T., Band, L. E., & Fisher, G. T. (2004). Nitrogen fluxes and retention in urban watershed ecosystems. *Ecosystems*, *7*(4), 393–403. https://doi.org/10.1007/s10021-003-0039-x

Gröning, M., Lutz, H. O., Roller-lutz, Z., Kralik, M., Gourcy, L., & Pöltenstein, L. (2012). A simple rain collector preventing water re-evaporation dedicated for d 18 O and d 2 H analysis of cumulative precipitation samples, *449*, 195–200. https://doi.org/10.1016/j.jhydrol.2012.04.041

Haggerty, R. (2002). Power-law residence time distribution in the hyporheic zone of a 2nd-order mountain stream. *Geophysical Research Letters*, *29*(13), 1–4. https://doi.org/10.1029/2002GL014743

Harman, C. J. (2015). Time-variable transit time distributions and transport: Theory and application to storage-dependent transport of chloride in a watershed. *Water Resources Research*, *51*(1), 1–30. https://doi.org/10.1002/2014WR015707

Hewlett, J. D., & Hibbert, A. R. (1963). Moisture and energy conditions within a sloping soil mass during drainage. *Journal of Geophysical Research*, *68*(4), 1081–1087. https://doi.org/10.1029/JZ068i004p01081

Hewlett, J. D., & Hibbert, A. R. (1967). Factors affecting the response of small watershed to precipitation in humid areas. *Forest Hydrology*, 275–290. Retrieved from http://coweeta.ecology.uga.edu/publications/851.pdf

Holbrook, W. S., Riebe, C. S., Elwaseif, M., Hayes, J. L., Basler-Reeder, K., Harry, D. L., et al. (2014). Geophysical constraints on deep weathering and water storage potential in the Southern Sierra Critical Zone Observatory. *Earth Surface Processes and Landforms*, *39*(3), 366–380. https://doi.org/10.1002/esp.3502

Horton, R. E. (1933). The role of infiltration in the hydrologic cycle. *Transcations American Geophysical Union*, *14*(1), 446–460.

Hursh, C. R., & Brater, E. F. (1941). Separating storm-hydrographs from small drainage-areas into surface- and subsurface-flow. *Transactions, American Geophysical Union*, *22*(3), 863–871. https://doi.org/10.1029/TR022i003p00863

Jencso, K. G., & McGlynn, B. L. (2011). Hierarchical controls on runoff generation: Topographically driven hydrologic connectivity, geology, and vegetation. *Water Resources Research*, *47*(11), 1–16. https://doi.org/10.1029/2011WR010666

Jencso, K. G., McGlynn, B. L., Gooseff, M. N., Wondzell, S. M., Bencala, K. E., & Marshall, L. A. (2009). Hydrologic connectivity between landscapes and streams: Transferring reach- and plot-scale understanding to the catchment scale. *Water Resources Research*, *45*(4), 1–16. https://doi.org/10.1029/2008WR007225

Kendall, C., & McDonnell, J. J. (Eds.). (2006). *Isotope Tracers In Catchment Hydrology*. New York: Elsevier.

Kirchner, J. W. (2009). Catchments as simple dynamical systems: Catchment characterization, rainfall-runoff modeling, and doing hydrology backward. *Water*

Resources Research, *45*, 1–34. https://doi.org/10.1029/2008WR006912

Kirchner, J. W., Feng, X., & Neal, C. (2000). Fractal stream chemistry and its implications for contaminant transport in catchments. *Nature*, *403*(6769), 524–527. https://doi.org/10.1038/35000537

Klaus, J., & McDonnell, J. J. (2013). Hydrograph separation using stable isotopes: Review and evaluation. *Journal of Hydrology*, *505*, 47–64. https://doi.org/10.1016/j.jhydrol.2013.09.006

Kling, H., Fuchs, M., & Paulin, M. (2012). Runoff conditions in the upper Danube basin under an ensemble of climate change scenarios. *Journal of Hydrology*, *424–425*, 264–277. https://doi.org/10.1016/j.jhydrol.2012.01.011

Kulin, G., & Compton, P. R. (1975). *A Guide to Methods and Standards for the Measurement of Water Flow*. National Bureau of Standards (U.S.).

LeGrand, H. E. (1967). Ground Water of the Piedmont and Blue Ridge Provinces in the Southeastern States. *Geological Survey Circular*, (538).

Lindsey, B. D., Phillips, S. W., Donnelly, C. A., Speiran, G. K., Plummer, L. N., Böhlke, J.-K., et al. (2003). *Residence Times and Nitrate Transport in Ground Water Discharging to Streams in the Chesapeake Bay Watershed. Water-Resources Investigations Report* (Vol. 03-4035). New Cumberland, Pennsylvania. Retrieved from lit searches / groundwater

Loheide, S. P., Butler, J. J., & Gorelick, S. M. (2005). Estimation of groundwater consumption by phreatophytes using diurnal water table fluctuations: A saturated-unsaturated flow assessment. *Water Resources Research*, *41*(7), 1–14.

https://doi.org/10.1029/2005WR003942

Markewich, H. W., Pavich, M. J., & Buell, G. R. (1990). Contrasting soils and landscapes of the Piedmont and Coastal Plain, eastern United States. *Geomorphology*, *3*(3–4), 417–447. https://doi.org/10.1016/0169-555X(90)90015-I

McDonnell, J. J. (1990). A Rationale for Old Water Discharge Through Macropores in a Steep, Humid Catchment. *Water Resources Research*, *26*(11), 2821–2832. https://doi.org/10.1029/WR026i011p02821

McDonnell, J. J., McGuire, K., Aggarwal, P., Beven, K. J., Biondi, D., Destouni, G., et al. (2010). How old is streamwater? Open questions in catchment transit time conceptualization, modelling and analysis. *Hydrological Processes*, *24*(12), 1745–1754. https://doi.org/10.1002/hyp.7796

McGlynn, B. L., & McDonnell, J. J. (2003). Quantifying the relative contributions of riparian and hillslope zones to catchment runoff. *Water Resources Research*, *39*(11), n/a-n/a. https://doi.org/10.1029/2003WR002091

McGlynn, B. L., McDonnell, J. J., Seibert, J., & Kendall, C. (2004). Scale effects on headwater catchment runoff timing, flow sources, and groundwater-streamflow relations. *Water Resources Research*, *40*(7), W075041–W0750414. https://doi.org/10.1029/2003WR002494

McGuire, K., & McDonnell, J. J. (2006). A review and evaluation of catchment transit time modeling. *Journal of Hydrology*, *330*, 543–563. Retrieved from http://www.google.com/search?client=safari&rls=10_7_4&q=A+review+and+evaluation+of+catchment+transit+time+modeling&ie=UTF-8&oe=UTF-8

Monteith, J. L. (1965). Evaporation and environment. *Symposia of the Society for Experimental Biology*, *19*, 205–34. Retrieved from http://www.ncbi.nlm.nih.gov/pubmed/5321565

Mosley, M. (1979). Streamflow generation in a forested watershed, New Zealand. *Water Resources Research*, *15*(4), 795–806. Retrieved from http://onlinelibrary.wiley.com/doi/10.1029/WR015i004p00795/full

Nutter, L. J., & Otton, E. G. (1969). *Ground-Water Occurrence in the Maryland Piedmont*.

Ocampo, C. J., Sivapalan, M., & Oldham, C. E. (2006). Field exploration of coupled hydrological and biogeochemical catchment responses and a unifying perceptual model. *Advances in Water Resources*, *29*(2), 161–180. https://doi.org/10.1016/j.advwatres.2005.02.014

Otton, E. G., Cleaves, E. T., Crowley, W. P., Kuff, K. R., & Reinhardt, J. (1975). Cockeysville Quadrangle: Geology, Hydrology and Mineral Resources. Maryland Geological Survey.

Pavich, M. J. (1989). Regolith residence time and the concept of surface age of the Piedmont "Peneplain." *Geomorphology*, *2*(1–3), 181–196. https://doi.org/http://dx.doi.org/10.1016/0169-555X(89)90011-1

Peters, N. E., & Aulenbach, B. T. (2011). Water storage at the Panola Mountain Research Watershed, Georgia, USA. *Hydrological Processes*, *25*(25), 3878–3889. https://doi.org/10.1002/hyp.8334

Pinder, G. F., & Jones, J. F. (1969). Determination of the Ground-Water Component of

Peak Discharge from the Chemistry of Total Runoff. *Water Resources Research*, *5*(2), 438–445.

Ragan, R. M. (1968). An Experimental Investigation of Partial Area Contributions. *International Association of Scientific Hydrology*, *76*, 241–249.

Richardson, C. A. (1980). Ground water in the Piedmont upland of central Maryland. *Water-Resources Investigations Report*. U.S. Geological Survey, Water Resources Division.

Riebe, C. S., Hahm, W. J., & Brantley, S. L. (2016). Controls on deep critical zone architecture: a historical review and four testable hypotheses. *Earth Surface Processes and Landforms*, *156*(November 2016), 128–156. https://doi.org/10.1002/esp.4052

Riegger, J., & Tourian, M. J. (2014). Characterization of runoff-storage relationships by satellite gravimetry and remote sensing. *Water Resources Research*, *50*(4), 3444–3466. https://doi.org/10.1002/2013WR013847

Roa-García, M. C., & Weiler, M. (2010). Integrated response and transit time distributions of watersheds by combining hydrograph separation and long-term transit time modeling. *Hydrology and Earth System Sciences*, *14*(8), 1537–1549. https://doi.org/10.5194/hess-14-1537-2010

Roa-García, M. C., Brown, S., Schreier, H., & Lavkulich, L. M. (2011). The role of land use and soils in regulating water flow in small headwater catchments of the Andes. *Water Resources Research*, *47*(5). https://doi.org/10.1029/2010WR009582

Salama, W., González-álvarez, I., & Anand, R. R. (2017). Significance of weathering and regolith / landscape evolution for mineral exploration in the NE Albany-Fraser Orogen , Western Australia Significance of weathering and regolith / landscape evolution for mineral exploration in the NE Albany-Fraser Orogen. *Ore Geology Reviews*, *73*(October), 500–521. https://doi.org/10.1016/j.oregeorev.2015.07.024

Sayama, T., McDonnell, J. J., Dhakal, A., & Sullivan, K. (2011). How much water can a watershed store? *Hydrological Processes*, *25*(25), 3899–3908. https://doi.org/10.1002/hyp.8288

Sidle, R. C., Tsuboyama, Y., Noguchi, S., Hosoda, I., Fujieda, M., & Shimizu, T. (2000). Stormflow generation in steep forested headwaters: A linked hydrogeomorphic paradigm. *Hydrological Processes*, *14*(3), 369–385. https://doi.org/10.1002/(SICI)1099-1085(20000228)14:3<369::AID-HYP943>3.0.CO;2-P

Sklash, M. G., Stewart, M. K., & Pearce, A. J. (1986). Storm runoff generation in humid headwater catchments 2. A case study of hillslope and low-order stream response. *Water Resources Research*, *22*(8), 1273–1282. https://doi.org/10.1029/WR022i008p01273

Sklash, M. M. G., & Farvolden, R. N. R. (1979). The Role Of Groundwater In Storm Runoff. *Developments in Water Science*, *12*(C), 45–65. Retrieved from http://www.sciencedirect.com/science/article/pii/0022169479901641

Soil Survey Staff, Natural Resources Conservation Service, United States Department of Agriculture. Web Soil Survey. Available online at the following link: https://websoilsurvey.sc.egov.usda.gov/. Accessed [06/27/2018].

St Clair, J., Moon, S., Holbrook, W. S., Perron, J. T., Riebe, C. S., Martel, S. J., et al. (2015). Geophysical imaging reveals topographic stress control of bedrock weathering. *Science (New York, N.Y.)*, *350*(6260), 534–8. https://doi.org/10.1126/science.aab2210

Thompson, S. E., Sivapalan, M., Harman, C. J., Srinivasan, V., Hipsey, M. R., Reed, P., et al. (2013). Developing predictive insight into changing water systems: use-inspired hydrologic science for the Anthropocene. *Hydrology and Earth System Sciences*, *17*(12), 5013–5039. https://doi.org/10.5194/hess-17-5013-2013

Tiner, R. W., & Burke, D. G. (1995). *Wetlands of Maryland*.

Trapp Jr., H., & Horn, M. A. (1997). *Ground Water Atlas of the United States: Segment 11, Delaware, Maryland, New Jersey, North Carolina, Pennsylvania, Virginia, West Virginia*. *Hydrologic Atlas 730-L*.

Tromp-van Meerveld, H. J., & McDonnell, J. J. (2006). Threshold relations in subsurface stormflow: 2. The fill and spill hypothesis. *Water Resources Research*, *42*(2), n/a-n/a. https://doi.org/10.1029/2004WR003800

van der Velde, Y., Torfs, P. J. J. F., van der Zee, S. E. A. T. M., & Uijlenhoet, R. (2012). Quantifying catchment-scale mixing and its effect on time-varying travel time distributions. *Water Resources Research*, *48*. https://doi.org/10.1029/2011WR011310

Vepraskas, M. J. (2005). Predicting contaminant transport along quartz veins above the water table in a mica-schist saprolite. *Geoderma*, *126*(1–2), 47–57. https://doi.org/10.1016/j.geoderma.2004.11.006

Wagener, T., Sivapalan, M., Troch, P., & Woods, R. (2007). Catchment Classification and Hydrologic Similarity. *Geography Compass*, *1*, 1–31. https://doi.org/10.1111/j.1749-8198.2007.00039.x

Wald, J. A., Graham, R. C., & Schoeneberger, P. J. (2012). Distribution and properties of soft weathered bedrock at ≤ 1m depth in the contiguous United States Distribution and properties of soft weathered bedrock at ≤ 1 m depth in the contiguous United States. https://doi.org/10.1002/esp.3343

Wolman, M. G. (1987). Sediment movement and knickpoint behavior in a small piedmont drainage basin. *Geografiska Annaler, Series A*, *69*(1), 5–14. https://doi.org/Doi 10.2307/521362

Wolman, M. G., & Miller, J. P. (1960). Magnitude and Frequency of Forces in Geomorphic Processes. *The Journal of Geology*, *68*(1), 54–74. https://doi.org/10.1086/626637

Vita

Shane Michael Putnam was born in Springfield, Vermont on June 23, 1990. He grew up in the small town of Chester, Vermont, spending much of his time exploring the streams and woods of the Green Mountain State, where he developed his love for nature. He graduated from Green Mountain Union High School in Chester, Vermont in June 2008. He graduated *summa cum laude* from the State University of New York College at Oneonta in Oneonta, New York in May 2012 with a B.S. in Water Resource Science and minors in Mathematics and Chemistry. During his undergraduate education, he researched a variety of topics including the impact of best management practices on water quality as well as the photodegradation of environmental contaminants of emerging concern. He received a M.S. in Environmental Science in May 2016 and a Ph.D. in Geography and Environmental Engineering in December 2018 from Johns Hopkins University in Baltimore, Maryland. His graduate research combined field data and modeling in order to understand the influence of landscape structure on the storage of water and generation of streamflow in deeply weathered landscapes. Upon leaving Johns Hopkins University, he plans to do applied research at a state or federal government agency with the goal of influencing policies that aim to protect and improve surface water quality.